



This is to certify that the

thesis entitled

Synthesis Of Novel Mixed-Metal Oxide Materials From Salts Comprised Of Dinuclear Homoleptic Acetonitrile Metal Cations And Polyoxometalate Anions

presented by

Stacey Nanette Bernstein

has been accepted towards fulfillment of the requirements for

M.S degree in Chemistry

Major professor

Date February 13, 1992

LIBRARY Michigan State University

PLACE IN RETURN BOX to remove this checkout from your record. TO AVOID FINES return on or before date due.

DATE DUE	DATE DUE	DATE DUE
	-	

MSU Is An Affirmative Action/Equal Opportunity Institution

SYNTHESIS OF NOVEL MIXED-METAL OXIDE MATERIALS FROM SALTS COMPRISED OF DINUCLEAR HOMOLEPTIC ACETONITRILE METAL CATIONS AND POLYOXOMETALATE ANIONS

By

Stacey Nanette Bernstein

A THESIS

Submitted to
Michigan State University
in partial fulfillment of the requirements
for the degree of

MASTER OF SCIENCE

Department of Chemistry

1992



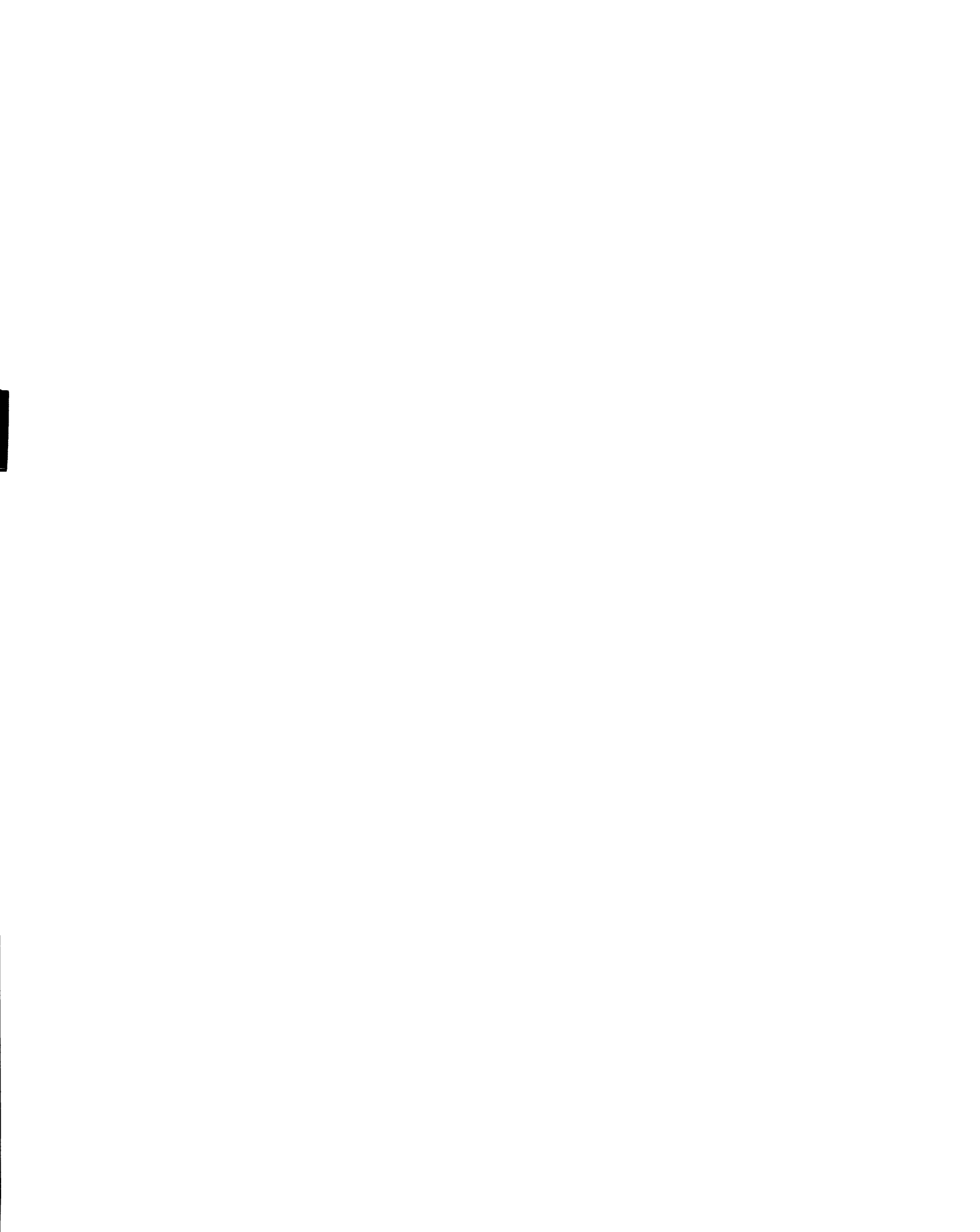
ABSTRACT

SYNTHESIS OF NOVEL MIXED-METAL OXIDE MATERIALS FROM SALTS COMPRISED OF DINUCLEAR HOMOLEPTIC ACETONITRILE METAL CATIONS AND POLYOXOMETAL ATE ANIONS

By

Stacey Nanette Bernstein

An interesting feature of cationic homoleptic acetonitrile complexes is their potential use as catalysts due to the weakly ligating nature of acetonitrile. In addition, these complexes are excellent synthons for a variety of applications in coordination, organometallic, and materials chemistry. Complexes such as $[M_2(NCCH_3)]_x^{4+}$ (M = Rh, Mo, Re; x = 8, 10) are excellent precursors for the facile preparation of new mixed metal oxide materials. The approach consists of co-crystallizing the dinuclear cations with polyoxometalates of general formulae $[M'_6O_{19}]^{2-}$ and $[M'_8O_{26}]^{4-}$ (M'= Mo, W) that are not capable of undergoing nucleophilic substitution; this strategy therefore yields salts of general formulae $[M_2(NCCH_3)_x][M'_6O_{19}]_2$ and $[M_2(NCCH_3)_x][M'_8O_{26}]$ (M= Rh, Mo, Re; x = 8, 10; M'= Mo, W). These materials may serve as bifunctional catalysts due to the possibility of both ions being active. In addition, an advantage of these salts is their ability to be "desolvated" to form new molecular oxide clusters containing very specific metal

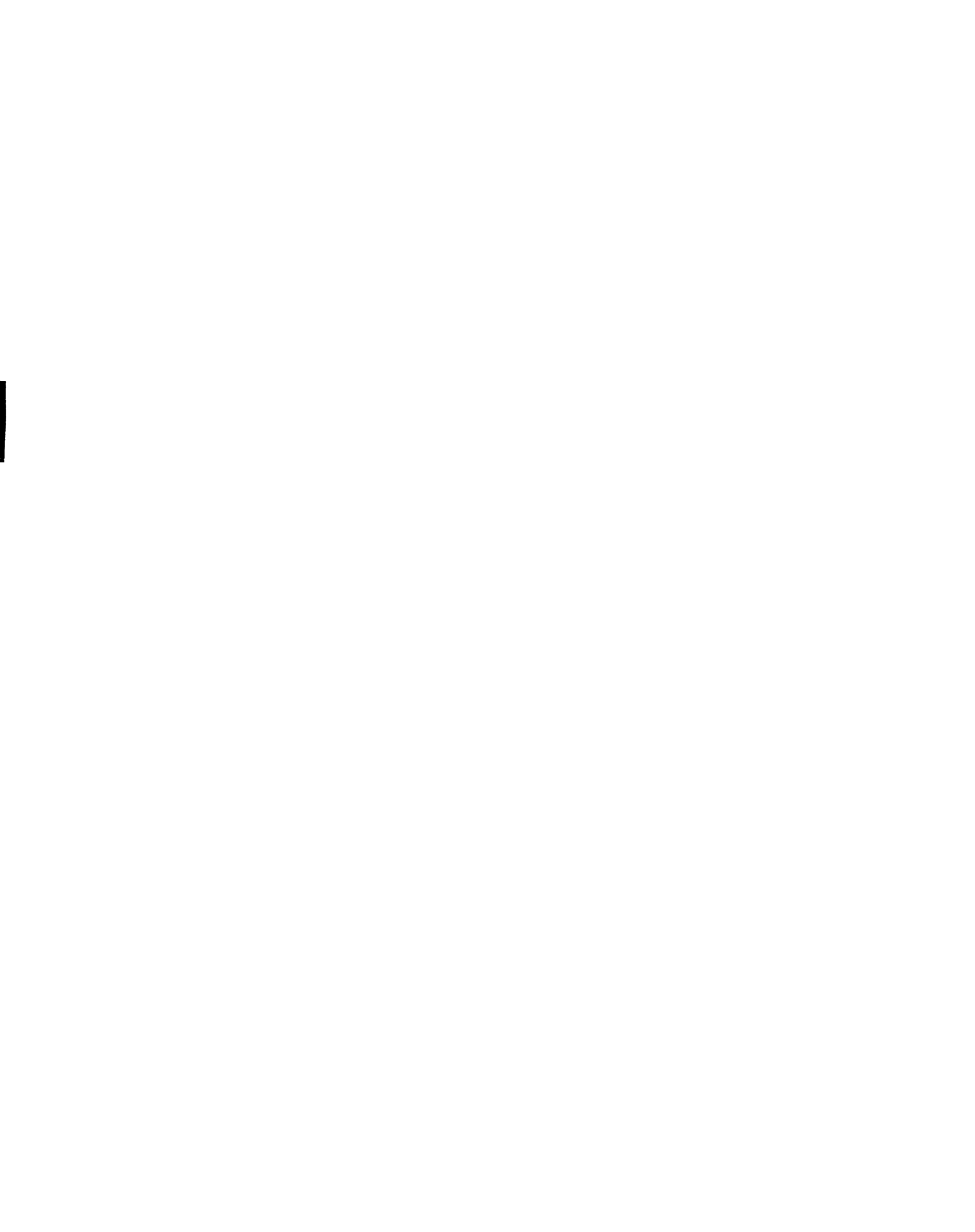


stoichiometries. Based on thermal gravimetric analysis results, these new oxides should be quite pure, with little or no carbonaceous or nitrogenous impurities.

The techniques of single crystal and powder X-ray diffraction, thermal gravimetric analysis, infrared spectroscopy, and cyclic voltammetry have been applied to the characterization of the new compounds. These results as well as the synthesis of polyoxometalate salts containing mononuclear phosphine cations of rhodium are reported herein.



to my family



ACKNOWLEDGMENTS

I wish to express my sincere appreciation to Professor Kim R. Dunbar for her inspiring guidance, support, encouragement, and for the freedom allowed during the course of this work. I am also appreciative that Professors Nocera, Leroi, and Eick have served on my committee.

It is a pleasure to thank the members of Dr. Dunbar's research group, both past and present for their cooperation, suggestions, and aid. Special thanks to Dr. Sue Jane Chen, Steve Haefner, Anne Quillevéré, Helen Chifotides, John Matonic, Dr. Vijay Saharan, Xiang Ouyang, Stuart Bartely, Jui-Sui Sun, and my labmates in room 416.

Of my friends and colleagues I would like to thank Dr. Rui Huang and Dr. Jay Amaraseka for their patience and invaluable help and discussions. A special mention of thanks to Carolyn Hsu who has unselfishly given her equal support and friendship.

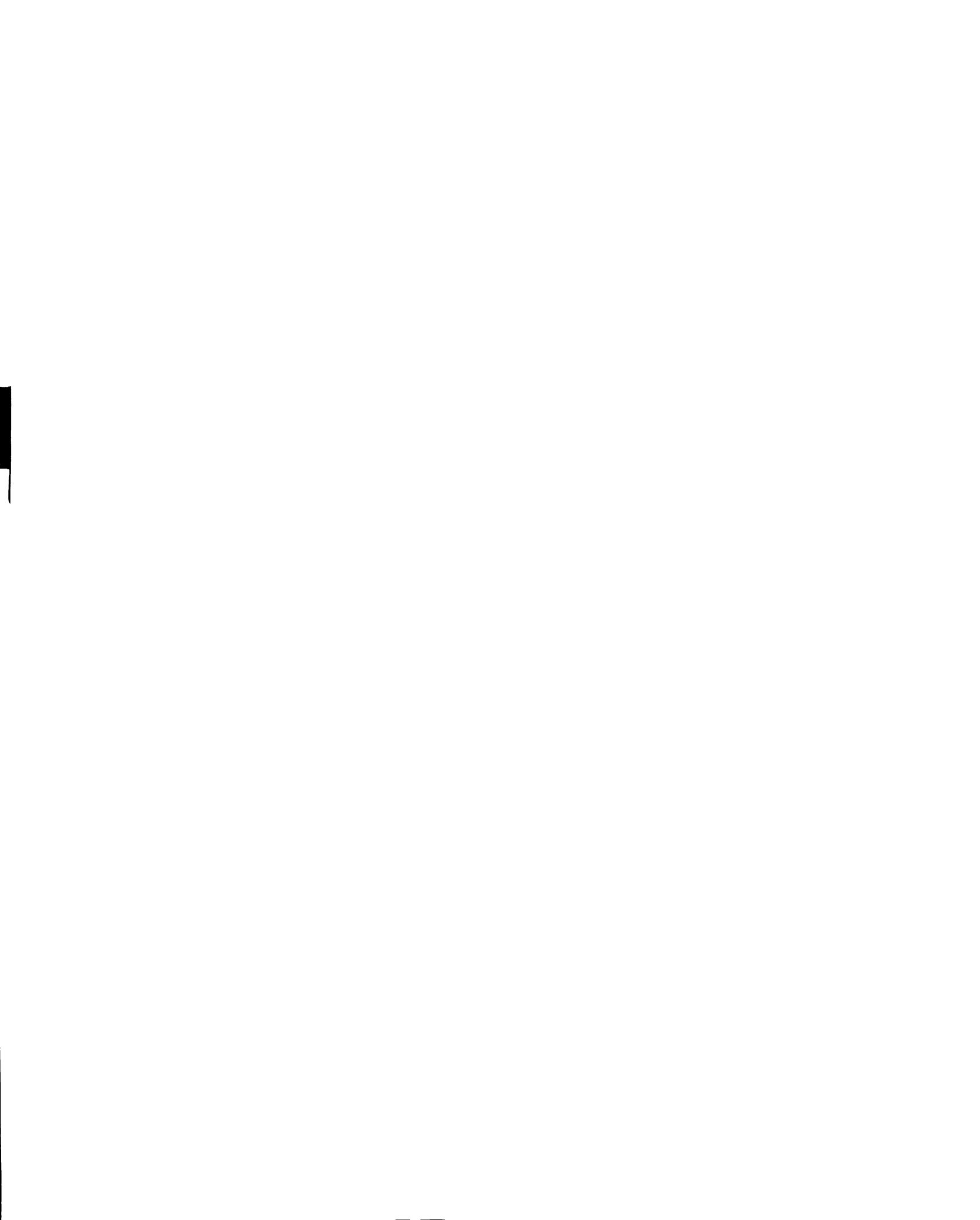
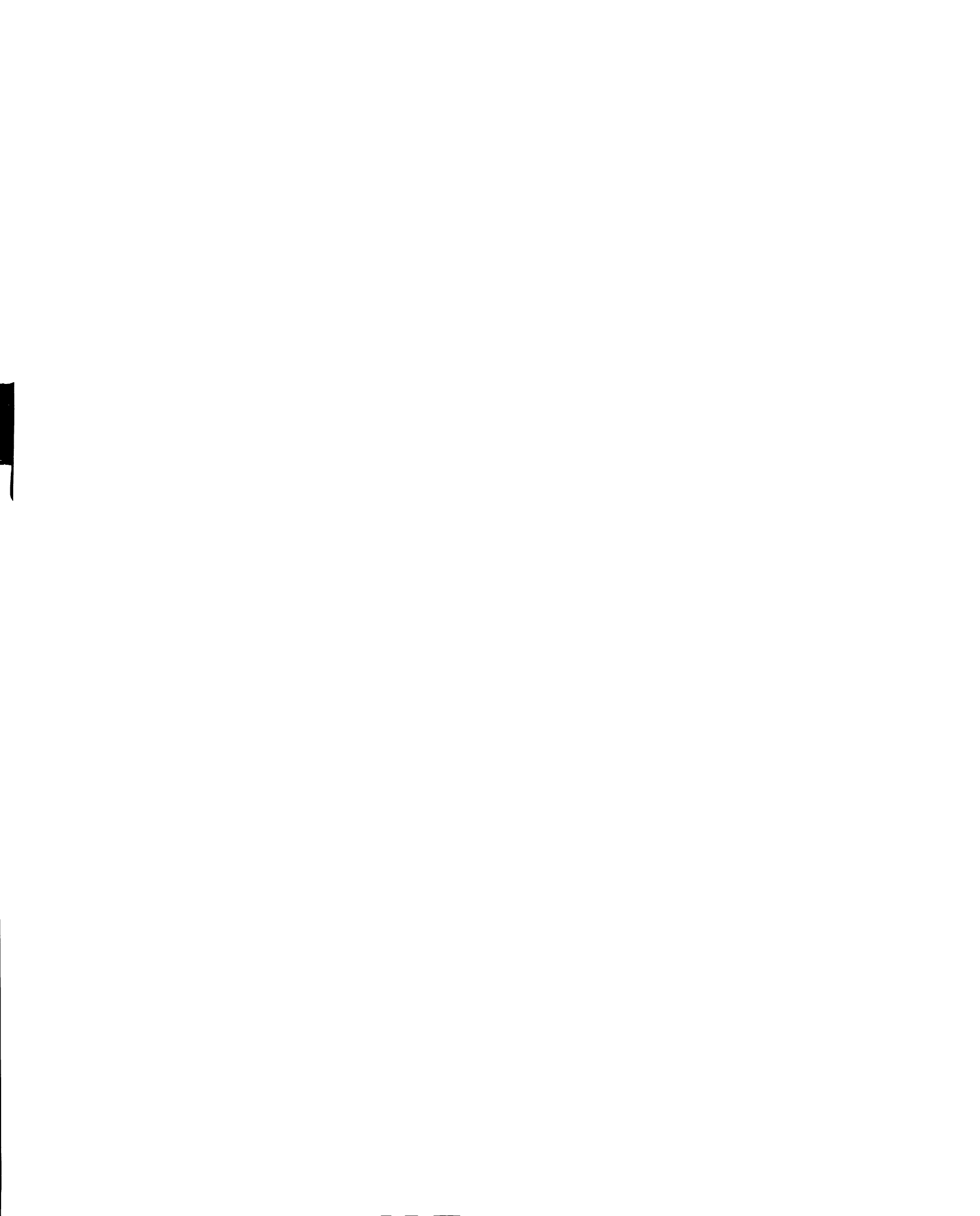


Table of Contents

page
LIST OF TABLESix
LIST OF FIGURESxi
Chapter 1 Introduction
A. Background
1. Cationic Acetonitrile Complexes
2. Anionic Polyoxometalate Complexes
3. Organometallic Polyoxometalate Complexes11
Chapter 2 Experimental
A. Synthesis of Dinuclear Cationic Acetonitrile Complexes18
1. General Procedures
2. Rh ₂ (O ₂ CCH ₃) ₄ · 2CH ₃ OH
3. [Rh ₂ (NCCH ₃) ₁₀][BF ₄] ₄
4. [Mo ₂ (NCCH ₃) ₈][BF ₄] ₄
5. [Re ₂ (NCCH ₃) ₈][BF ₄] ₄
B. Synthesis of Polyoxometalate Complexes
1. $[(n-C_4H_9)_4N]_2[Mo_6O_{19}]$
2. $[(n-C_4H_9)_4N]_4[Mo_8O_{26}]$
3. $[(n-C_4H_9)_4N]_2[W_6O_{19}]$
C. New Members of a Class of Oxymetalates
1. Synthesis of [Rh ₂ (NCCH ₃) ₁₀][Mo ₆ O ₁₉] ₂ 23

2. Reaction of [Rh ₂ (NCCH ₃) ₁₀][BF ₄] ₄ with	
$[(n-C_4H_9)_4N]_4[Mo_8O_{26}]$	23
3. Synthesis of $[Rh_2(NCCH_3)_{10}][W_6O_{19}]_2$	24
4. Synthesis of [Mo ₂ (NCCH ₃) ₈][Mo ₆ O ₁₉] ₂	24
5. Reaction of [Mo ₂ (NCCH ₃) ₈][BF ₄] ₄ with	
$[(n-C_4H_9)_4N]_4[Mo_8O_{26}]$	24
6. Synthesis of $[Mo_2(NCCH_3)_8][W_6O_{19}]_2$	25
7. Synthesis of $[Re_2(NCCH_3)_8][Mo_6O_{19}]_2$	25
8. Synthesis of $[Rh(\eta^3-TMPP)_2][Mo_6O_{19}]$	25
9. Synthesis of $[Rh(\eta^3-TMPP)_2][W_6O_{19}]$	26
10. Reaction of $[Rh(\eta^3-TMPP)_2][Mo_6O_{19}]$ with CO	26
D. Physical Techniques	26
1. Infrared Spectroscopy	26
2. Electronic Absorption Spectroscopy	27
3. Powder X-ray Diffraction	27
4. Electrochemistry	27
5. Thermogravimetric Analysis	28
6. Nuclear Magnetic Resonance	28
7. Electron Paramagnetic Resonance	28
8. Magnetic Susceptibility Measurements	29
9. Elemental Analyses	29
10. Single X-ray Crystallography	29
Chapter 3 Results and Discussion	30
A. Synthetic Methodology	30
1. Synthesis of Solvated Systems	30

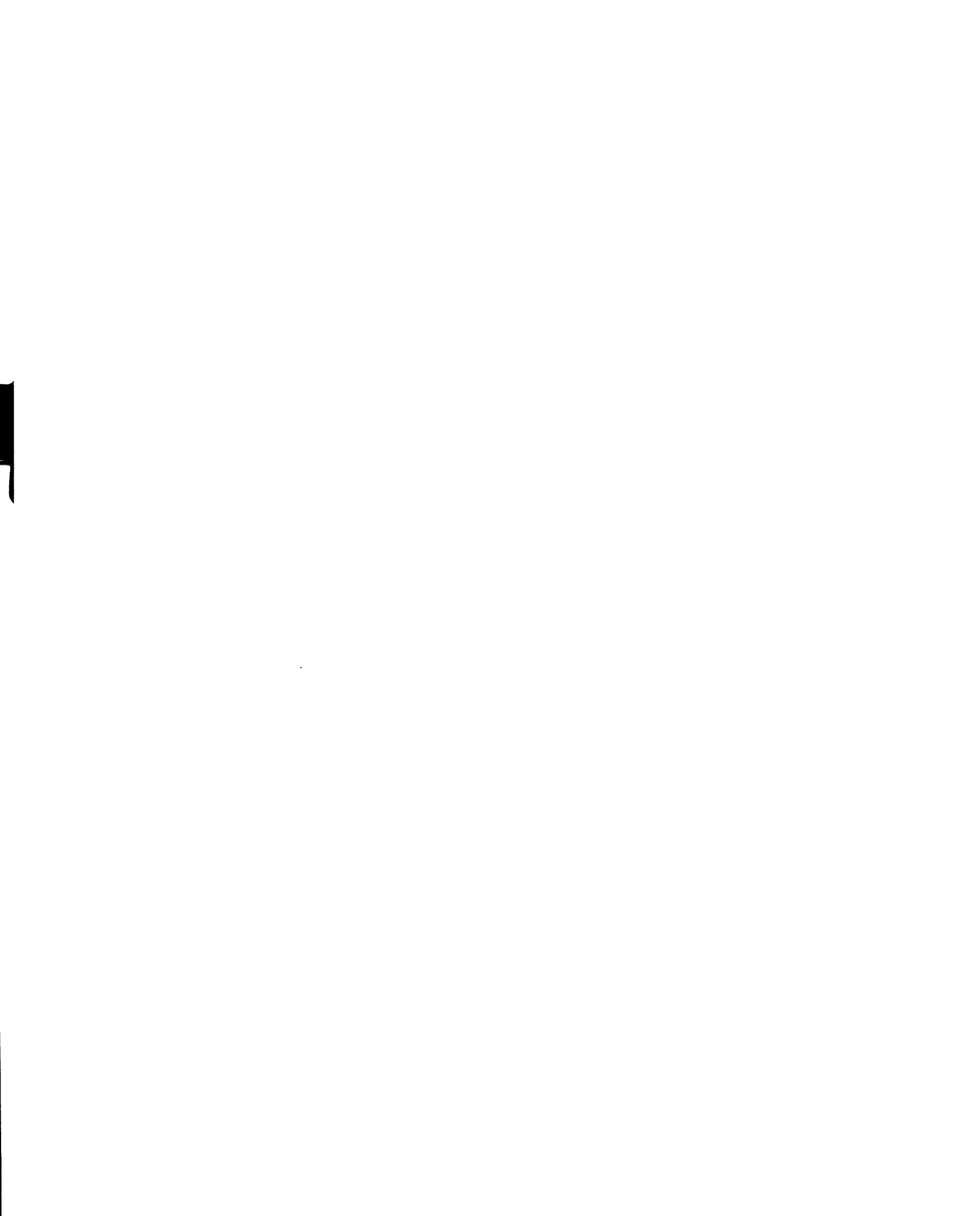
page



LIST OF TABLES

•	D	a	g
	~	_	_

1.	Average Bond Lengths (Å) for the $[M_6O_{19}]^{n-}$ Anions7
2.	Observed v(M-O) Stretching Frequencies (cm ⁻¹) of the New
Oxyn	netalate Complexes Compared to the
n-Tei	trabutylammonium Salts47
3.	Electron Paramagnetic Resonance and Magnetic Susceptibility
Meas	surements for the Dication $[Rh(\eta^3-TMPP)_2]^{2+}$ 55
4.	The Peak Positions and Indices of the X-ray Diffraction Pattern of the
TGA	Product for [Mo ₂ (NCCH ₃) ₈][Mo ₆ O ₁₉] ₂ 69
5.	Crystal Data for
[Re ₂ ($NCCH_3)_8(CH_3CN)_2][Mo_6O_{19}]_2 \cdot 4CH_3CN \cdot 2H_2O \dots 73$
6.	Selective Bond Distances (Å) and Angles (deg) for the Molecular
[Re ₂ (NCCH ₃) ₈ (CH ₃ CN) ₂] ²⁺ Cation74
7.	Selective Bond Distances (Å) and Angles (deg) for the [Mo ₆ O ₁₉] ²⁻
Anio	n75
8.	Crystal Data for [Rh ₂ (NCCH ₃) ₁₀][BF ₄] ₄ 81



9.	Selective Bond Distances (Å) and Angles (deg) for the Molecular	
[Rh ₂	(NCCH ₃) ₁₀] ⁴⁺ Cation Derived from Orthorhombic and Monoclinic	
Cry	stal Systems	32
10.	Crystal Data for [Rh ₂ (NCCH ₃) ₁₀][Mo ₆ O ₁₉] ₂ • 4CH ₃ CN	35
11.	Selective Bond Distances (Å) and Angles (deg) for	
[Rh ₂	(NCCH ₃) ₁₀][Mo ₆ O ₁₉] ₂ • 4CH ₃ CN	36
12.	Crystal Data for $[Rh(\eta^3-TMPP)_2][W_6O_{19}] \cdot 4CH_3CN$	9 0
13.	Some Important Bond Distances (Å) and Angles (deg) for	
[Rh($[\eta^3-TMPP)_2][W_6O_{19}]$)1

LIST OF FIGURES

page

1.	Representations of the general polyoxometalate structures:
(a) K	Leggin structure; (b) Anderson structure; (c) icosahedral
struc	eture6
2.	The structure of the $[M_6O_{19}]^{2-}$ unit: (a) 'bond' structure;
(b) 'p	polyhedral' model; (c) space-filling model8
3.	A model of the $[M_6O_{19}]^{2-}$ anion depicting the different types of
oxyg	ens10
4.	Structures of organometallic polyoxometalates: (a) $[\eta^5$ -
C ₅ H ₅	$_{5}$)TiMo ₅ O ₁₈] ³⁻ ; (b) [(η^{5} -C ₅ H ₅)Ti(Mo ₅ O ₁₈)MoCl ₂] ²⁻ ; (c) [(η^{5} -
C ₅ H ₅	$_{5}$)Ti(Mo ₅ O ₁₈)Mn(CO) ₃] ²⁻ ; (d) [(η^{4} -C ₈ H ₁₂)Ir(C ₅ Me ₅)TiW ₅ O ₈] ²⁻ ;
(e) [($(OC)_3MNb_2W_4O_{19}]^{3-}$, $(M = Mn^I, Re^I)$;
(f) {[$[(CH_3)_5C_5Rh(cis)-Nb_2W_4O_{19}]^2$; (g) $\{[(C_7H_8)Rh]_5(Nb_2W_4O_{19})_2\}^3$;
(h) [((C_5H_5) TiSiW ₉ V ₃ O ₄₀] ⁴⁻ , $[(C_5Me_5)$ RhSiW ₉ V ₃ O ₄₀] ⁵⁻ ;
(i) [($C_5Me)_5RhP_2W_{15}Nb_3O_{62}]^{7-}$, $[(C_6H_6)RuP_2W_{15}Nb_3O_{62}]^{7-}$,
[(C(OD) $IrP_2W_{15}Nb_3O_{62}]^{8-}$
5.	The ¹ H NMR spectrum of [Re(NCCH ₃) ₈][BF ₄] ₄ in (a) CD ₃ NO ₂
solve	ent and (b) CD ₃ CN solvent33

6.	Infrared spectrum of [Re ₂ (NCCH ₃) ₈][BF ₄] ₄ : (a) 2500 cm ⁻¹ to
200	0 cm ⁻¹ region; (b) 2500 cm ⁻¹ to 400 cm ⁻¹ region35
7.	Cyclic voltammetry of [Re ₂ (NCCH ₃) ₈][BF ₄] ₄ in 0.05 M TBABF ₄ -
CH ₃	CN at 200 mV/sec: (a) a voltammogram showing only the
accs	sible reduction process at $E_{1/2} = +0.24$ V displaying a
peak	x-to-peak separation of 110 mV; (b) a voltammogram consisting
of th	aree separate sweeps that show the appearance of several
irrev	versible reductions at potentials greater than 0 V vs Ag/AgCl36
8.	Electronic absorption spectrum of [Re ₂ (NCCH ₃) ₈][BF ₄] ₄ : (a) in
dry,	deoxygenated CH ₃ CN and (b) as a DMAA solution
9.	Infrared spectra of (a) [Rh ₂ (NCCH ₃) ₁₀][Mo ₆ O ₁₉] ₂ and
(b) [$Mo_2(NCCH_3)_8][Mo_6O_{19}]_2$ 41
10.	Infrared spectrum of $[Re_2(NCCH_3)_8][Mo_6O_{19}]_2$
11.	Infrared spectra of (a) [Rh ₂ (NCCH ₃) ₁₀][W ₆ O ₁₉] ₂ and
(b) [$Mo_2(NCCH_3)_8][W_6O_{19}]_2$
12.	Infrared spectra of (a) [Rh ₂ (NCCH ₃) ₁₀][Mo ₈ O ₂₆] and
(b) [$Mo_2(NCCH_3)_8][Mo_8O_{26}]$ 44
13.	Infrared spectra of $[(n-C_4H_9)_4N]_2[M_6O_{19}]$: (a) M = Mo;
(b) l	M = W
14	Infrared spectrum of $[(n-C_4H_0)_4N]_4[M_{00}O_{26}]$

15.	Electronic absorption spectrum of [Re ₂ (NCCH ₃) ₈][Mo ₆ O ₁₉] ₂ 48
16.	Electronic absorption spectra of (a) $[Rh_2(NCCH_3)_{10}][Mo_6O_{19}]_2$ and
(b) []	$Mo_2(NCCH_3)_8][Mo_6O_{19}]_2$
17.	Infrared spectrum of $[Rh(\eta^3-TMPP)_2][Mo_6O_{19}]$
18.	Electron paramagnetic spectra of $[Rh(\eta^3-TMPP)_2][Mo_6O_{19}]$:
(a) li	quid sample at 103 K (9.6226 GHz, 2658.15 - 3702.5 G); (b) solid
samp	ole at 103 K (9.6096 GHz, 2658.4 - 3702.3 G); (c) solid sample at
300k	X (9.5993 GHz, 2316.5 - 4402.5 G)52
19.	The χ_M vs 1 / T plot for [Rh(η^3 -TMPP) ₂][Mo ₆ O ₁₉]54
20.	Infrared spectrum from the reaction of $[Rh(\eta^3-TMPP)_2][Mo_6O_{19}]$
with	CO at 50 psi56
21.	Display of the thermogravimetric analysis measurements of
(a) []	$Rh_2(NCCH_3)_{10}][Mo_6O_{19}]_2$ and (b) $[Mo_2(NCCH_3)_8][Mo_6O_{19}]_258$
22.	Display of the thermogravimetric analysis measurement of
[Re ₂	$(NCCH_3)_8][Mo_6O_{19}]_2$
23.	Infrared spectra of the desolvated materials (a) "Re ₂ (Mo ₆ O ₁₉) ₂ "
and ((b) $"Mo_2(Mo_6O_{19})_2"$
24.	Infrared spectrum of the desolvated material "Rh ₂ (Mo ₆ O ₁₉) ₂ "61

25.	Powder X-ray diffraction patterns for (a) [Rh ₂ (NCCH ₃) ₁₀][Mo ₆ O ₁₉] ₂
and	(b) $[Re_2(NCCH_3)_8][Mo_6O_{19}]_2$
26.	Powder X-ray diffraction patterns for (a) [Rh ₂ (NCCH ₃) ₁₀][W ₆ O ₁₉] ₂
and	(b) $[Mo_2(NCCH_3)_8][W_6O_{19}]_2$ 64
27.	Powder X-ray diffraction pattern for [Rh ₂ (NCCH ₃) ₁₀][Mo ₈ O ₂₆]65
28.	Powder X-ray diffraction patterns for $[(n-C_4H_9)_4N]_2[M_6O_{19}]$:
(a) N	M = Mo; (b) $M = W$
29.	Powder X-ray diffraction pattern for [(n-C ₄ H ₉) ₄ N] ₄ [Mo ₈ O ₂₆]67
30.	Powder X-ray diffraction pattern for the desolvated material
obta	ined from the TGA of $[Mo_2(NCCH_3)_8][Mo_6O_{19}]_2$
31.	ORTEP drawing of [Re ₂ (NCCH ₃) ₈ (CH ₃ CN) ₂][Mo ₆ O ₁₉] ₂ , showing
the a	atom labeling scheme. Unlabeled atoms are related to labeled ones
by a	a two-fold axis at the midpoint of the Re-Re* bond
32.	Computer generated space-filling model of the [Re ₂ (NCCH ₃) ₈] ⁴⁺
catio	on. The Re atom is denoted by the black ball77
33.	ORTEP diagram of [Rh ₂ (NCCH ₃) ₁₀][BF ₄] ₄ in an orthorhombic
crys	tal system

34.	ORTEP diagram of [Rh ₂ (NCCH ₃) ₁₀][Mo ₆ O ₁₉] ₂ showing the atom
label	ling scheme. Unlabeled atoms are related to labeled ones by a
two	-fold axis at the midpoint of the Rh-Rh* bond87
35.	ORTEP drawing of $[Rh(\eta^3-TMPP)_2][W_6O_{19}]$. The $[W_6O_{19}]^{2-}$ anion
resid	les on a site of two-fold symmetry92
36.	A view of a packing diagram of [Rh(η ³ -TMPP) ₂][W ₆ O ₁₉] along
the b	o - axis93

Chapter 1 INTRODUCTION

A. Background

1. Cationic Acetonitrile Complexes.

The earliest reports of metal-nitrile complexes date from circa 1850 [1]. Nearly thirty years ago, extensive reviews on the structures, spectral properties, and reactivity of such complexes were published [2]. In recent years, there has been a renewed interest in the chemistry of transition metal cationic acetonitrile complexes. Most of the attention has focused on the experimental evidence pointing to their use as precursors for preparative routes to new coordination compounds, biologically relevant complexes, and as various catalysts.

For many years, the known homoleptic transition metal acetonitrile cations included most of the first row transition metal elements (groups 4-12). Syntheses with various counterions such as [SbF₆]⁻, [BiF₆]⁻, [AlCl₄]⁻, [ClO₄]⁻, and [BF₄]⁻ have been outlined by Reedijk and Groeneveld, and Hathaway [3, 4]. The most facile method of preparation includes the use of NOBF₄ with the appropriate metal powder or filings in acetonitrile to form the mononuclear divalent [M(CH₃CN)₆]ⁿ⁺ (n = 2, 3) tetrafluoroborate salts. The chemistry of the homoleptic acetonitrile complexes has not been as extensive for the second and third row transition elements. Indeed, the only mononuclear homoleptic acetonitrile complexes known for these include Ru^{II}, Pd^{II}, Ag^I, Cd^{II}, Pt^{II}, and Au^I [5]. The only extension of the

chemistry of these mononuclear cations to date is the synthesis of the lanthanide metal acetonitrile complex [Eu(CH₃CN)₃(BF₄)₃]_x which was synthesized by Sen and co-workers [6]. Characterization by molecular weight measurements revealed that the cation actually exists as a dimer via a bridging tetrafluoroborate in acetonitrile solutions.

In 1983, Mayer and Abbott managed to synthesize the very first dinuclear homoleptic acetonitrile complex, viz., [Mo₂(NCCH₃)₁₀][F₃CSO₂]₄ [7]; even more recently Cotton and co-workers have succeeded in preparing the tetrafluoroborate complex in high yield [8]. Interest in dinuclear species was initially sparked by a desire for an organic soluble form of the fully solvated complex cation [Mo₂(aq)]⁴⁺, which was reported by Bowen and Taube [9]. One of the more interesting properties of the [Mo₂(NCCH₃)₈]⁴⁺ cation is that it is an example of a dinuclear Mo₂^(II,II) species that possesses a quadruple bond without the extra stability afforded by any bridging ligands, such as phosphines or carboxylates.

In addition to the interest in dinuclear molybdenum solvated systems, the prospect for an analogous rhodium complex had also been investigated by Dunbar [10] and independently by Baranovskii et al. [11]. A crystallographic study of the tetrafluoroborate salt confirmed the formulation as the unbridged cation $[Rh_2(NCCH_3)_{10}]^{4+}$. Each rhodium atom has a d⁷ configuration, and the molecule retains a single metal-metal bond.

The instances of these dinuclear solvated cations have been rare, and so there is current interest to prepare more examples, especially of the third row transition elements since the potential chemistry for these complexes is vast; for example, as synthons for many new ionic materials, and as precursors for metal containing polymers and molecular materials [12].

A prominent feature of the chemistry of homoleptic acetonitrile complexes is that they are all cationic, and only soluble in polar organic solvents such as acetonitrile, dimethylsulfoxide, and nitromethane. An important advantage in using these complexes is their enhanced reactivity since they are only supported by the weakly ligating acetonitrile ligand and possess non-coordinating counterions. These characteristics are desirable traits for complexes to be potential catalysts. Sen and co-workers have attracted considerable attention in this area by demonstrating the usefulness $[Pd(CH_3CN)_4][BF_4]_2$, $[Mo(NO)_2(CH_3CN)_4][BF_4]_2$, of $[W(NO)_2(CH_3CN)_4][BF_4]_2$, and $[Eu(CH_3CN)_3(BF_4)_3]_x$ as good homogeneous catalysts for the polymerization of acetylenes and olefins, and the selective activation of C=C, C-C, and C-H bonds [6, 13]. Since these complexes have the ability to create vacant coordination sites due to the dissociation of their weakly held ligands, the metals are then free to interact with organic substrates. In this regard, an investigation of the catalytic behavior of acetonitrile cations, especially rhodium, might lead to interesting results, especially in light of the extensive work of Doyle, et al. involving the use of Rh₂(bridge)₄ compounds as excellent catalysts for the asymmetric cyclopropanation of olefins from the decomposition of diazo compounds to carbenes [14].

2. Anionic Polyoxometalate Complexes.

Polyoxometalates are anionic molecular oxide clusters of the early transition metal elements. They are one of the most remarkable classes of compounds known, as they have found applications in many of the most significant research areas of chemical interest. Much attention has been given to the solid state properties, since it is well known that polyoxometalates serve as diverse heterogeneous catalysts [15]. In addition, polyoxometalates are useful in analytical and clinical chemistry, biochemistry, and medicinal chemistry. They are known to be biologically active as highly selective inhibitors of enzyme function, as in vitro and in vivo antitumor agents, as antiviral activity agents (e.g. against rabies and scrapie, the sheep version of "mad cow disease"), and even as anti-retroviral agents (e.g. against HIV infections, connected with AIDS, SAIDS). The heteropolytungstate [(Na)(Sb₃O₇)₂(SbW₇O₂₄)₃]⁸⁻, also known as HPA-23, has been used exclusively as a treatment for AIDS patients in France [16].

The first reports of polyoxometalates emerged more than 150 years ago, and since then a vast number of examples have been structurally elucidated. In 1826, Berzelius initiated the fertile research area of molybdenum polyoxometalate chemistry by noting the formation of yellow products from the reaction of sodium molybdate with phosphoric acid [17]. Hence, the discovery of the heteropolyanion [PMo₁₂O₄₀]³. Heteropolytungstates were characterized almost forty years later by Marignac, but it was not until 1933 that Keggin reported the structure of the heteropoly acid [H₃PW₁₂O₄₀] • 6H₂O [18, 19].

A prominent feature of the polyoxoanion structure is the presence of MO_x units in an octahedral or square pyramidal arrangement. In most cases, the metal lies at the vertex, or an edge of a polyhedron. Many years ago, Lipscomb predicted that the polyanion structures would not form MO_6 octahedra with more than two unshared oxygen atoms, and in fact since then, very few structures have violated this statement [20]. Among the

metals that form discrete polyoxoanions, molybdenum and tungsten exhibit the most polyoxoanion chemistry due, in part, to their size and the accessibility of empty d orbitals for metal-oxygen $d\pi$ -p π bonding. The transition elements of groups V and VI meet the requirements to form the main structures of polyoxoanions, whereas almost any element may function as a heteroatom in heteropolyanions.

In terms of geometry, there are three general polyoxometalate structures to be considered. These include tetrahedral, octahedral, and icosahedral. The exceptions to the structures are usually derivatives that include fragments of the basic structures. Figure 1 depicts a model for each of these broad classes. Among the tetrahedral heteropolyanions, the Keggin structure and its isomers are the most well known. The structure consists of an arrangement of four edge-shared M₃O₁₃ octahedra situated around a PO₄ tetrahedron. Other isomers have been discovered by modifying the heteroatom. A rotation of one of the four sets of three octahedra by 60° and reattachment to the same vertices reduces the T_d symmetry to a structure with a threefold axis. For example, replacement of the heteroatom from phosphorous to silicon or germanium gives the $[XM_{12}O_{40}]^{4-}$ (X=Si, Ge) anions. The majority of heteropolytung states exhibit either the Keggin structure or structures derived from its fragments, while far fewer heteropolymolybdates adopt the Keggin geometry [21].

The parent structure for an octahedral polyoxometalate, $[(XO_6)(M_{12}O_{32})]$, where the X heteroatom has octahedral XO_6 geometry, has not yet been observed, but several derivatives have been reported. The most familiar octahedral (XM_6) heteratom, is known as the Anderson structure. The first one of this type to be reported is $[TeMo_6O_{24}]^{6-}$ [22];

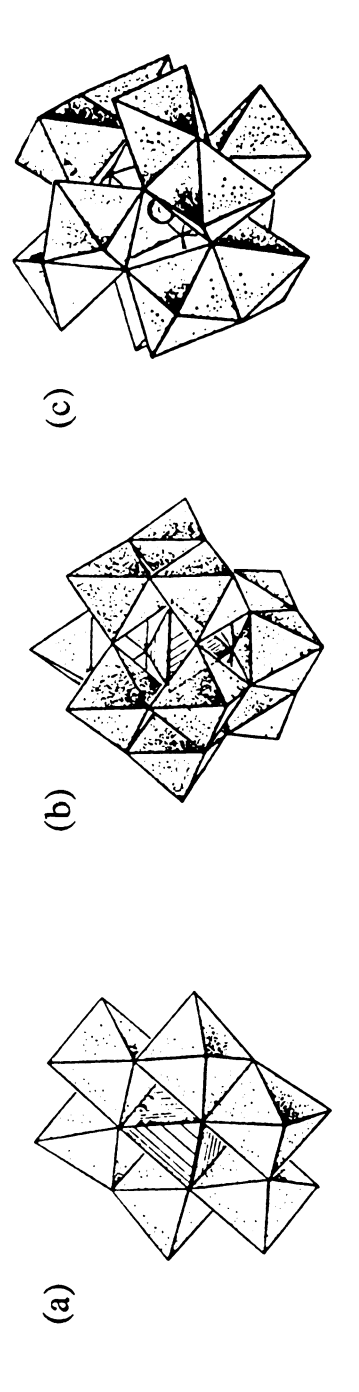


Figure 1. Representations of the general polyoxometalate structures: (a) Keggin structure; (b) Anderson structure; (c) icosahedral structure.

subsequently, a multitude of heteropolyanions with this structure have been demonstrated to exist with heteroatoms ranging in oxidation states from +2 to +7.

The icosahedral polyoxoanion structures were first described twenty-five years ago. In this case, the parent structure is $[(XO_{12})(M_{12}O_{30})]$; an early example is $[Ce^{IV}Mo_{12}O_{42}]^{3-}[23]$. The structure is also known for molybdates with Ce^{III} , Th^{IV} , U^{IV} , U^{V} , and Np^{IV} heteroatoms.

Isopolyanions, also known as the Lindqvist structure, are constructed of a hexametalate M_6O_{19} unit. Examples include $[Nb_6O_{19}]^{8-}$, $[Ta_6O_{19}]^{8-}$, $[Mo_6O_{19}]^{2-}$, $[W_6O_{19}]^{2-}$, and are represented in Figure 2. The arrangement of M_6O_{19} in nearly all structures is close to octahedral symmetry, O_h . The 'bond' structure representation reveals the placement of atoms within the polyhedron. Table 1 gives the average bond lengths for several isopoly hexametalates [16]. The 'polyhedral' representation is generally used to provide a comprehensive picture for the more complicated polyanions, and space filling models are used to reveal the metal oxide surface, a characteristic that enhances their catalytic properties.

Table 1. Average Bond Lengths (Å) for the $[M_6O_{19}]^{n-}$ Anions.^a

Anion	M-O _t	M-O _b	M-O _c
$[Mo_6O_{19}]^{2-}$	1.68	1.93	2.32
$[W_6O_{19}]^{2-}$	1.69	1.92	2.33
$[{\rm Ta_6O_{19}}]^{2-}$	1.80	1.99	2.38

^a O_t, terminal oxygens; O_b, bridging OM₂ oxygens; O_c, central OM₆ oxygens.

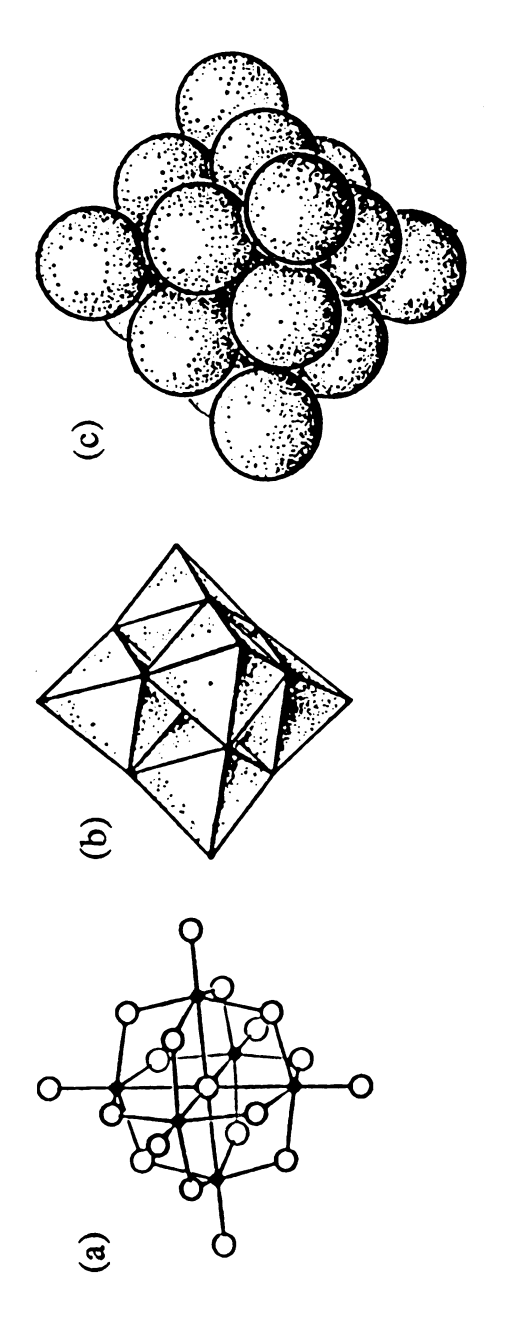


Figure 2. The structure of the [M₆O₁₉]²- unit: (a) 'bond' structure; (b) 'polyhedral' model; (c) space-filling model.

For many years now, polyoxometalates have been of academic interest to chemists. Rocchiccioli-Deltcheff and co-workers have extensively studied the vibrational spectra of the polyanions by using a normal coordinate analysis [24]. This technique has provided a good basis for understanding the structural properties of the Lindqvist and Keggin ion structures. On the basis of being able to propose reasonable force constants, and by performing labelling studies, Rocchiccioli-Deltcheff have calculated, and assigned the stretching and bending frequencies for the hexamolybdate anion $[M_6O_{19}]^{2-}$ according to each type of oxygen in the structure (Figure 3).

The influence of counterions on the vibrational spectra of polyanions in the solid state leads to observations that the anion-anion interactions may influence the physical properties of polyoxometalates [24]. The infrared spectral approach to studying the polyanions has the advantage of affording information about intermolecular interactions without knowledge of the crystal structure. Rocchiccioli-Deltcheff showed that the cation size determines the anion-anion interactions; the larger cations result in longer O-O interanion distance, and due to electrostatic repulsion, lead to weaker anion-anion interactions [24]. The correlation between cation size and the metal-oxygen stretching frequencies was investigated, with the result that cation size determined the infrared frequencies of the M-O stretches [24]. Complexes with smaller cations have higher frequency shifts. n-tetrabutylammonium salts were chosen as good models for isolated anions in the crystal lattice and are used as references, for only negligible electrostatic forces exist between the external oxygens of the adjacent anions.

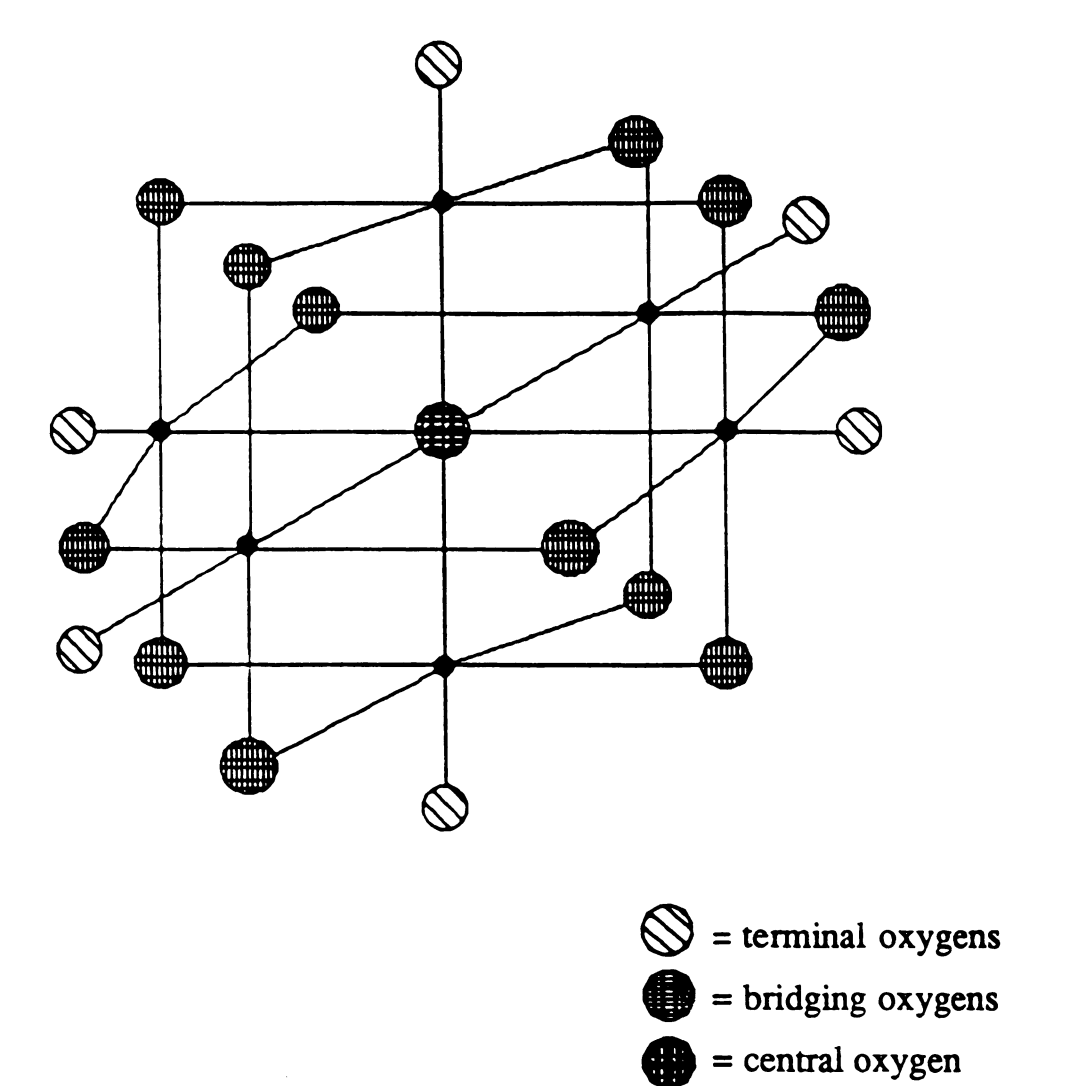


Figure 3. A model of the $[M_6O_{19}]^{2-}$ anion identifying the different types of oxygens.

Numerous polyoxometalate complexes are capable of being reversibly reduced by addition of one or more electrons. These reduction species, frequently deep blue in color, usually retain the general structures of their oxidized precursors, and comprise a very important group of complexes generally known as the "heteropoly blues." The extra electrons are delocalized over numerous atoms in the structure, and are involved in the process of "electron hopping," a process that involves the mobility of activated electrons from one metal to another through the pi bonding of the bridging oxygens from a reduced metal atom to its neighbors [16].

3. Organometallic Polyoxometalate Complexes.

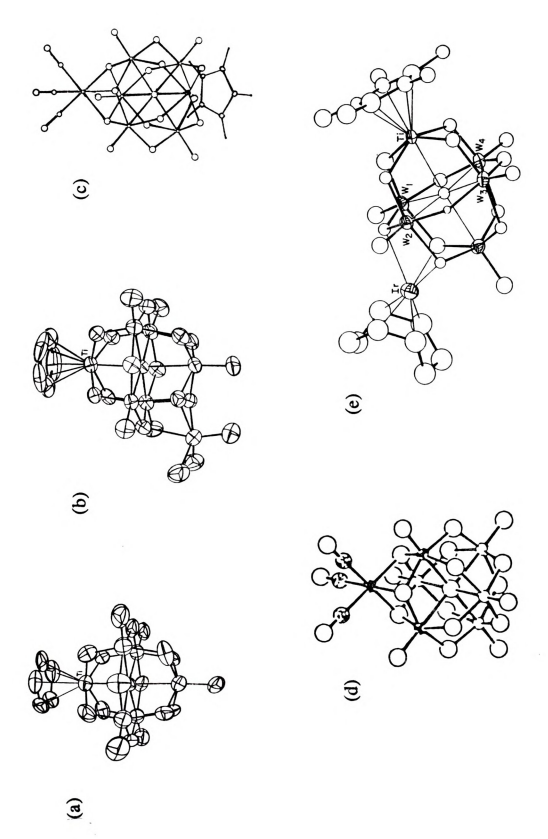
Molecular catalysts supported by various metal oxides combine the advantages of both homogeneous and heterogeneous systems [15, 25]. Specifically, the organometallic and coordination chemistry of metal centers coordinated to oxoanion "ligands" supplies useful information regarding the nature of the metal-oxygen interaction and its importance in catalytic reactions. Molecular clusters containing polyoxoanions have contributed substantially to the development of new solid state materials that contain organometallic cluster units. This new class of compounds bridge the gap between the solution chemistry of polyoxoanions and the solid-state chemistry of metal-oxide materials [26].

During the past decade, Klemperer and co-workers have investigated the reaction chemistry of early transition metal polyoxoanions with a variety of organotransition metal compounds [26]. Their work has primarily focused on the chemistry of the hexametalate polyoxoanions closely related to $[M_6O_{19}]^{2-}$ (M = Mo, W), which contain either one or two metal sites that have been partially replaced by other low valent early

transition metal atoms. An advantage of this approach is that it increases the nucleophilicity of the anion which affords greater reactivity towards the highly electrophilic organometallic compounds. This new class of complexes are usually structurally characterized by X-ray diffraction, but can also be investigated by ¹⁷O NMR spectroscopy. The structure of the salt $[(n-C_4H_9)_4N]_3[(\eta^5-C_5H_5)TiM_5O_{18}]$ (M = Mo, W) was first proposed purely on the basis of its ¹⁷O NMR, and later confirmed by single X-ray diffraction (Figure 4a). The molecule exhibits a structural modification of the $[M_6O_{19}]^{2-}$ anion in that one terminal M=O unit has been replaced by the (n⁵-C₅H₅)Ti unit [27]. An examination of the reactivity of the anion towards electrophiles demonstrated the utility of polyoxometalates in determining the stability of oxoanion supported organometallic chemistry. Upon addition of aqueous HCl, the anion $[(\eta^5-C_5H_5)Ti(Mo_5O_{18})Mo_2Cl]^{2-}$ is formed, and has a structure wherein the MoO₂Cl⁺ unit is bonded to a triangle of three bridging oxygens of the Mo₅O₁₈ unit (Figure 4b); similarly, $[(OC)_3Mn(NCCH_3)_3][PF_6]$ reacts with $[(\eta^5-C_5H_5)Ti(Mo_5O_{18}]^{3-}$ to vield the bifunctional polyoxoanion supported organometallic hydrocarbylcarbonyl derivative $[(\eta^5-C_5H_5)Ti(Mo_5O_{18})Mn(CO)_3]^{2-}$ (Figure 4c) [28]. Recently, investigations into the reaction chemistry of cyclooctadieneiridium (I) complexes performed by Klemperer and Yagasaki, resulted in the isolation of the polyanion [(n⁴-C₈H₁₂)Ir(C₅Me₅)TiW₅O₈]²⁻ (Figure 4d) [29]. The structural determination of these new complexes illustrated that the organometallic adducts were all supported on the oxoanion via the same $[(\eta^5-C_5H_5)TiMo_6O_{18}]^{2-}$ oxygens that were bound to the MoO₂Cl⁺ metal center.

The chemistry of electrophilic organometallic complexes with [(cis)-Nb₂W₄O₁₉]⁴⁻ has also been explored but different behavior was observed.

Figure 4. Structures of organometallic polyoxometalates: (a) $[\eta^5-C_5H_5)TiMo_5O_{18}]^3$; (b) $[(\eta^5-C_5H_5)Ti(Mo_5O_{18})Mo_2Cl]^2$; (c) $[(\eta^5-C_5H_5)Ti(Mo_5O_{18})Mn(CO)_3]^2$; (d) $[(\eta^4-C_8H_{12})Ir(C_5Me_5)TiW_5O_8]^2$; (e) $[(OC)_3MNb_2W_4O_{19}]^3$ -, (M = Mn^I, Re^I); (f) $\{[(CH_3)_5C_5Rh(cis)-Nb_2W_4O_{19}]^2$ -; (g) $\{[(C_7H_8)Rh]_5(Nb_2W_4O_{19})_2\}^3$ -; (h) $[(C_5H_5)TiSiW_9V_3O_40]^4$ -, $[(C_5Me_5)RhSiW_9V_3O_40]^5$; (i) $[(C_5Me)_5RhP_2W_{15}Nb_3O_{62}]^7$ -, $[(C_6H_6)RuP_2W_{15}Nb_3O_{62}]^7$ -, $[(COD)IrP_2W_{15}Nb_3O_{62}]^8$ -.



igure 4

In solution, the anion forms several diastereomers with the metal tricarbonyl adducts $[(CO)_3M]$ ($M = Mn^I$, Re^I) and $[(CH_3)_5C_5]Rh^I$ to produce $[(OC)_3MNb_2W_4O_{19}]^{3-}$ and $\{[(CH_3)_5C_5Rh(\mathit{cis})-Nb_2W_4O_{19}\}^{2-}$ respectively (Figure 4e,f) [30]. On the contrary, if the norbornadiene Rh^I species $[(C_7H_8)Rh(NCCH_3)_2]^+$ is combined with $[Nb_2W_4O_{19}]^{4-}$, a structurally unique complex in which the $Nb_2W_4O_{19}$ unit uses both terminal and bridging oxygens is formed (Figure 4g) [31]. The iridium analogue was recently reported along with an investigation of its reactivity towards carbon monoxide and oxygen [32].

The partial substitution of metal atoms of the heteropoly Dawson and Keggin anions has been extensively investigated by Finke and co-workers [33]. Replacement with early transition metals such as vanadium or niobium provides a more nucleophilic and more reactive system, that may be capable of forming stable as well as catalytically active organometallic adducts. Since the discovery of the [SiW₉M₃O₄₀]⁷⁻ (M=V^V, NbV) series, polyoxoanion-supported CpTi³⁺, (C₅Me₅)Rh²⁺ (Figure 4h), and (C₆H₆)Ru²⁺ complexes of C_{3V} symmetry have been obtained [34]. These complexes have the advantage of forming K³-oxygen organometallic adducts that do not produce isomers as in the case of the Nb₂W₄O₁₉ unit. Preparation of polyoxoanion supported organometallics of [P₂W₁₅Nb₃O₆₂]⁸have proven fruitful since they serve as excellent precursors to active and long-lived hydrogenation catalysts. The organometallic adducts of CpTi, Cp*Rh, (C₆H₆)Ru, and (1,5-COD)Ir (Figure 4i) proved to be useful precursors for forming metal-supported polyoxoanions in which the organometallic species is rigidly attached to a K³-O site of the surface oxygens [34]. This placement is directly related to the proposed bonding situation in oxide-supported heterogeneous catalysts.

Of much contemporary interest is a novel class of complexes wherein the metal species or organometallic complex is incorporated into a vacant of interstitial lattice sites and is not supported by or incorporated into the polyoxoanion framework. Currently at 3M Corporate Research Laboratories, Siedle reports the function of the Keggin ions in establishing a lattice that may contain catalytically active species [35]. These methods have been effective in stabilizing coordinatively unsaturated organometallic cations that function along with the oxometalate as active catalysts [36]. The general synthetic strategy involves simple metathetic reactions of the Keggin ion salts with organometallic cations which contain a labile protective group that may be easily removed as indicated in Equation 1.

[L_nM'(PG)]₃XM₁₂O₄₀ — (L_nM')₃XM₁₂O₄₀ + PG (1) L_nM'(PG)⁺ represents a metal center, M' bonded to the protective group PG, and an accompanying array of ligands, L [37]. Consequently we sought to develop a preparation for complexes which accommodate reactive species such as the dinuclear acetonitrile cations, as well as an unsaturated rhodium (II) monomeric cation, that may function along with oxometalates as active catalysts. This thesis describes the synthesis, structural characterization and preliminary reactivity and thermal decomposition products of some novel compounds comprised of solvated metal cations or metal phosphine complexes and polyoxoanions.

Chapter 2 EXPERIMENTAL

A. Synthesis of Dinuclear Cationic Acetonitrile Complexes

- 1. General Procedures. All manipulations were performed with use of standard Schlenk line, syringe, or drybox techniques. All solvents were predried over 4Å molecular sieves. Diethyl ether was distilled from sodium/potassium benzophenone ketyl radical, whereas acetonitrile, methylene chloride, and methanol were distilled under a nitrogen atmosphere from CaH₂, P₂O₅, and Mg(OCH₃)₂, respectively. Starting materials were purchased from Aldrich Chemical Co., Alfa Chemical Co., or Strem Chemical Co.
- 2. Rh₂(O₂CCH₃)₄ · 2CH₃OH. Dirhodium tetraacetate, Rh₂(O₂CCH₃)₄, was prepared as described in the literature [38], by gentle reflux of RhCl₃ · 3H₂O (3.00 g, 5.95 mmol) and sodium acetate trihydrate (6.00 g, 45 mmol) in a mixture of glacial acetic acid (50 mL, 875 mmol) and absolute ethanol (50 mL). After three hours of reflux under argon atmosphere, the blue reaction mixture was cooled to room temperature and filtered to collect a blue-green solid. The solid was recrystallized by dissolving in methanol (1 L) and removing the insoluble residue by filtration. The resulting solution was concentrated to yield the blue-green crystalline methanol adduct Rh₂(O₂CCH₃)₄ · 2CH₃OH. More compound is

obtained by repeating the recrystallization and by concentrating the resulting methanol solutions.

3. $[Rh_2(NCCH_3)_{10}][BF_4]_4$. The solvated dirhodium complex, $[Rh_2(NCCH_3)_{10}][BF_4]_4$, was prepared by a procedure involving esterification of the methanol adduct of $Rh_2(O_2CCH_3)_4$ [39]. In a typical reaction $Rh_2(O_2CCH_3)_4 \cdot 2CH_3OH$ (0.200 g, 0.500 mmol) was dissolved in CH_3CN (10 mL) to give a characteristic purple solution. The alkylating reagent ($CH_3CH_2)_3OBF_4$ (10 mL, 1M solution in CH_2Cl_2) was added by syringe. After gently refluxing the reaction mixture for 7-10 days, large red crystals were deposited on the bottom of the reaction vessel and separated from the red-orange solution by decanting via cannula and subsequently washed with a 1:5 mixture of CH_3CN and CH_2Cl_2 . More crystalline solid may be precipitated from the cooled solution after addition of CH_2Cl_2 . The additional solids were separated from the solution and washed with a 1:3 mixture of CH_3CN and CH_2Cl_2 ; combined yield: 327 mg (68%). IR (cm⁻¹, Nujol): v(CN) = 2353 (s), 2325 (ms), 2310 (w). v(B-F) = 1054 (s, vbr).

Alternatively, the complex may be prepared by the acidification of $Rh_2(O_2CCH_3)_4 \cdot 2CH_3OH$ with an etherate solution of tetrafluoroboric acid in refluxing acetonitrile.

4. $[Mo_2(NCCH_3)_8][BF_4]_4$. The solvated dimolybdenum complex $[Mo_2(NCCH_3)_8][BF_4]_4$ may be prepared by esterification of the acetate ligands of tetrakis(aceto)dimolybdenum (II) in acetonitrile, as in the synthesis of $[Rh_2(NCCH_3)_{10}][BF_4]_4$, although a more efficient and higher yield synthesis involving tetrafluoroboric acid was reported

more recently [40]. Tetrakis(aceto)dimolybdenum (II), $Mo_2(O_2CCH_3)_4$, was synthesized by the standard methods [41]. A suspension of bright yellow, crystalline $Mo_2(O_2CCH_3)_4$ (1.20 g, 2.80 mmol) was charged with CH₃CN (20 mL) and CH₂Cl₂ (100 mL). To this vigorously stirring suspension HBF₄ · Et₂O was added (6 mL, 85% HBF₄ solution) to produce a red solution. After thirty minutes, the solution progressed through color changes from red to purple and finally to blue. The reaction mixture was gently refluxed for an additional forty minutes and then cooled in an icebath to yield an intensely colored blue solid which was separated from the solution by decantation via cannula. The solid was washed with four 10 mL portions of CH₂Cl₂ until the washings were clear, and then further washed with three portions of diethyl ether (10 mL) to remove any residual HBF₄; yield: 2.16 mg (89%). IR (cm⁻¹, KBr): ν (CN) = 2325 (ms), 2295 (s), 2550 (w). ν (B-F) = 1025 (vs, vbr), 520 (s, sh). UV-visible (CH₃CN): λ max = 597 nm.

5. [Re₂(NCCH₃)₈][BF₄]₄. All manipulations were performed in a Schlenk flask that was evacuated for at least twenty-four hours prior to the onset of the reaction. Tetrabutylammonium octachlorodirhenate (III), [(n-C₄H₉)₄N]₂Re₂Cl₈ (1.00 g, 0.865 mmol) was dissolved in CH₃CN (50 mL) to give a green-blue solution. To this stirring solution, HBF₄ · Et₂O (5ml, 85% HBF₄ solution) was slowly added to generate a deep purple solution. After complete addition of the acid, the purple solution was periodically reduced in pressure to remove gaseous HCl released from the reaction. Following the subsequent removal of the gaseous HCl, methylene chloride (200 mL) was slowly added to the reaction vessel. After gently refluxing the reaction mixture for five hours, an intensely colored blue solution and

solid was produced. The solid was filtered under a blanket of argon, washed with three 10 mL portions of CH₂Cl₂ and three 10 mL portions of diethyl ether, then dried *in vacuo* to yield 125 mg (14%) of product. The product was recrystallized by slow diffusion of CH₂Cl₂ into an acetonitrile solution of the complex. Blue crystals suitable for an X-ray diffraction study appeared after five days. IR (cm⁻¹, CsI): v(CN) = 2328(m), 2295(w). v(B-F) = 1025 (vs, vbr), 520 (s, sh). UV-visible (CH₃CN): $\lambda_{max} = 663$ nm ($\epsilon = 629$ M⁻¹cm⁻¹), (DMAA): $\lambda_{max} = 715$ nm (sh), 551 nm ($\epsilon = 740$ M⁻¹cm⁻¹). ¹H NMR (CD₃NO₂): $\delta = 3.38$ ppm (s), (CD₃CN): $\delta = 3.37$ ppm (s).

B. Synthesis of Polyoxometalate Complexes

1. $[(n-C_4H_9)N]_2[Mo_6O_{19}]$. The hexametalate anion, $[Mo_6O_{19}]^{2-}$, may be obtained by Fuchs and Jahr's method by precipitation from acidified aqueous molybdate solution and recrystallization of the resulting mixture of polymolybdates from acetone [42]. A more direct synthesis of the same salt in dimethylformamide (DMF) has been described by Fournier, et al. and is preferred [43]. In a typical reaction, a quantity of $Na_2MoO_4 \cdot 2H_2O$ (19.33 g, 80 mmol) was stirred in DMF (33.30 ml). Acetic anhydride (16 mL) was slowly added and then followed by acidification with concentrated HCl (11 mL, 132 mmol) to form a white solid and yellow solution. The reaction was accompanied by significant heating. The hot solution was filtered and the yellow filtrate precipitated with a solution of $(n-C_4H_9)_4NBr$ (5.87 g, 19.12 mmol) in DMF (33.30 mL). The resulting yellow crystalline solid was filtered and washed with ethanol (20 mL) and diethyl ether (20 mL). Recrystallization from acetone is suggested in order to remove any remaining insoluble

polymolybdates. IR (cm⁻¹, KBr): ν (Mo-O) = 958 (vs, br), 798 (s, vbr), 598 (ms, vbr), 426 (ms, br). UV-visible (DMAA): λ_{max} = 325 nm.

- 2. $[(n-C_4H_9)_4N]_4[Mo_8O_{26}]$. The octamolybdate (VI) complex, $[(n-C_4H_9)_4N]_4[Mo_8O_{26}]$ was prepared as described in the literature [44]. An amount of Na₂MoO₄·2H₂O (5.00 g, 20.7 mmol) was dissolved in water (12 mL) and subsequently acidified with 6N HCl (5.17 mL, 31.0 mmol). After stirring for two minutes, a solution of $(n-C_4H_9)_4NBr$ (3.34 g, 10.40 mmol) in water (10 mL) was added to precipitate a white solid. The white solid was filtered from the solution and washed with four 20 mL portions of water, ethanol (20 mL), acetone (20 mL), and diethyl ether (20 mL). Recrystallization from acetone at -10°C yielded clear, colorless, block-shaped crystals that were collected by filtration. IR(cm⁻¹, KBr): v(Mo-O) = 952 (m), 923 (s, br), 882 (w), 805 (vs, vbr), 736 (w), 561 (m), 501 (m).
- 3. [(n-C₄H₉)₄N]₂[W₆O₁₉]. The hexatungstate anion, [W₆O₁₉]²⁻, is prepared in a manner similar to that of [(n-C₄H₉)₄N]₂[Mo₆O₁₉] [44]. A mixture of Na₂WO₄ · 2H₂O (11.00 g, 33.30 mmol), acetic anhydride (13.33 mL), and DMF (10 mL) was stirred at 100°C for three hours to yield a white, creamy solution. A solution of acetic anhydride (6.67 mL) and concentrated HCl (6 mL, 72 mmol) in DMF (50 mL) was added with stirring, and the resulting mixture was filtered. The solid was washed with CH₃OH (20 mL), and the clear filtrate was allowed to cool to room temperature. A solution of (n-C₄H₉)₄NBr (5.00 g, 15.67 mmol) in CH₃OH (50 mL) was added to give a white precipitate. After stirring for five additional minutes, the product was collected by filtration and washed with

CH₃OH (10 mL), and diethyl ether (20 mL). Recrystallization from DMSO (3 mL, 80° C) gives clear colorless crystals after two days at room temperature, that were collected by filtration. IR (cm⁻¹, KBr): v(Mo-O) = 976 (vs, br), 815 (vs, vbr), 586 (s, br), 444 (s, vbr).

C. New Members of a Class of Oxymetalates

1. Synthesis of $[Rh_2(NCCH_3)_{10}][Mo_6O_{19}]_2$. A quantity of $[Rh_2(NCCH_3)_{10}][BF_4]_4$ (34.0 mg, 0.035 mmol) was dissolved in 5 mL of acetonitrile, then added to a vigorously stirring solution of $[(n-C_4H_9)_4N]_2[Mo_6O_{19}]$ (95.5 mg, 0.070 mmol). The product that precipitated from the reaction mixture was separated by decanting the clear supernatant via cannula, then washed with fresh acetonitrile and vacuum dried to yield 71.4 mg (86%) of microcrystalline orange solid: Anal. Calcd. for $Rh_2Mo_{12}O_{38}N_{10}C_{20}H_{30}$: N, 5.90; C, 10.11; H, 1.27. Found: N, 5.16; C, 10.30; H, 1.27. IR (cm^{-1}, KBr) : $\nu(CN) = 2336$ (ms), 2310 (ms) 2282 (w). $\nu(Mo-O) = 963$ (vs, br), 800 (vs, br), 597 (ms, br), 429(m, br). UV-visible (DMAA): $\lambda_{max} = 519$ nm ($\varepsilon = 451$ M⁻¹cm⁻¹).

2. Reaction of [Rh₂(NCCH₃)₁₀][BF₄]₄ with

[(n-C₄H₉)₄N]₄[Mo₈O₂₆]. A solution of [(n-C₄H₉)₄N]₄[Mo₈O₂₆] (82 mg, 0.056 mmol) in 10 mL of acetonitrile was added via syringe to a stirred solution of [Rh(NCCH₃)₁₀][BF₄]₄ (53.7 mg, 0.056 mmol) in 10 mL of acetonitrile to form a very fine, floccuent, pale orange solid. After stirring for 5 min., the solid was isolated from the clear supernatant, washed with fresh acetonitrile and diethyl ether, and dried under a stream of argon for 2 hrs. to yield 71.3 mg (71%) of product. IR (cm⁻¹, KBr):

v(CN) = 2336 (ms), 2311 (ms), 2247 (w). v(Mo-O) = 948 (vs), 913 (vs), 845 (ms), 806 (m), 714 (s, br), 556 (w, sh), 522 (w).

- 3. Synthesis of $[Rh_2(NCCH_3)_{10}][W_6O_{19}]_2$. A flask was charged with a sample of $[Rh_2(NCCH_3)_{10}][BF_4]_4$ (24.6 mg, 0.025 mmol, $[(n-C_4H_9)_4N]_2[W_6O_{19}]$ (94.5 mg, 0.050 mmol), and CH₃CN (10 mL). After 5 min. of vigorous stirring, the orange product was separated from the clear supernatant, washed with fresh acetonitrile, then vacuum dried to yield 75.5 mg (88%) microcrystalline orange solid. IR (cm⁻¹, KBr): v(CN) = 2337 (s), 2310 (s), 2283 (w), 2249 (vw), 2242 (vw). v(W-O) = 982 (vs,br), 814 (vs, vbr), 585 (ms), 444 (ms, br).
- 4. Synthesis of [Mo₂(NCCH₃)₈][Mo₆O₁₉]₂. A solution of [Mo₂(NCCH₃)₁₀][BF₄]₄ (24.6 mg, 0.053 mmol) in 5mL of acetonitrile was added via syringe to a stirred solution of $[(n-C_4H_9)_4N]_2[Mo_6O_{19}]$ (144.5 mg, 0.106 mmol) in 5mL of acetonitrile. The resulting sky blue precipitate was washed with fresh acetonitrile, and dried *in vacuo* to yield 115 mg (92%) of a sky blue-green product. IR (cm⁻¹, KBr): v(CN) = 2315 (m), 2284 (ms), 2255 (w). v(Mo-O) = 972 (vs, br), 800 (vs, vbr), 600 (ms, vbr), 416 (ms, br). UV-visible (DMAA): $\lambda_{max} = 718$ nm.

5. Reaction of [Mo₂(NCCH₃)₈][BF₄]₄ with

[(n-C₄H₉)₄N]₄[Mo₈O₂₆]. A 10 mL acetonitrile solution of [(n-C₄H₉)₄N]₄[Mo₈O₂₆] (67.5 mg, 0.046 mmol) was slowly added to a stirred solution of [Mo₂(NCCH₃)₈][BF₄]₄ (40.0 mg, 0.046 mmol) in 10 mL of acetonitrile to form a black solid. After stirring for 10 min., the solid was filtered and washed with copious amounts of acetonitrile and 10 mL of

diethyl ether, and dried in vacuo to yield 57.5 mg (74%) of product. IR (cm⁻¹, KBr): v(CN) = 2321 (w), 2315 (vw), 2257 (w). v(Mo-O) = 980 (s), 717 (vs, br), 486 (m).

- 6. Synthesis of $[Mo_2(NCCH_3)_8][W_6O_{19}]_2$. To a flask containing $[Mo_2(NCCH_3)_{10}][BF_4]_4$ (44.0 mg, 0.046 mmol) and $[(n-C_4H_9)_4N]_2[W_6O_{19}]$ (174 mg, 0.092 mmol) was added 10 mL of acetonitrile. The reaction mixture was vigorously stirred for 5 min. and then filtered to isolate a bright sky blue solid. The solid was washed with CH₃CN, and dried under a dynamic vacuum to yield 140 mg (89%) of product. IR (cm^{-1}, KBr) : v(CN) = 2316 (m), 2284 (s), 2255 (w). v(W-O) = 991 (vs, br), 810 (vs, vbr), 586 (s), 443 (s, br).
- 7. Synthesis of [Re₂(NCCH₃)₈][Mo₆O₁₉]₂. A quantity of [Re₂(NCCH₃)₈][BF₄]₄ (33.5 mg, 0.032 mmol) dissolved in CH₃CN (5 mL) was added dropwise to a vigorously stirring acetonitrile (5 mL) solution of $[(n-C_4H_9)_4N]_2[Mo_6O_{19}]$ (55.0 mg, 0.022 mmol) to form a blue-green microcrystalline solid. The solid was washed with two 10 mL portions of acetonitrile and dried *in vacuo*, whereby the solid turned blue-gray to yield 55 mg (69%) of material. Anal. Calcd. for Re₂Mo₁₂O₃₈N_{8.5}C₁₇H_{25.5}: N, 4.80; C, 8.23; H, 1.04. Found: N, 478; C, 8.39; H, 1.20. IR (cm⁻¹, KBr): ν (CN) = 2350 (m), 2285 (w), 2250 (w). ν (Mo-O) = 956 (vs, br), 793 (vs, vbr), 598 (m, br), 492 (m, br).
- 8. Synthesis of $[Rh(\eta^3-TMPP)_2][Mo_6O_{19}]$. The complex $[Rh_2(\eta^3-TMPP)_2][BF_4]_2$ (TMPP = Tris(2,4,6-trimethoxyphenyl)phosphine) was prepared as reported in the literature [45]. An equimolar amount of

[Rh₂(η^3 -TMPP)₂][BF₄]₂ (170 mg, 0.083 mmol) and [(n-C₄H₉)₄N]₂[Mo₆O₁₉] (113 mg, 0.083 mmol) were each separately dissolved in acetonitrile. In a long 0.50 cm diameter pyrex tube, the rhodium solution was carefully layered over the molybdate solution. After one week, diffusion of the two layers was sufficient to afford long purple needles of X-ray quality. Yield: 96.7 mg (86%). Anal. Calc. for RhMo₆P₂O₃₇C₅₄H₆₆: C, 31.68; H, 2.67. Found: C, 31.97; H, 3.14. IR (cm⁻¹, KBr): ν (TMPP) = 1942 (ms), 1933 (ms), 1918 (m). ν (Mo-O) = 952 (vs, br), 795 (vs, vbr), 592 (m, br), 432 (m, br).

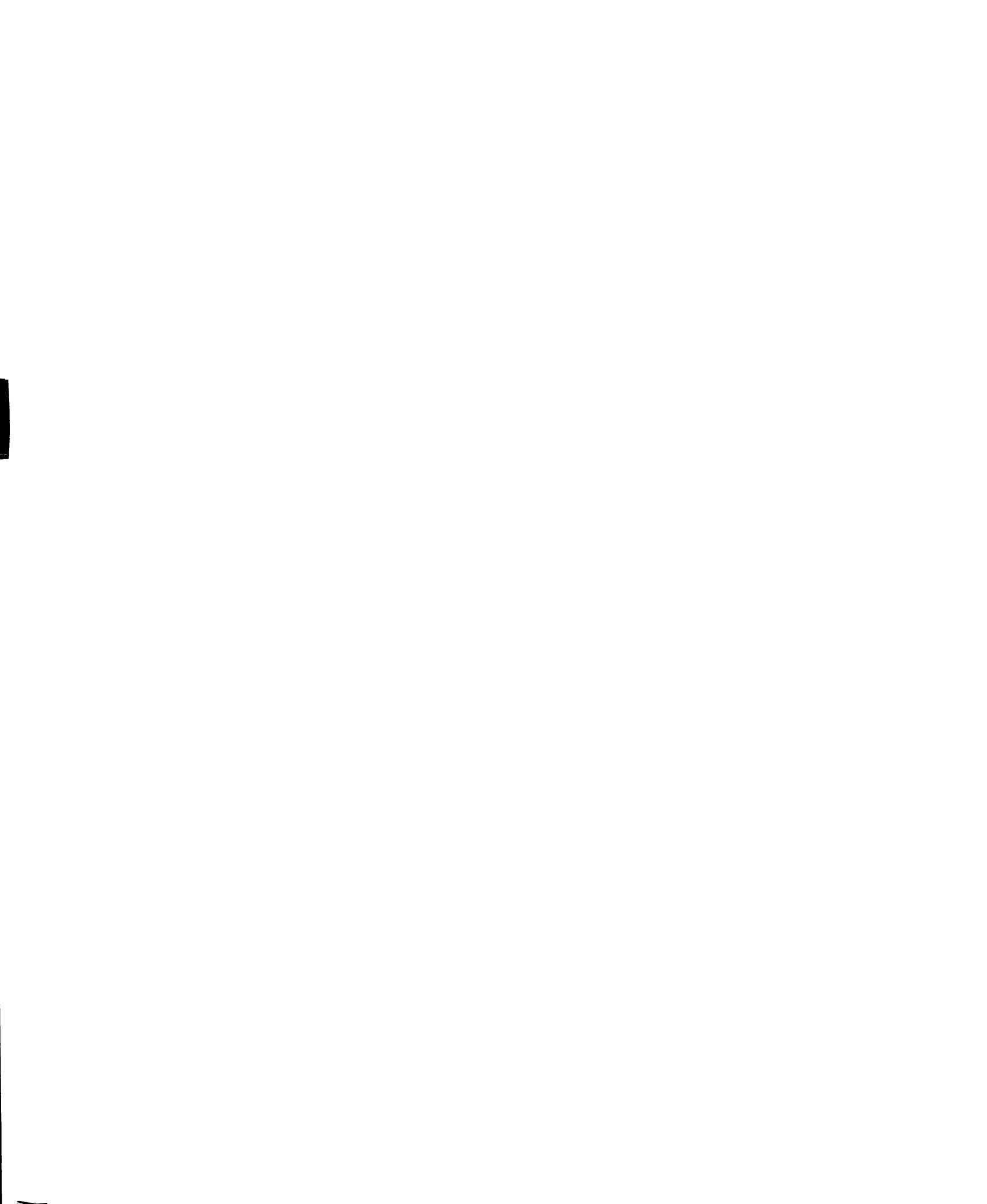
- 9. Synthesis of $[Rh(\eta^3-TMPP)_2][W_6O_{19}]$. The complex was prepared according to the method described previously for $[Rh(\eta^3-TMPP)_2][Mo_6O_{19}]$. IR (cm⁻¹, KBr): $\nu(TMPP) = 1599$ (vs), 1572 (s), 1560 (m). $\nu(W-O) = 951$ (vs, br), 792 (vs, vbr), 587 (m, br).
- 10. Reaction of [Rh(η³-TMPP)₂][Mo₆O₁₉] with CO. A small quantity of finely divided starting complex (13 mg) in a polyethylene vial was placed in a Parr reactor. After several fillings and subsequent purging with CO, the reactor was pressurized to approximately 50 psi. After 2.5 hrs., the vessel was depressurized and a drop of Nujol was added to the sample and quickly transferred to CsI plates for infrared spectral measurements.

D. Physical Techniques

1. Infrared Spectroscopy. Infrared spectra were recorded on a Perkin-Elmer 599 or Nicolet FT IR/42 equipped with IBM PC/IR system software; in the latter case, an average of 32 scans were used for data

collection. IR specimens were prepared as KBr or CsI disks containing ~5 weight percent of dried samples or as Nujol mulls with CsI plates.

- 2. Electronic Absorption Spectroscopy. Electronic absorption spectra were measured on a Hitachi U-2000 Spectrophotometer with matching 1.00-cm pathlength quartz cell. All spectra were recorded in N,N-dimethylacetamide (DMAA) or acetonitrile (CH₃CN), from which a spectrum of the neat solvent in a matched cell was subtracted.
- 3. Powder X-ray Diffraction. The powder diffraction patterns were recorded on a Rotoflex system by Rigaku. The Cu- K_{α} and Cu- K_{β} lines were obtained from a rotating Cu anode (45 kV, 100 mA) and collimated towards the sample chamber using a 1/6° scattering slit and a 1/6° receiving slit. The K_{β} line of the diffracted X-ray beam was removed by a curved graphite single crystal monochromator (0.45° receiving slit and 0.45 mm monochromator receiving slit) which was set for detection of the deflected X-ray diffraction line. The samples were mounted by pressing dried powder on a piece of double-sided tape attached to a 1" x 2" glass slide. The resulting data were recorded and processed using the manufacturer provided software DMAXB on a microVAX computing system.
- 4. Electrochemistry. Electrochemical measurements were performed by using an EG&G Princeton Applied Research Model 362 scanning potentiostat in conjunction with a BAS Model RXY recorder. Cyclic voltammetry experiments were carried out at $22\pm2^{\circ}$ C in the appropriate solvent containing 0.05M [$(n-C_4H_9)_4N$][BF₄], or



n-tetrabutylammonium hexafluophosphate (TBAH) as the supporting electrolyte. $E_{1/2}$ values, determined as $(E_{p,a}+E_{p,c})/2$, were referenced to the Ag/AgCl electrode and are uncorrected for junction potentials. The $(C_5H_5)Fe/(C_5H_5)Fe^+$ couple occurs at +0.46 V under the same conditions on the equipment.

- 5. Thermogravimetric Analysis. Thermal gravimetric experiments were performed on a Cahn TGA 121. Samples were placed inside a quartz bucket and heated at 1°C/min under a dinitrogen atomosphere. The temperature method included isotherms at 30°C (20 min), 250°C (60 min), 300°C (60 min), 320°C (30 min), 350°C (30 min).
- 6. Nuclear Magnetic Resonance. ¹H NMR spectra were measured on a Varian 300 MHz spectrometer. Chemical shifts were referenced relative to the residual proton impurities of either CD₃CN (1.93 ppm with respect to TMS) or CD₃NO₂ (4.33 ppm with respect to TMS).
- 7. Electron Paramagnetic Resonance. X-band EPR spectra were measured by using a Bruker ER200D Spectrometer equipped with an Oxford ESR-9 liquid helium cryostat. To obtain an accurate measure of g values and line widths, a Bruker ER035M NMR Gaussmeter and a Hewlett-Packard 5245L frequency counter (with a 3-12 GHz adaptor) were used to measure magnetic field strength and the microwave frequency, respectively. Variation of temperature was achieved by controlling the flow rate of a gas generated from liquid nitrogen.

- 8. Magnetic Susceptibility Measurements. Variable temperature magnetic susceptibility measurements were performed on a Quantum Design MPMS Susceptometer in the Physics and Astronomy Department of Michigan State University. Data points were collected over a temperature range from 5 to 280 K at 10 or 20 degree intervals in a field of 1000 Gauss.
- 9. Elemental Analyses. Elemental Analyses were performed by Desert Analysis, Tucson, AZ.
- 10. Single X-ray Crystallography. Geometric and intensity data for $[Rh_2(NCCH_3)]_{10}[Mo_6O_{19}]_2$ were collected on a Nicolet P3/F upgraded to a Siemens P3/V diffractometer with graphite monochromated Cu K_{α} (λ_{α} = 1.541780 Å) radiation; data for $[Rh(\eta^3\text{-TMPP})_2][W_6O_{19}]$ was collected with Mo K_{α} (λ_{α} = 0.71073 Å) radiation. Crystallographic data for the complexes $[Rh_2(NCCH_3)_{10}][BF_4]_4$, $[Re_2(NCCH_3)_8][Mo_6O_{19}]_2$, and $[Rh(\eta^3\text{-TMPP})_2][Mo_6O_{19}]$ were collected on a Rigaku AFC6-S diffractometer with monochromated Mo K_{α} radiation (λ_{α} = 0.71069 Å). Calculations were performed by using the Texsan crystallographic software package of Molecular Structure Corporation [46].

Chapter 3 RESULTS AND DISCUSSION

- A. Synthetic Methodology
- 1. Synthesis of Solvated Systems.
 - i. $[Re_2(NCCH_3)_8][Mo_6O_{19}]_2$

Explorations towards extending the instances of dinuclear solvated cations have been successful in this laboratory. The use of a strong acid such as tetrafluoroboric acid with dinuclear homoleptic chlorides, as $[Re_2Cl_8]^{2-}$, provides a previously unknown route to dinuclear acetonitrile cations such as $[Re_2(NCCH_3)_8][BF_4]_4$. The reaction is successfully carried out in an acetonitrile:dichloromethane solvent ratio of 1:4 to first yield a deep purple solution at room temperature, which converts to the intensely colored blue product after gently refluxing for ~5 hours. This product may also be recrystallized from the same solvent ratio to produce a sample of pure hexagonal shaped crystals suitable for single X-ray crystallography. Several attempts to solve the crystal structure of this product have been undertaken, but unfortunately the cubic lattice has not yielded a unique solution that refines well. In this case, the molecule packs in a body-centered cubic crystal symmetry with all dimensions equal to 29.22(1) Å, and the volume equal to 24,947(22) Å³.

The formulation of the new complex as a Re^{II,II} unit is particularly interesting. Each rhenium atom has a d⁵ configuration, which denotes the

presence of a triple bond. From this, one must conclude that the molecule has undergone a spontaneous reduction during the reaction. It is possible that the formation of other metal containing species are produced in the reaction, and this may account for the low yields that have been obtained thus far.

ii. New Oxymetalate Complexes

The general synthetic strategy employed in the synthesis of the new polyoxometalate containing complexes involves simple metathetic reactions performed in acetonitrile. The important advantage of this new class of polyoxometalates is that they contain bimetallic cationic moieties located in interstitial lattice sites that are not covalently bonded to the oxygen atoms of the surrounding metal oxide clusters. These moieties are only protected by weakly supporting acetonitrile ligands, and this is of material importance for these complexes to behave as potential bifunctional catalysts.

2. Synthesis of Desolvated Systems.

Desolvation reactions of the $[Mo_6O_{19}]^{2-}$ complexes were followed by thermogravimetric analysis under a nitrogen atmosphere. The temperature at which the complete release of CH₃CN occurs at a rate of 1 °C/min is ~350 °C. If the rate is increased the final temperature needed for complete desolvation is lower than 350 °C. These data revealed that when the complexes are heated, the loss of the coordinated acetonitrile ligands is essentially quantitative to produce new amorphous materials; an exception is the desolvation of $[Mo_2(NCCH_3)_8][Mo_6O_{19}]_2$, a process that leads to a

highly crystalline deep blue material. These new materials are all insoluble in the polar solvents that dissolve the parent solvated precursors.

B. Spectroscopic and Magnetic Measurements

1. Solvated Systems.

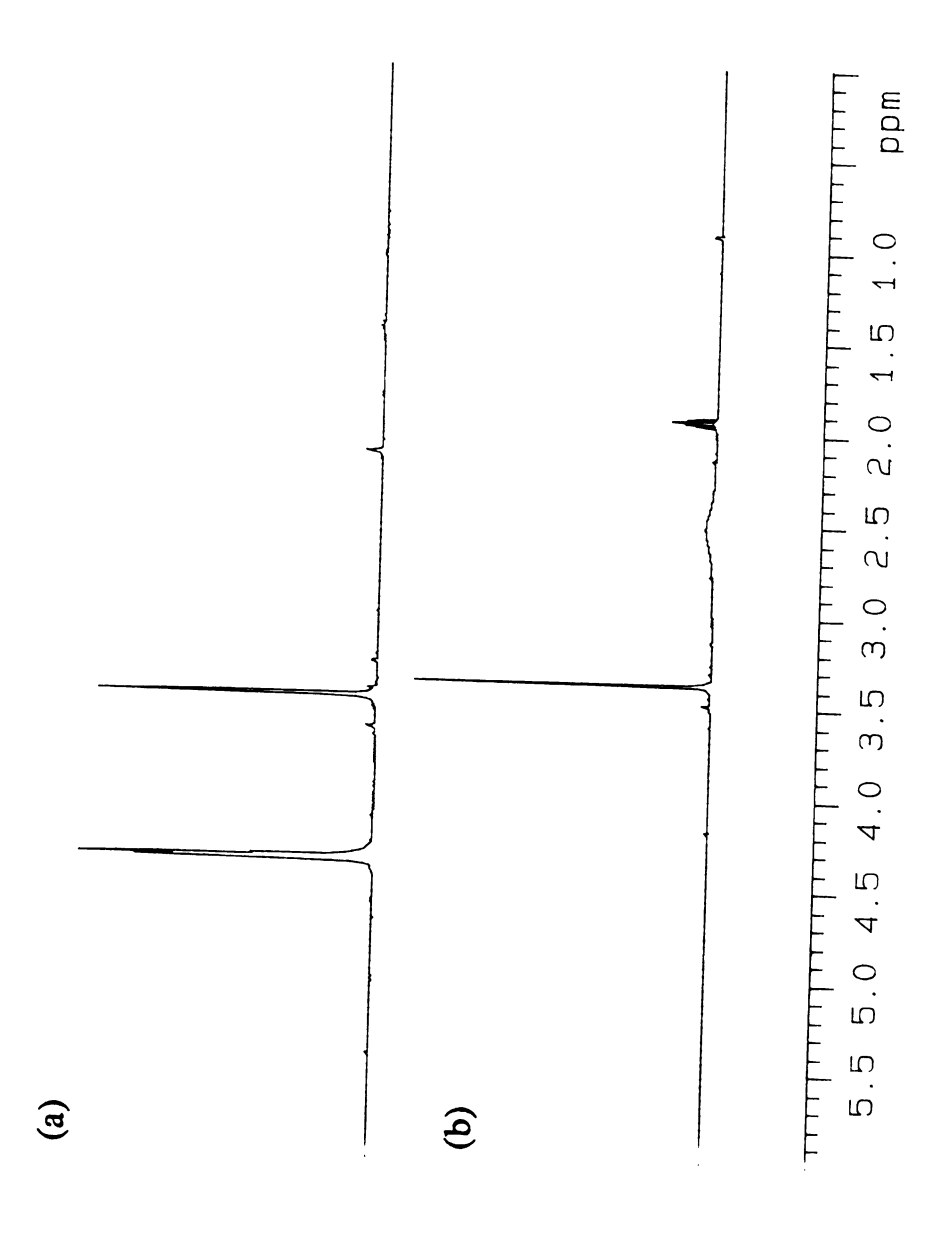
i. $[Re_2(NCCH_3)_8][BF_4]_4$

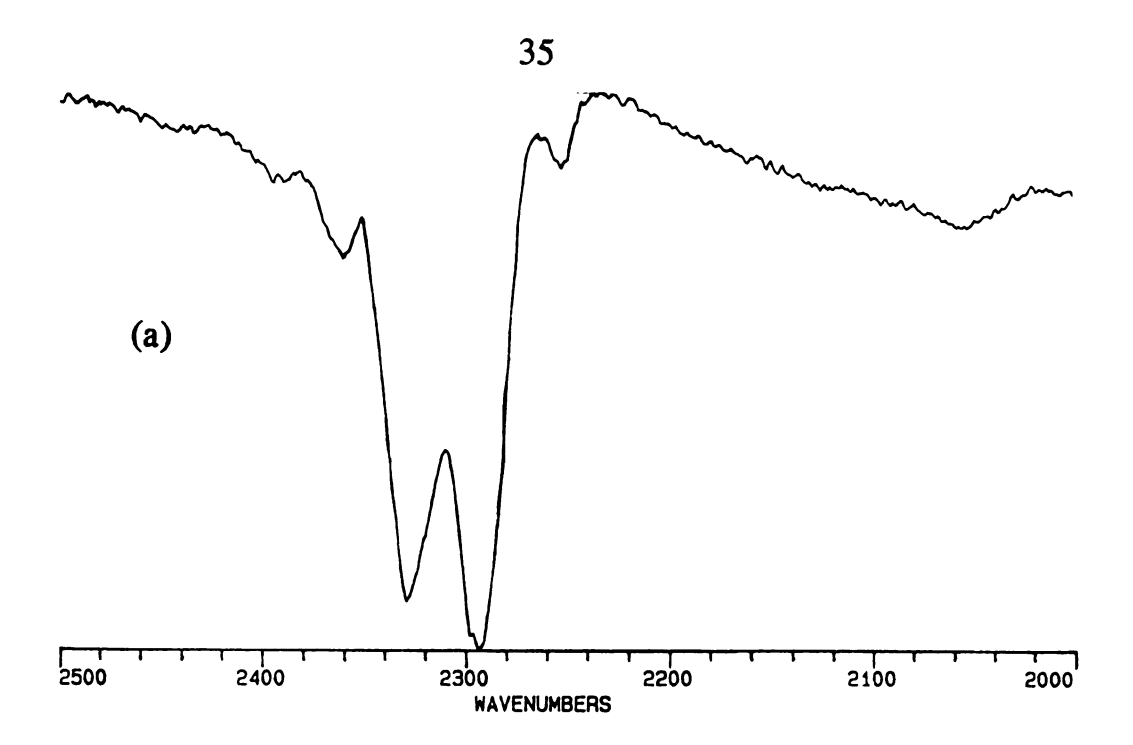
The room temperature 1H NMR spectrum of $[Re_2(NCCH_3)_8][BF_4]_4$ in CD_3NO_2 reveals the presence of equatorial acetonitrile ligands as a single resonance at $\delta = +3.39$ ppm. In addition, a second minor resonance occurs at $\delta = +2.00$ ppm, assigned to free acetonitrile (Figure 5a). Likewise the 1H NMR spectrum in CD_3CN displays a single resonance at $\delta = +3.37$ ppm and $\delta = +1.95$ ppm (Figure 5b). These spectra demonstrate that the equatorial acetonitrile ligands do not undergo facile exchange, even in the CD_3CN solvent. This is in direct contrast to that reported for the analogous dirhodium and dimolybdenum acetonitrile complexes; these were shown to undergo rapid ligand exchange with the CD_3CN solvent.

The infrared spectra in Figure 6a depict the general features in the 2500 cm⁻¹-2000 cm⁻¹ region which are used to verify the presence of the coordinated acetonitrile ligands. The bands at 2328 cm⁻¹ and 2295 cm⁻¹ are shifted to higher energy compared to free acetonitrile. Figure 6b reveals the full spectrum, which is basically featureless except for the strong bands at 1025 cm⁻¹ and 520 cm⁻¹, which correspond to the v(B-F) of the [BF₄]⁻ counterion.

The electrochemical properties have been investigated and determined by cyclic voltammetry. Studies in $[(n-C_4H_9)_4N][BF_4]_4-CH_3CN$ (0.05 M) revealed a quasi-reversible reduction at $E_{1/2}$ =

Figure 5. The ¹H NMR spectrum of [Re₂(NCCH₃)₈][BF₄]₄ in (a) CD₃NO₂ solvent and (b) CD₃CN solvent.





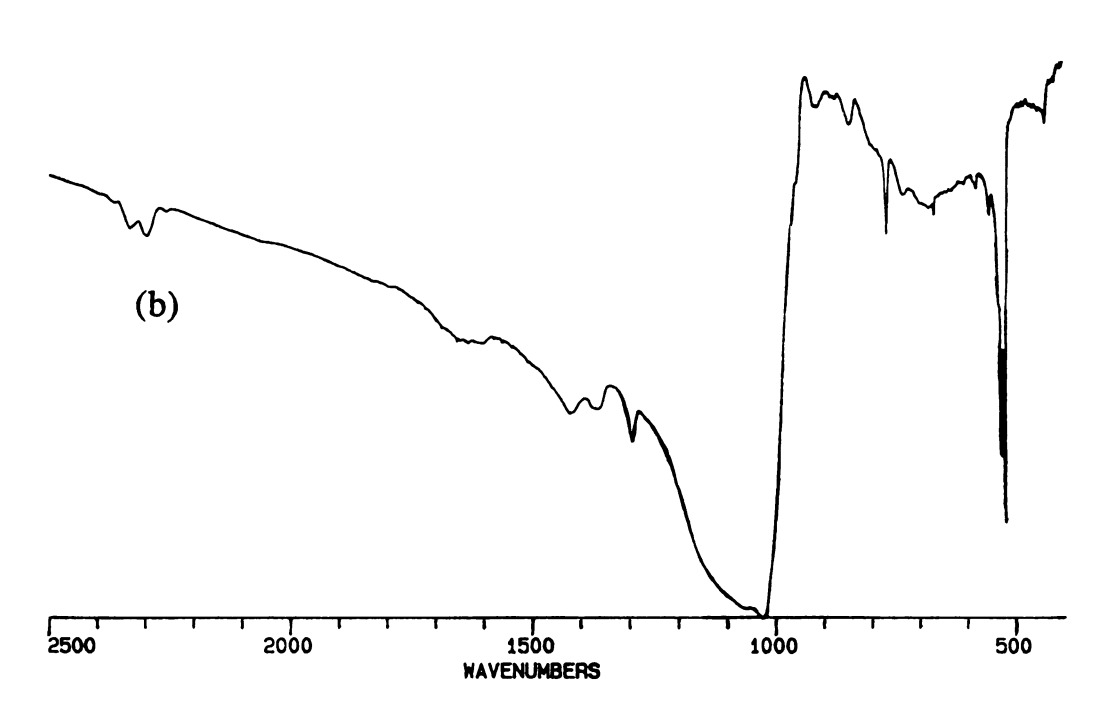
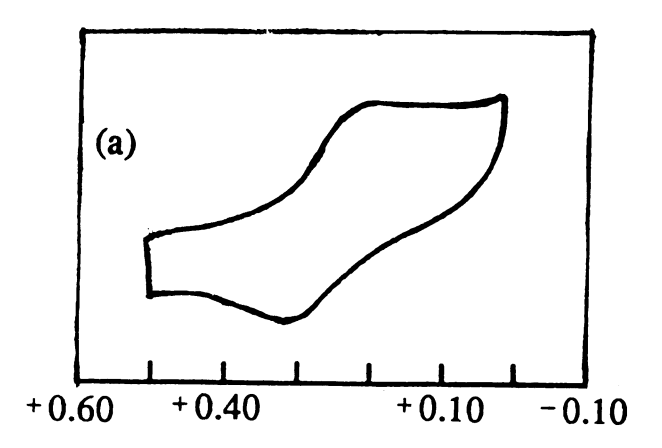


Figure 6. Infrared spectrum of [Re₂(NCCH₃)₈][BF₄]₄: (a) 2500 cm⁻¹ to 2000 cm⁻¹ region; (b) 2500 cm⁻¹ to 400 cm⁻¹ region.

Figure 7. Cyclic voltammetry of $[Re_2(NCCH_3)_8][BF_4]_4$ in 0.05 M TBABF₄-CH₃CN at 200 mV/sec: (a) a voltammogram showing only the accessible reduction process at $E_{1/2} = +$ 0.24 V displaying a peak-to-peak separation of 110 mV; (b) a voltammogram consisting of three separate sweeps that show the appearance of several irreversible reductions at potential greater than 0 V vs Ag/AgCl.



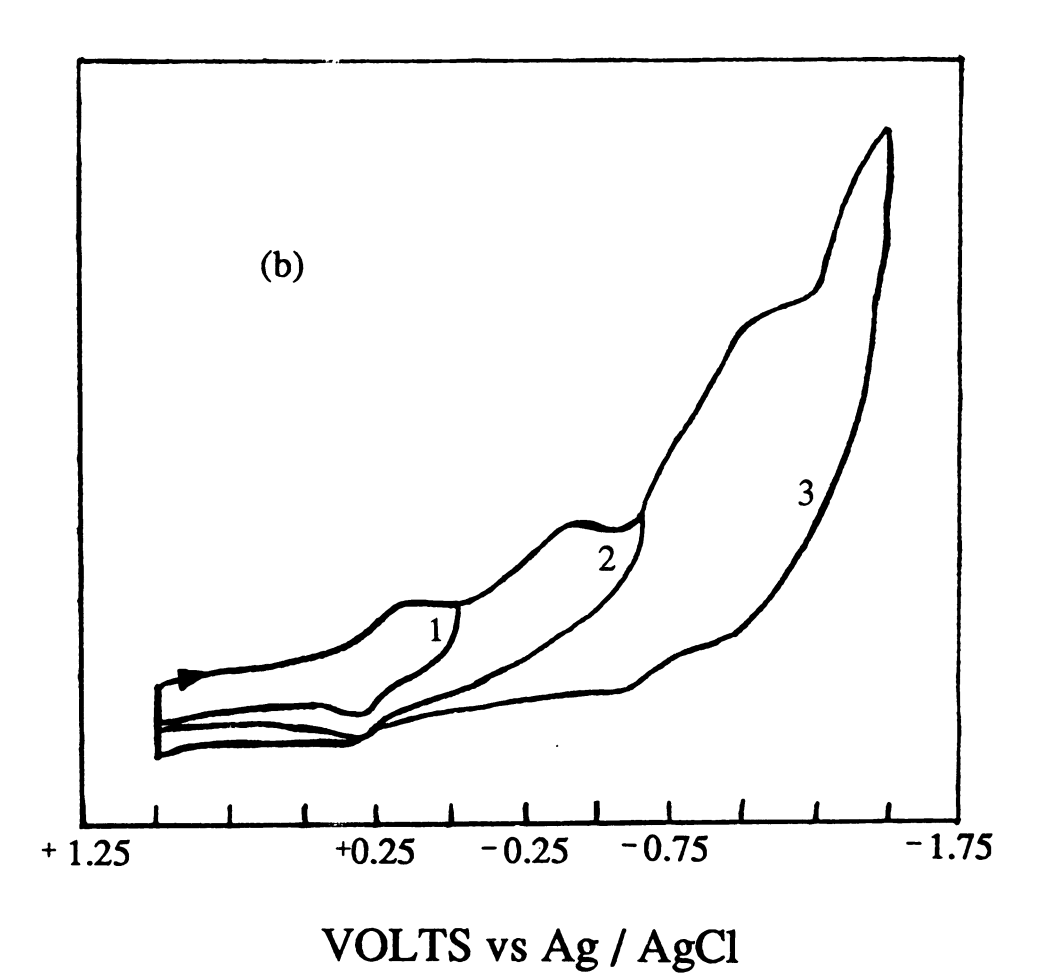
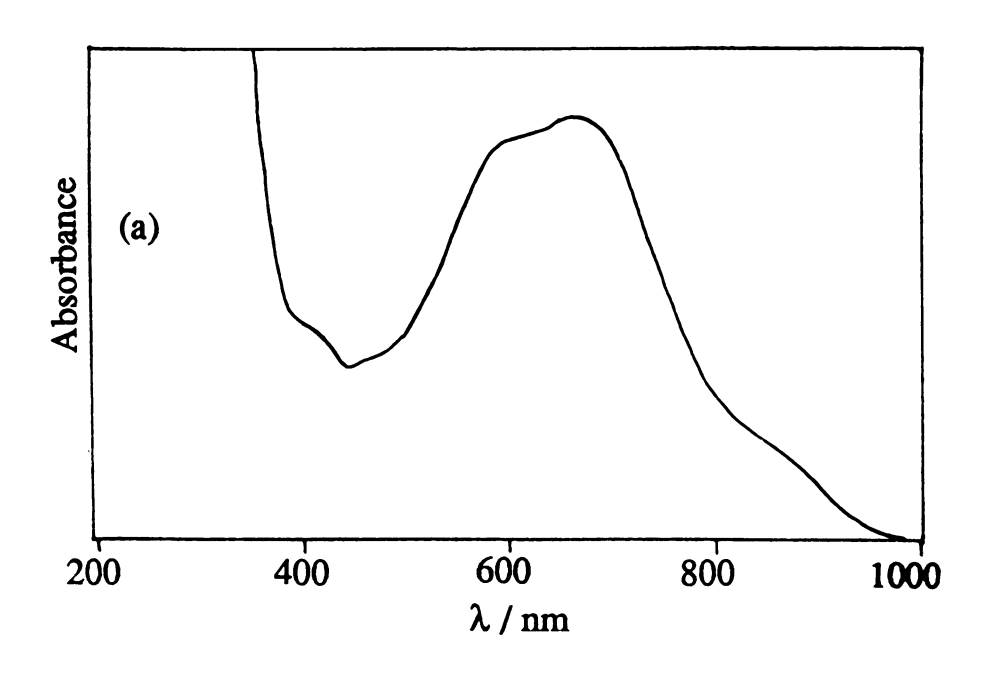


Figure 7



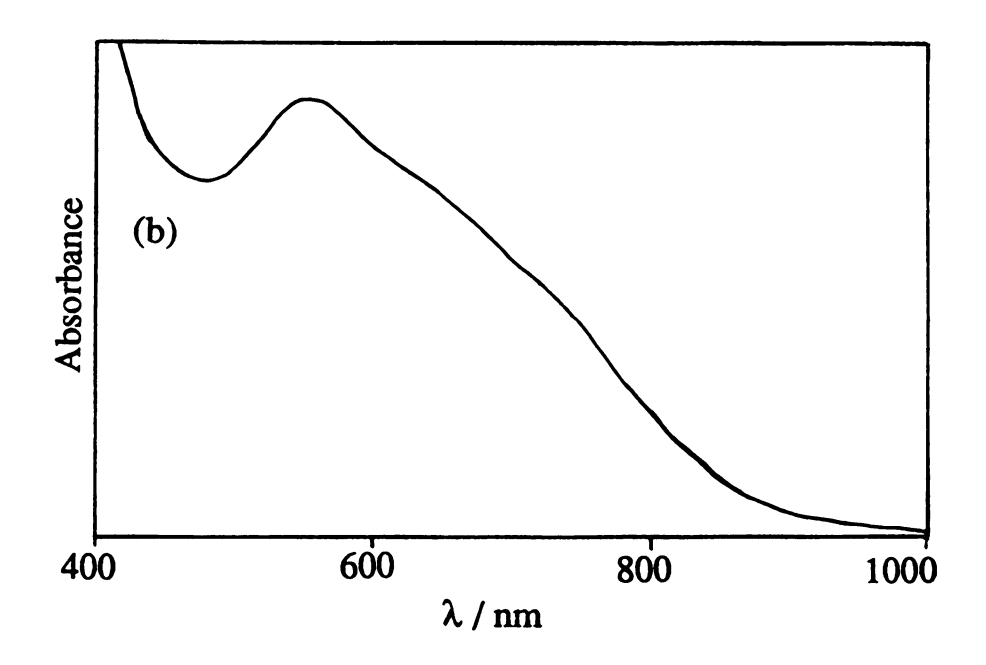


Figure 8. Electronic absorption spectrum of [Re₂(NCCH₃)₈][BF₄]₄: (a) in dry, deoxygenated CH₃CN and (b) as a DMAA solution.

+0.24 V with a peak-to-peak separation of 110 mV at a scan speed of 200 mV/sec (Figure 7a); the $(C_5H_5)Fe/(C_5H_5)Fe^+$ couple occurs at +0.46 V under the same conditions on the equipment. In addition, the spectrum displayed two irreversible reductions at $E_{p,c}$ = -0.20 V and $E_{p,c}$ = -0.76 V (Figure 7b).

The electronic spectral properties in CH₃CN solvent exhibit a very broad low energy transition at λ_{max} (nm) = 663 (ϵ = 629 M⁻¹cm⁻¹) in addition to a strong feature of almost equal intensity at 593 (591) and very weak shoulders at 458 and 866; two additional bands are located at 244 (2.7 × 10⁴) and 203 (5.1 × 10⁴) (Figure 8a). A spectrum of the complex as a DMAA solution (Figure 8b) reveals the presence of a very broad band in the visible region at 551 nm with a low-energy shoulder at ~715 nm.

ii. New Oxymetalate Complexes

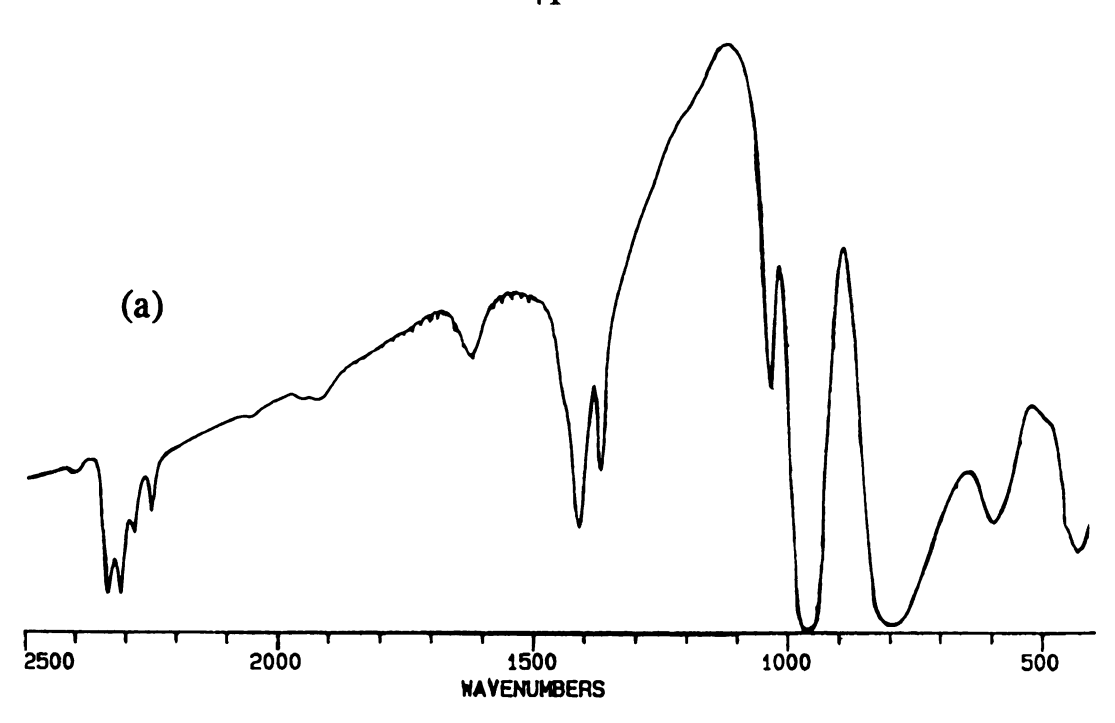
Since polyoxometalates are of great interest for various applications, various properties of the new salts obtained in this work have been studied. Researchers in the past have used structural properties in order to better understand observed phenomena. The influence of counterions on the vibrational spectra of these complex anions is suitable for this purpose.

As mentioned earlier, some important assignments of the vibrational spectra of these complexes include the 6 terminal oxygens (O_t) , 12 bridging oxygens (O_b) , and 1 central oxygen (O_c) (Figure 3). Since the *n*-tetrabutylammonium counterion exhibits a very low polarizing power, researchers have chosen this polyoxometalate salt as an idealized model for comparison. The infrared spectra of the $[Mo_6O_{19}]^{2-}$, $[Mo_8O_{26}]^{4-}$, and $[W_6O_{19}]^{2-}$ complexes with the dinuclear acetonitrile cations are depicted in

Figures 9-12, along with the n-tetrabutylammonium starting materials for comparison (Figures 13-14). A salient feature of these spectra is a shift of the observed v(Mo-O) stretching frequencies, which occurs as a result of the presence of different counterions. This type of effect was referred to earlier as a consequence of the anion-anion interactions; the higher the shift, the shorter the interanionic O-O distances, and therefore the stronger the interaction. A comparison of the cations studied throughout this report with the n-tetrabutylammonium cation, summarized in Table 2, shows that this is clearly the case.

The electronic spectra of the $[Mo_6O_{19}]^{2-}$ complexes as DMAA solutions contain very broad bands in the visible region in addition to a band associated with the $[Mo_6O_{19}]^{2-}$ anion found in the UV region. These broad bands are slightly more intense than the corresponding bands associated with the analogous $[BF_4]^-$ salts, and are centered at lower energies. The spectrum of $[Re_2(NCCH_3)_8][Mo_6O_{19}]_2^{2-}$ (Figure 15) is qualitatively similar to that of $[Re_2(NCCH_3)_8][BF_4]_4$. The lowest energy transitions occur at $\lambda_{max} = 715$ nm and 552 nm; one additional absorption located at 324 nm is assigned as the LMCT band of the $[Mo_6O_{19}]^{2-}$ anion.

Figure 16 depicts the electronic absorption spectra of $[Rh_2(NCCH_3)_{10}][Mo_6O_{19}]_2$ and $[Mo_2(NCCH_3)_8][Mo_6O_{19}]_2$. $[Rh_2(NCCH_3)_{10}][Mo_6O_{19}]_2$ exhibits a broad band at a λ_{max} value of 519 nm and a higher energy band at 318 nm. The complex $[Mo_2(NCCH_3)_8][Mo_6O_{19}]_2$ undergoes a rapid decomposition upon dissolution. In DMAA, the complex forms a green solution which has a very broad absorption in the visible region with a maximum at 718 nm. An additional band occurring in the UV region at 324 nm suggests that the $[Mo_6O_{19}]^{2-}$ anion remains intact. These data suggests that the DMAA



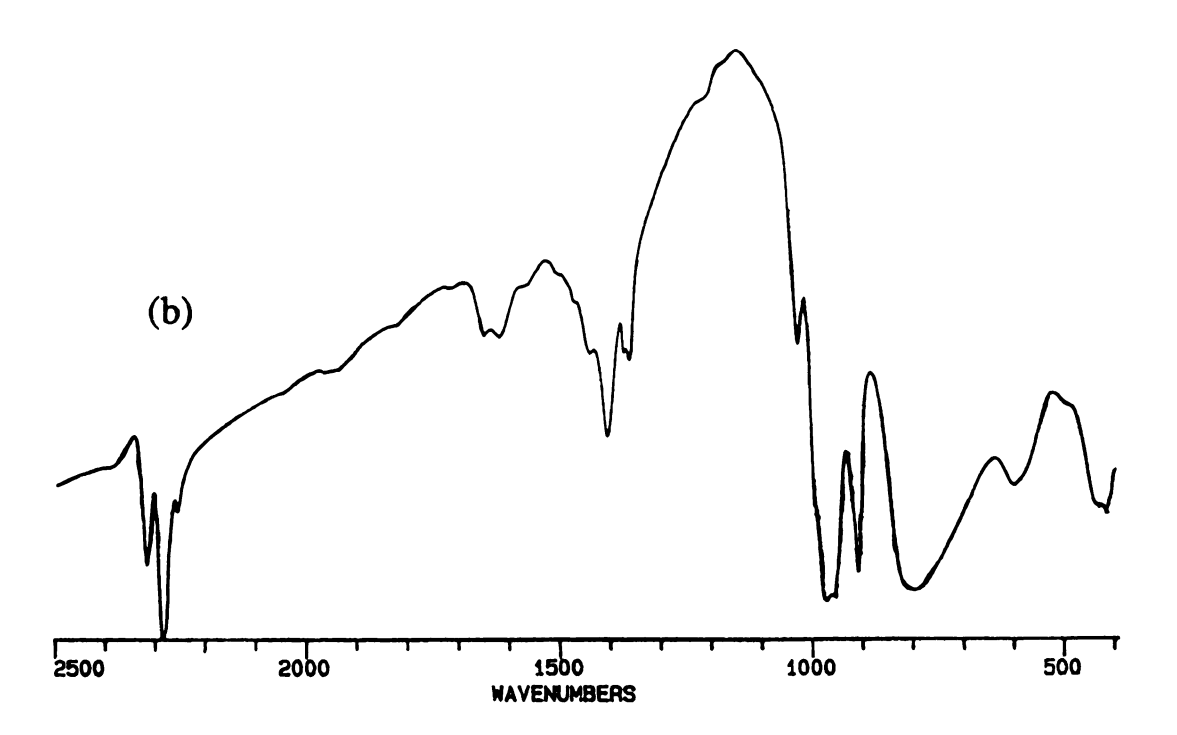


Figure 9. Infrared spectra of (a) $[Rh_2(NCCH_3)_{10}][Mo_6O_{19}]_2$ and (b) $[Mo_2(NCCH_3)_8][Mo_6O_{19}]_2$.

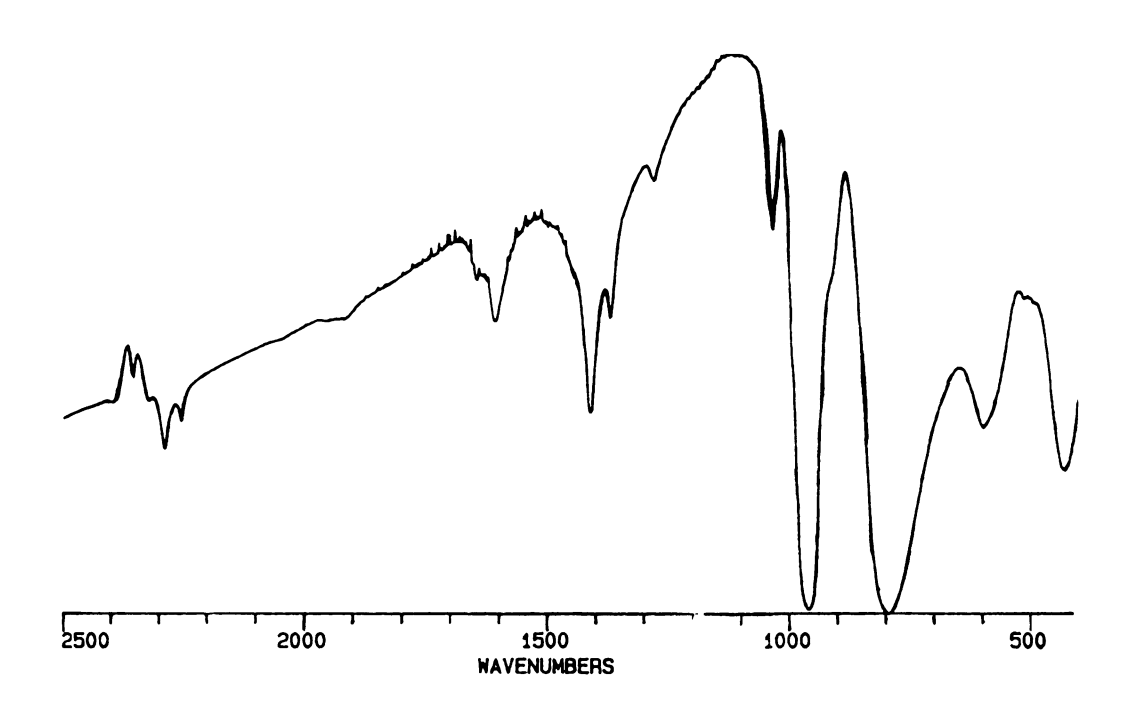
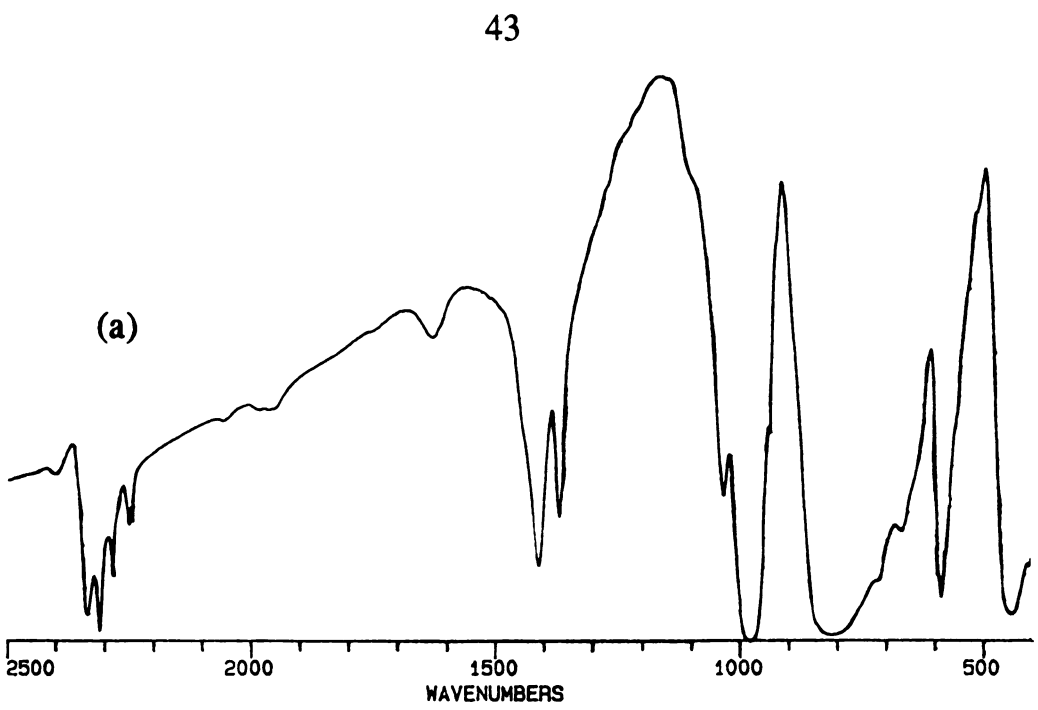


Figure 10. Infrared spectrum of $[Re_2(NCCH_3)_8][Mo_6O_{19}]_2$.





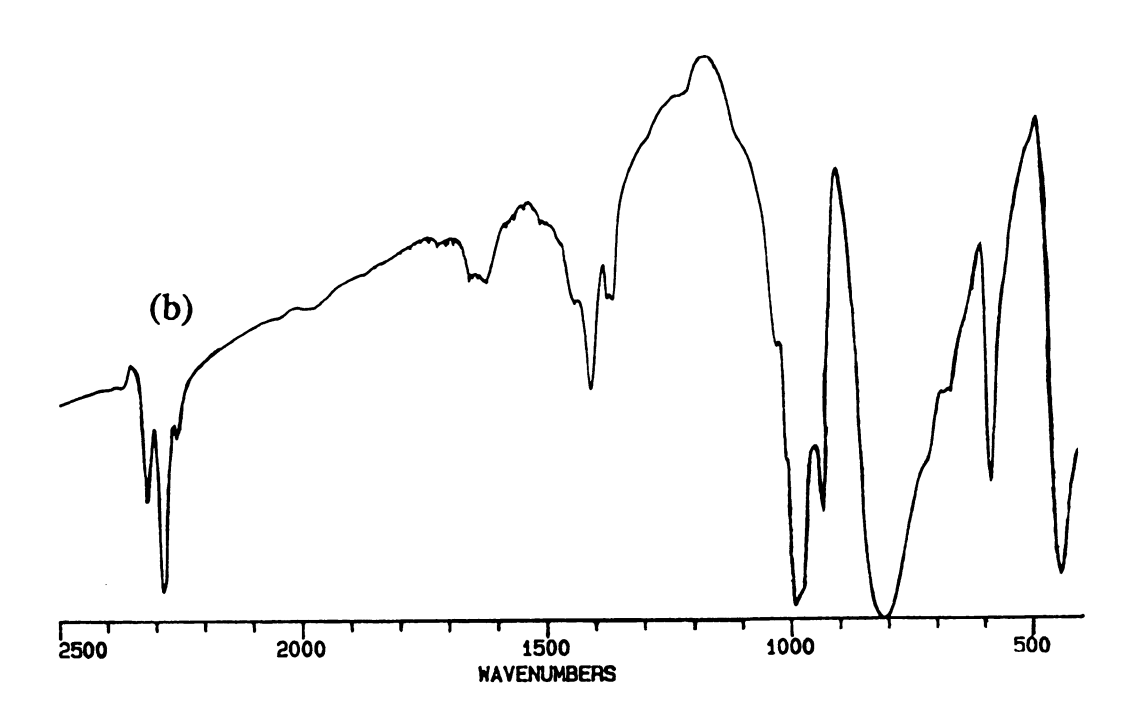
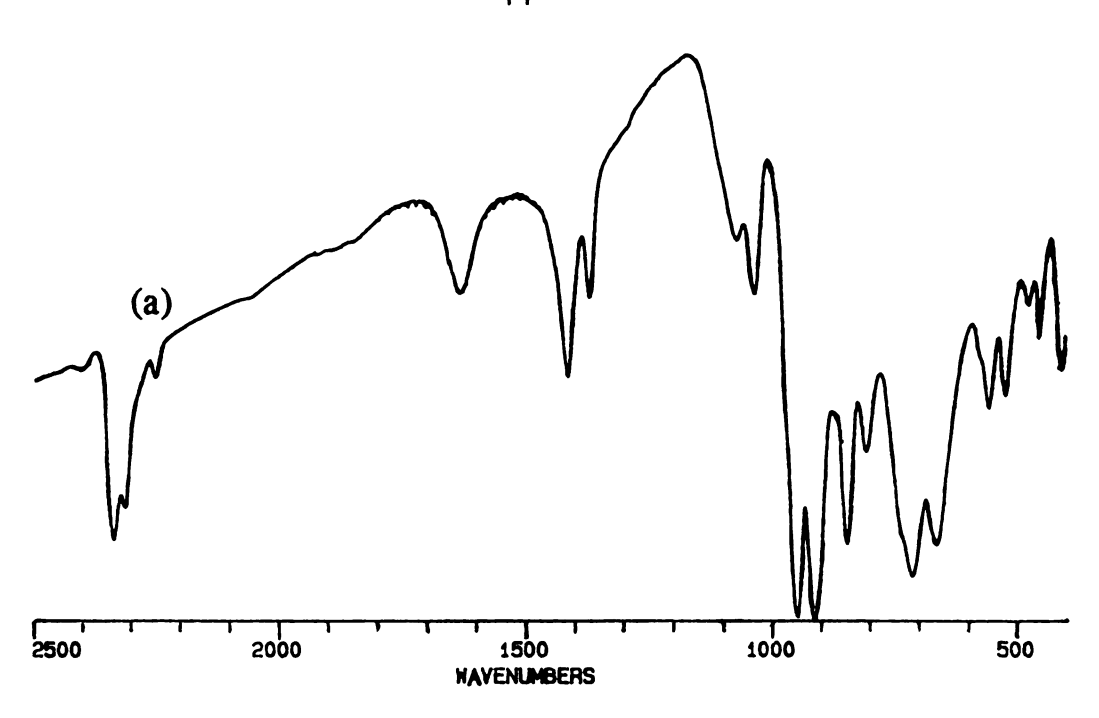


Figure 11. Infrared spectra of (a) $[Rh_2(NCCH_3)_{10}][W_6O_{19}]_2$ and (b) $[Mo_2(NCCH_3)_8][W_6O_{19}]_2.$



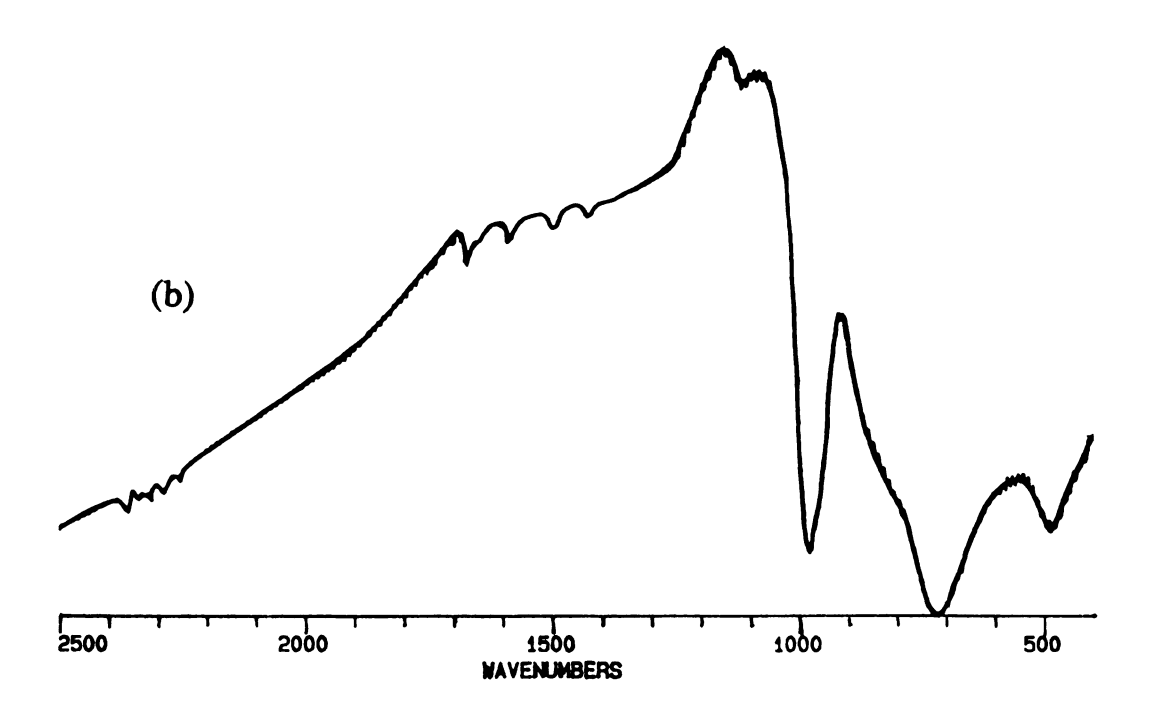
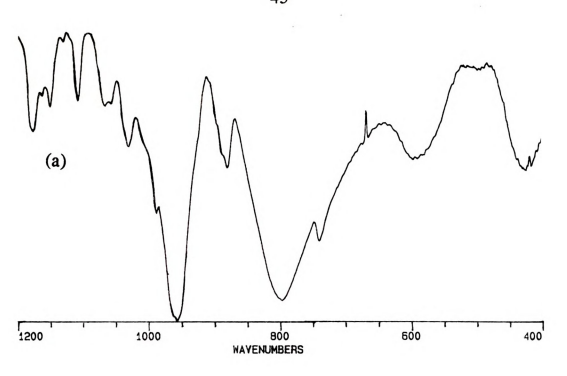


Figure 12. Infrared spectra of (a) $[Rh_2(NCCH_3)_{10}][Mo_8O_{26}]$ and (b) $[Mo_2(NCCH_3)_8]Mo_8O_{26}]$.



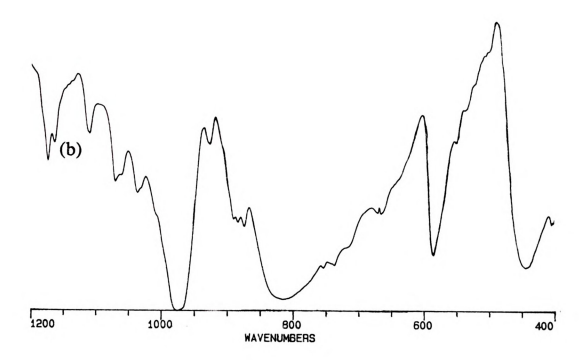


Figure 13. Infrared spectra of $[(n-C_4H_9)_4N]_2[M_6O_{19}]$: (a) M = Mo; (b) M = W.

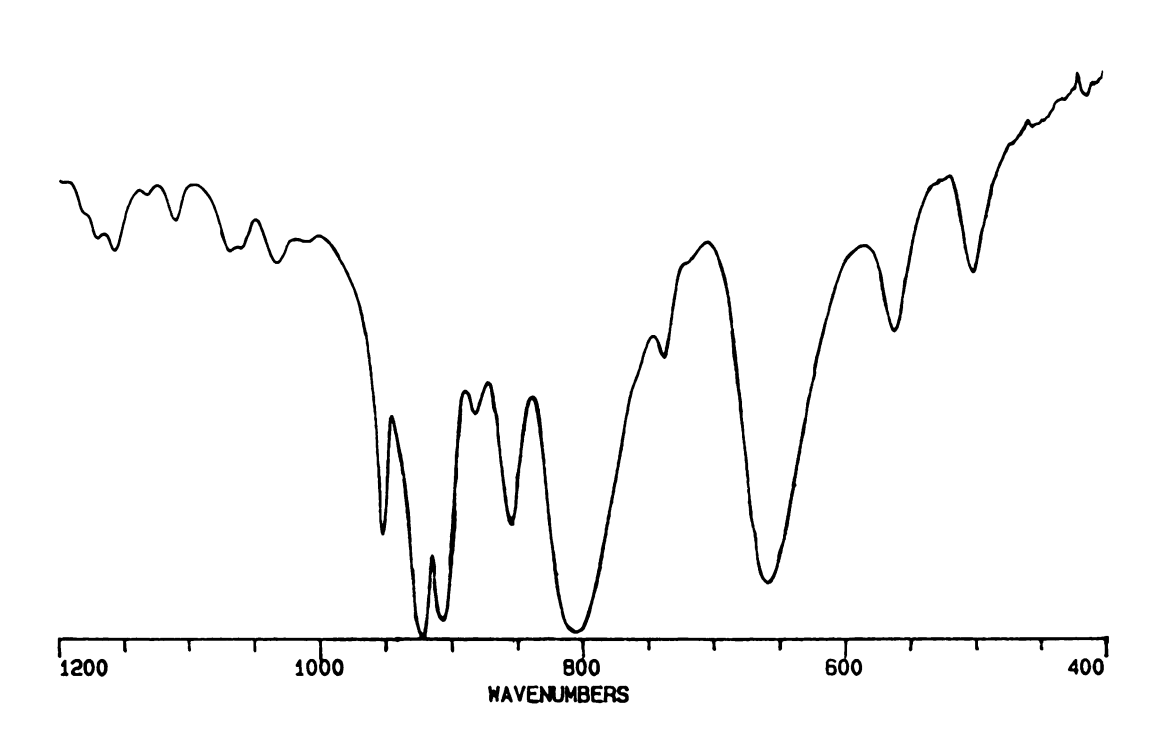


Figure 14. Infrared spectrum of $[(n-C_4H_9)_4N]_4[Mo_8O_{26}]$.

Table 2. Observed v(M-O) Stretching Frequencies (cm⁻¹) of the New Oxymetalate Complexes Compared to the n - Tetrabutylammonium Salts.

[M06O19] ² -	v(M-O _l)	$V(M-O_b)$	$v(M-O_b)$	$v(M-O_c)$
<u>Cation</u>				
$(n-C_4H_9)_4N]^+$	958	798	869	426
Rh ₂ (NCCH ₃) ₁₀] ⁴⁺	963	800	597	429
Mo ₂ (NCCH ₃) ₈] ⁴⁴	972	800	009	416
[Re ₂ (NCCH ₃) ₈] ⁴⁺	926	793	969	429
W ₆ O ₁₉] ² -				
Cation				
$(n-C_4H_9)_4N]^{\dagger}$	926	815	586	445
Rh ₂ (NCCH ₃) ₁₀] ⁴⁺	982	814	585	444
$Mo_2(NCCH_3)_8]^{4+}$	810	810	586	443

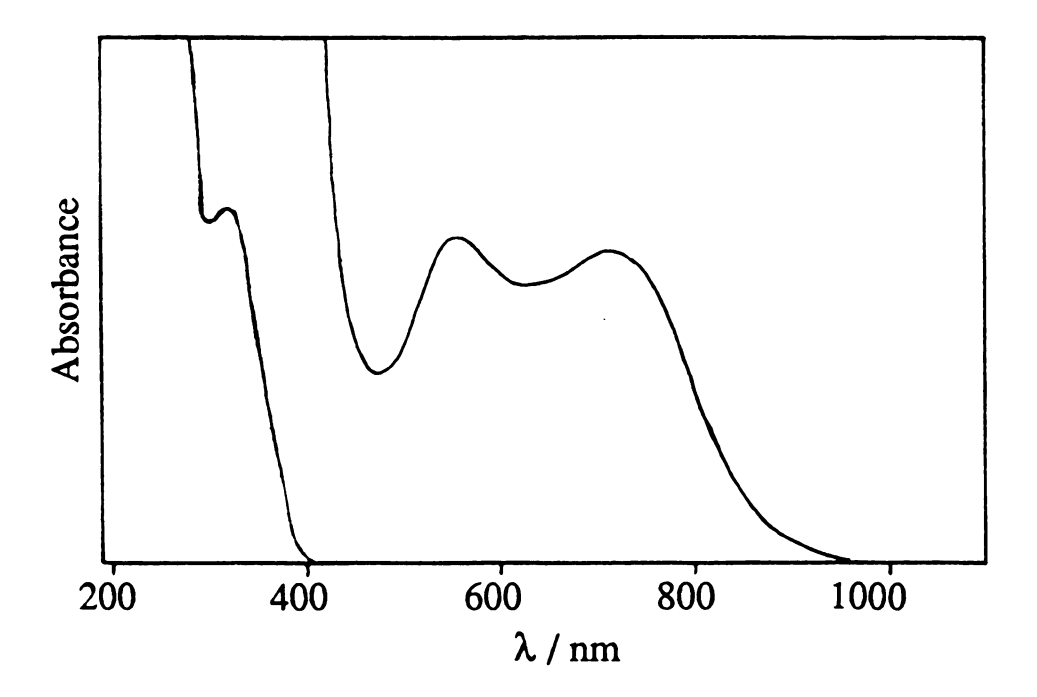
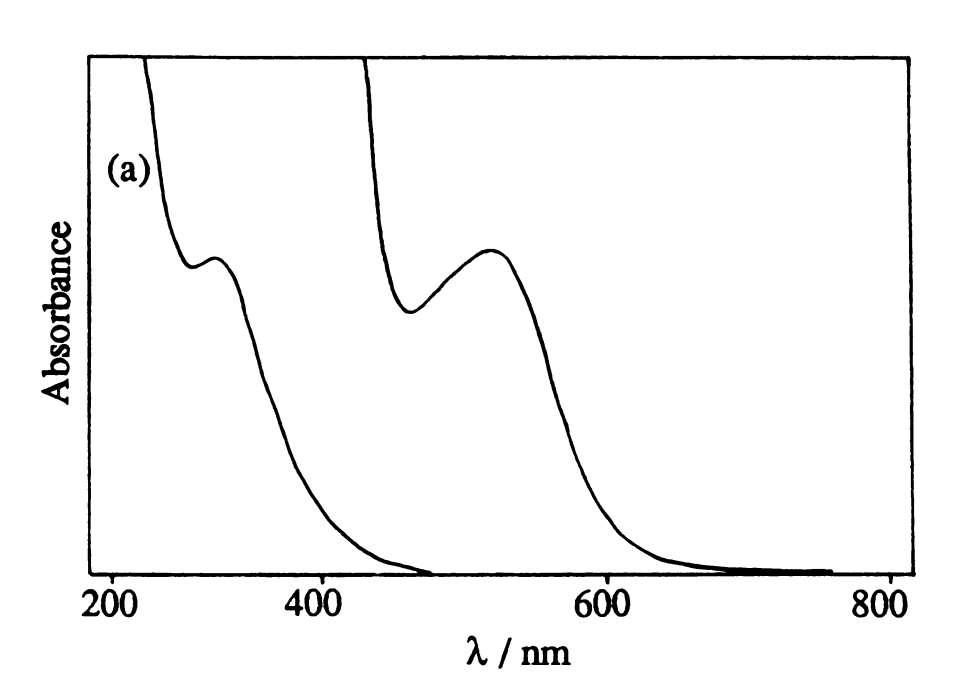


Figure 15. Electronic absorption spectrum of [Re₂(NCCH₃)₈][Mo₆O₁₉]₂.



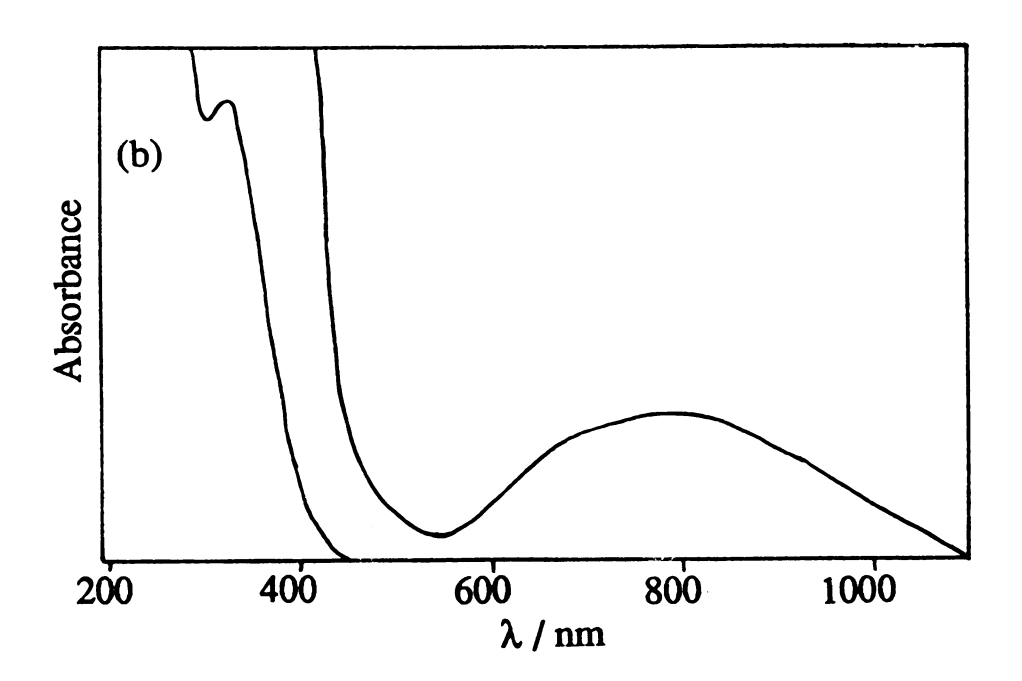


Figure 16. Electronic absorption spectra of (a) $[Rh_2(NCCH_3)_{10}][Mo_6O_{19}]_2$ and (b) $[Mo_2(NCCH_3)_8][Mo_6O_{19}]_2$.

solvent may be replacing the acetonitrile ligands which might also correspond to the presence of the two bands that are found in the spectra for the [Re₂(NCCH₃)₈]⁴⁺ salts.

iii. $[Rh(\eta^3-TMPP)_2][M_6O_{19}]$ (M = Mo, W)

The incorporation of the monomeric Rh(II) species into a polyoxometalate salt is also achieved by metathesis of $[Rh(\eta^3-TMPP)_2][BF_4]_2$ and $[(n-C_4H_9)_4N]_2[M_6O_{19}]$ in CH₃CN. The complex is very stable in DMAA solutions and as a solid sample. The infrared spectrum displays bands assignable to coordinated TMPP ligands, as well as the $\nu(Mo-O)$ bands of the $[M_6O_{19}]^{2-}$ anion that are only slightly shifted from that of the model $[(n-C_4H_9)_4N]_2[M_6O_{19}]$ salts (Figure 17). The electronic absorption spectrum recorded in DMAA exhibits a transition in the visible region at $\lambda_{max} = 545$ nm and higher energy bands at 334 nm and 303 nm.

EPR measurements of $[Rh(\eta^3\text{-TMPP})_2][Mo_6O_{19}]$ were performed by Steven Haefner in DMAA at room temperature and at 103 K (Figure 18). The g values of the liquid and solid samples are listed in Table 3, along with those of the $[BF_4]^-$ starting material for purposes of comparison. The magnetic moment of $[Rh(\eta^3\text{-TMPP})_2][Mo_6O_{19}]$ was measured as a solid over a temperature range of 5 to 280 K at 1000 Gauss (Figure 19). The complex exhibits Curie-Weiss behavior over the entire range of temperatures. The results of this investigation are also listed in Table 3. These studies serve to confirm the integrity of the cation in the new salt.

As previously reported by our group, the elucidation for the mechanism of the reaction between $[Rh(\eta^3-TMPP)_2][BF_4]_2$ with CO is of interest because of the demonstrated reversibility of the reaction. $[Rh(\eta^3-TMPP)_2][Mo_6O_{19}]$ reacts with carbon monoxide in the solid state under

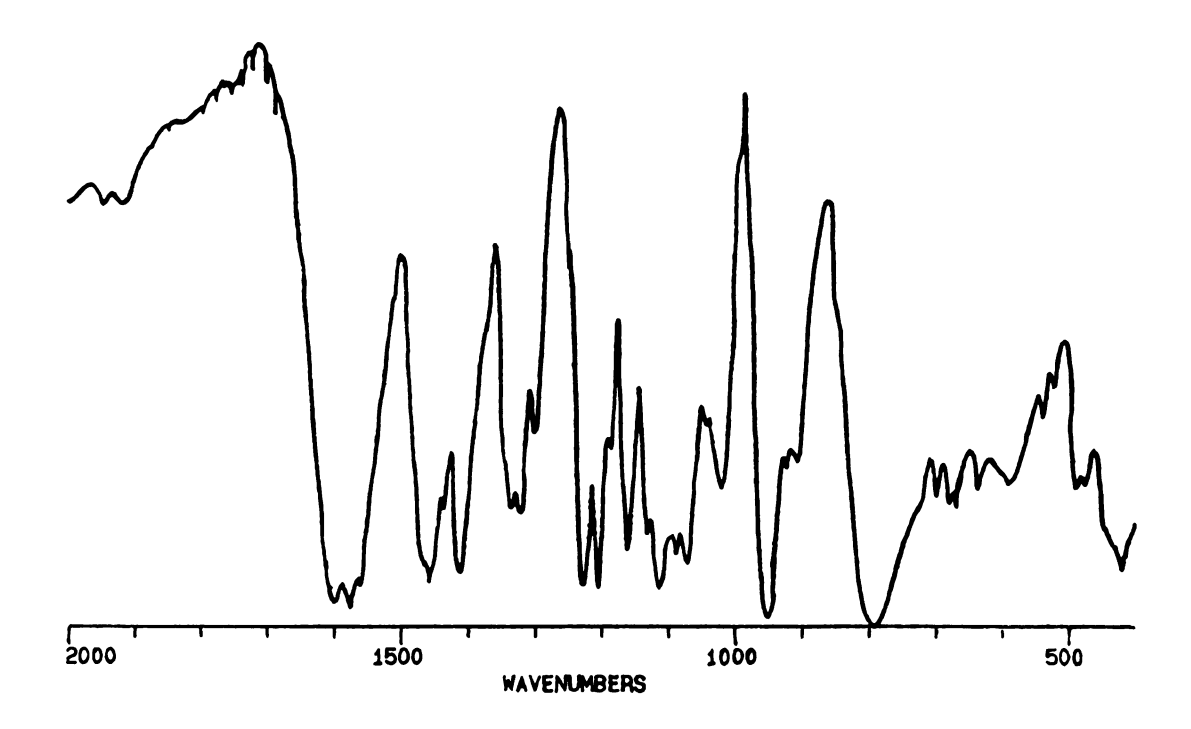


Figure 17. Infrared spectrum of $[Rh(\eta^3-TMPP)_2][Mo_6O_{19}]$.

Figure 18. Electron paramagnetic spectra of $[Rh(\eta^3-TMPP)_2][Mo_6O_{19}]$: (a) liquid sample at 103 K (9.6226 GHz, 2658.15 - 3702.5 G); (b) solid sample at 103 K (9.6096 GHz, 2658.4 - 3702.3 G); (c) solid sample at 300K (9.5993 GHz, 2316.5 - 4402.5 G).

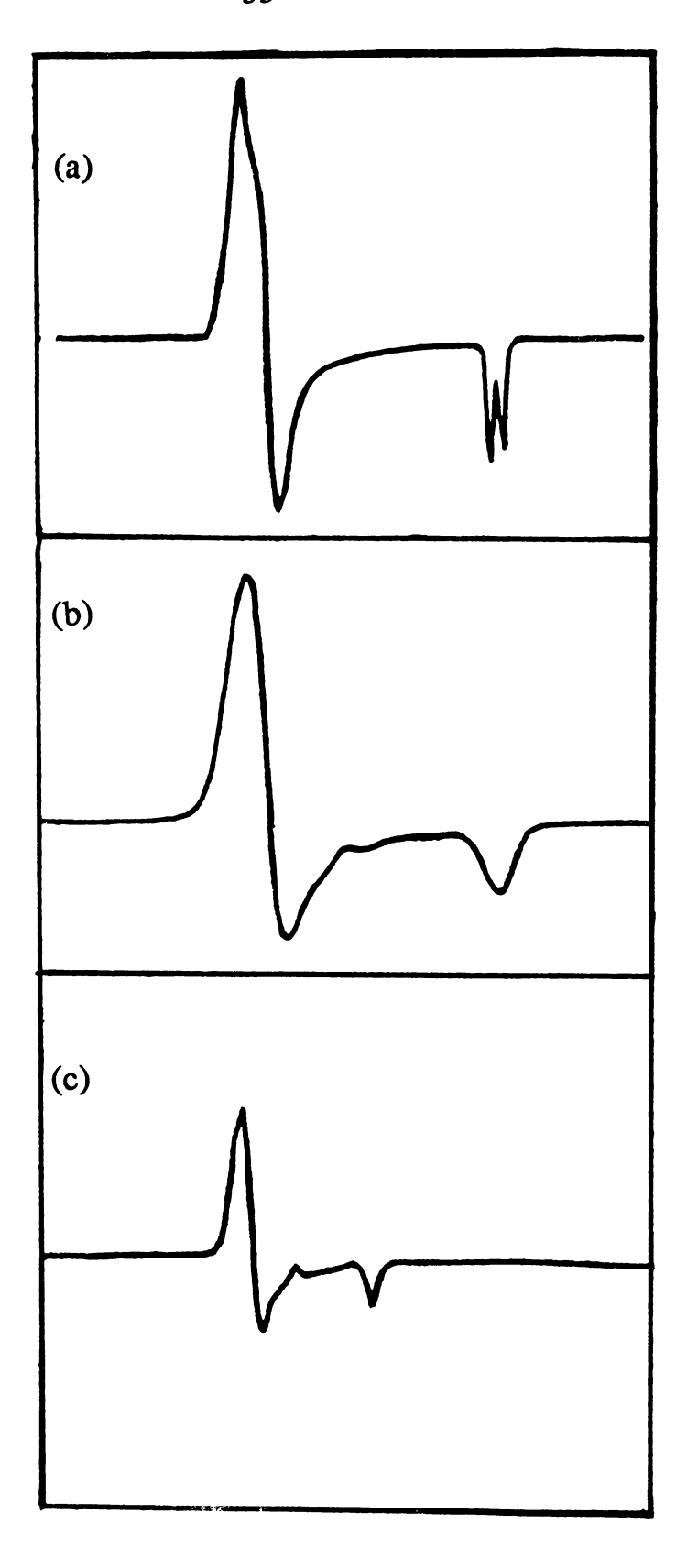


Figure 18

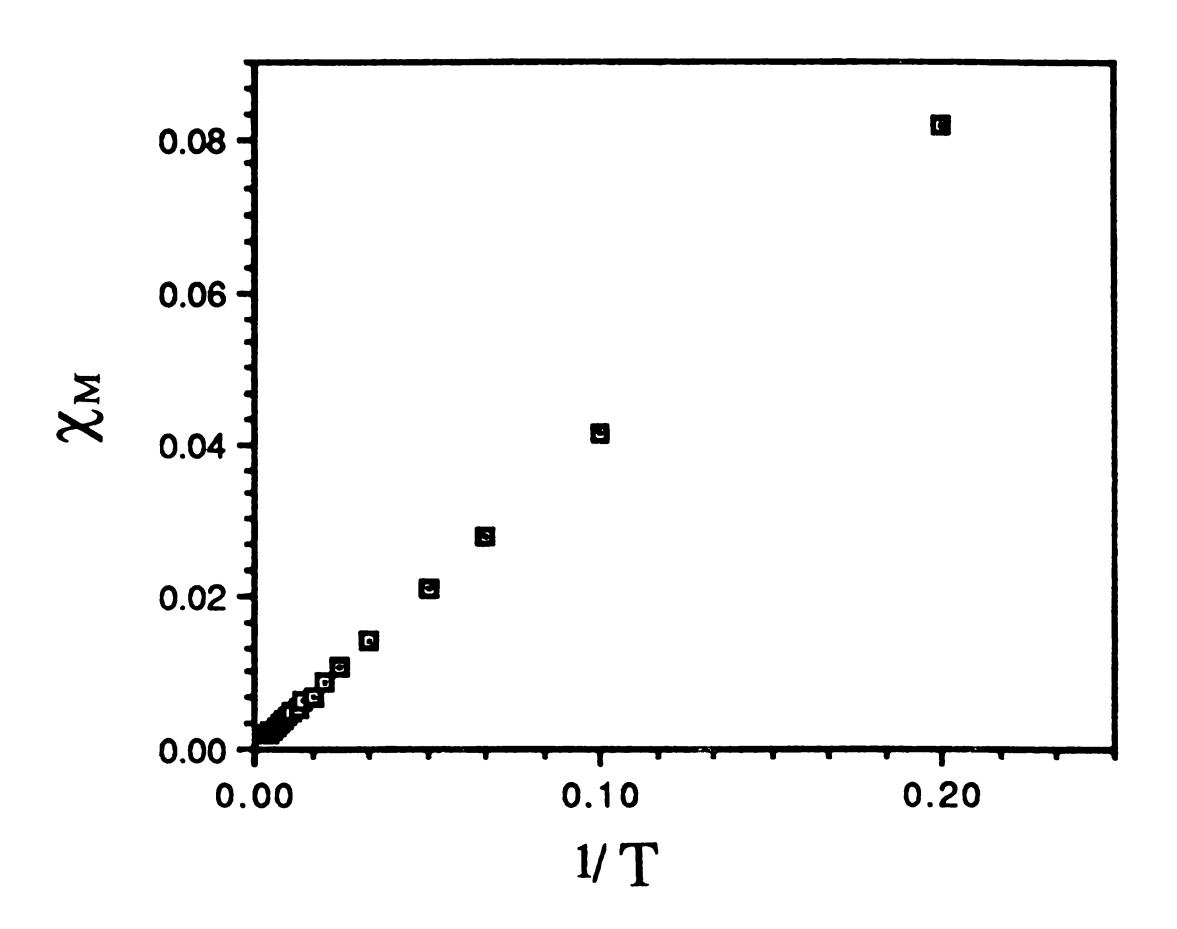


Figure 19. The χ_M vs 1/T plot for [Rh(η^3 -TMPP)₂][Mo₆O₁₉].

Table 3. Electron Paramagnetic Resonance and Magnetic Susceptibility Measurements for the Dication $[Rh(\eta^3-TMPP)_2]^{2+}$.

<u>Liquid</u> EPR (CH ₂ Cl ₂ /Me-THF glass) ^a , (DMAA)	77 K $[Rh(\eta^3\text{-TMPP})_2][BF_4]_2$	103 K [Rh(η ³ - TMPP) ₂][Mo ₆ O ₁₉]
g _{xx}	2.26	2.26
g _{yy}	2.30	2.30
g_{zz}	1.99	2.00
A_{zz} , G (cm ⁻¹)	22 (2 × 10 ⁻³)	22 (2 × 10 ⁻³)
Solid	<u>300 K</u>	<u>103 K</u>
[Rh(η ³ - TMPP) ₂][Mo ₆ O ₁₉]		
gı	2.26	2.25
g _{II}	1.99	2.00
magnetic moment ^{b,c} ,	1.89	
μ_{eff} , μ_{B}		

^aref. [45] ^b Average magnetic moment measured over a temperature range of 5-280 K. ^c A diamagnetic correction of -648 x 10^{-6} was applied based on -20 × 10^{-6} for Rh²⁺, -313 × 10^{-6} for TMPP, -414 × 10^{-6} for $[(n-C_4H_9)_4N]^+$, and -315 × 10^{-6} for $[Mo_6O_{19}]^2$.

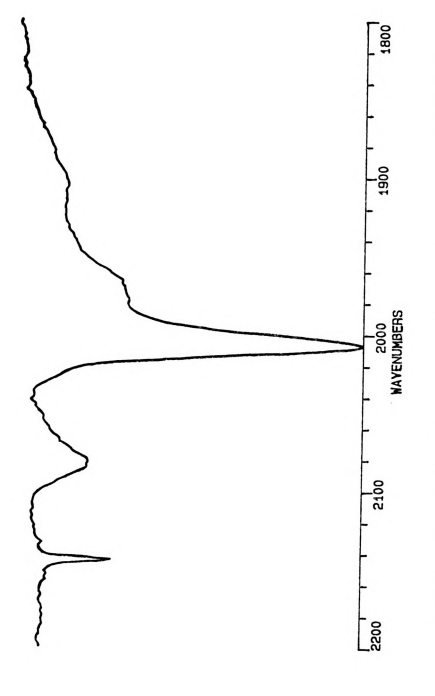
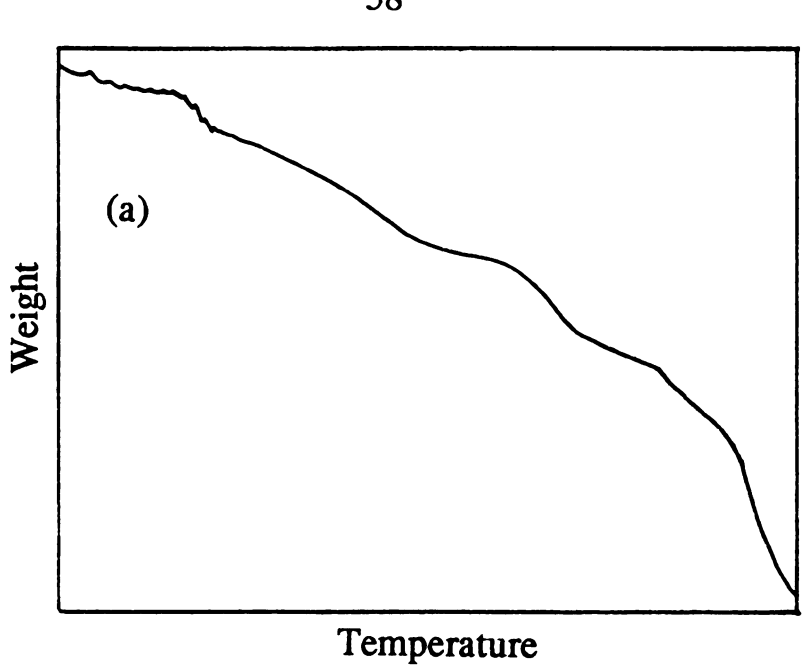


Figure 20. Infrared spectrum from the reaction of $[{\rm Rh}(\eta^{\,3} -$ TMPP)2][Mo₆O₁₉] with CO at 50 psi.

mild conditions to yield a brown solid. The infrared spectrum indicated that, as for the $[BF_4]^-$ salt in solution, a series of electron-transfer reactions occur to form two Rh(I) carbonyl complexes, $[Rh(TMPP)_2(CO)]^+$ and $[Rh(TMPP)_2(CO)_2]^+$ along with the oxidized complex, $[Rh(TMPP)_2]^{3+}$; one other as yet unidentified species was also detected by infrared spectroscopy (Figure 20). We believe that the species at $v(CO) = 2082 \text{ cm}^{-1}$ may be formulated as $[Rh(TMPP)_2(CO)]^{2+}$ since CO reactions of the other intermediates in the reaction, viz., $[Rh(TMPP)_2]^{3+}$ and $[Rh(TMPP)(CO)]^+$ either do not contain CO at all, or do not give rise to v(CO) bands in this region.

2. Desolvated Systems.

As pointed out in a preceding section, the solvated $[Mo_6O_{19}]^2$ -acetonitrile complexes show quantitative loss of acetonitrile upon heating. For example, upon TGA analysis of $[Rh_2(NCCH_3)_{10}][Mo_6O_{19}]_2$ under a stream of nitrogen, a 17.20 % weight loss (calculated 17.26 %) was observed. The spectra of the TGA measurements are depicted in Figures 21-22. The TGA curves generally show three steps corresponding to the loss of four acetonitriles, with subsequent loss of either six, eight, or ten acetonitriles. Figures 23-24 show that the infrared spectra of the new materials are generally featureless, with the exception of strong bands present between 1000 cm⁻¹ and 400 cm⁻¹. Because these new materials are insoluble in all solvents, exploration of the heterogeneous catalytic chemistry is extremely attractive.



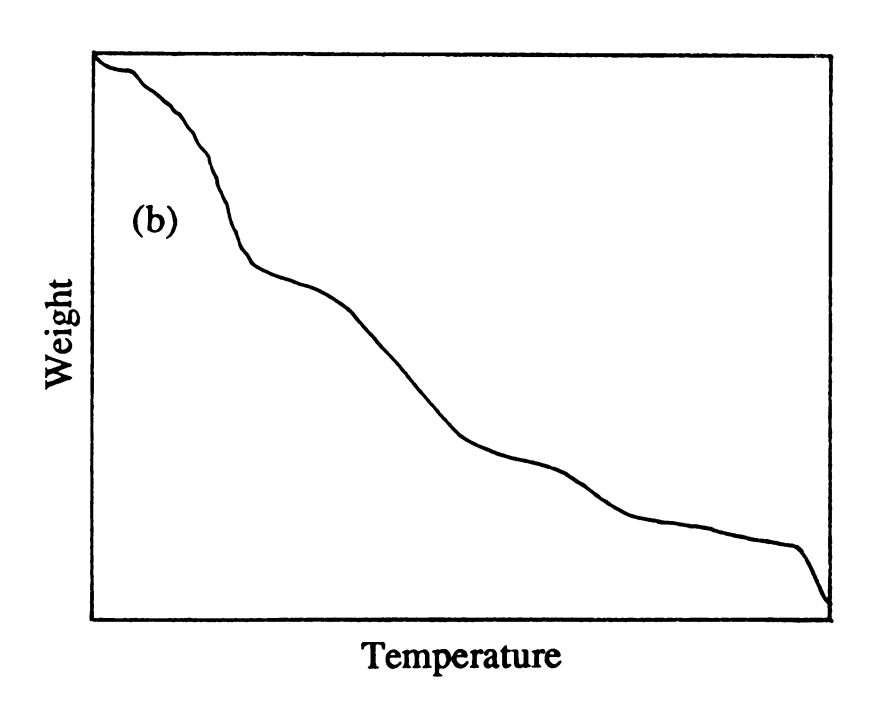


Figure 21. Display of the thermogravimetric analysis measurements of (a) $[Rh_2(NCCH_3)_{10}][Mo_6O_{19}]_2$, and (b) $[Mo_2(NCCH_3)_8][Mo_6O_{19}]_2$.

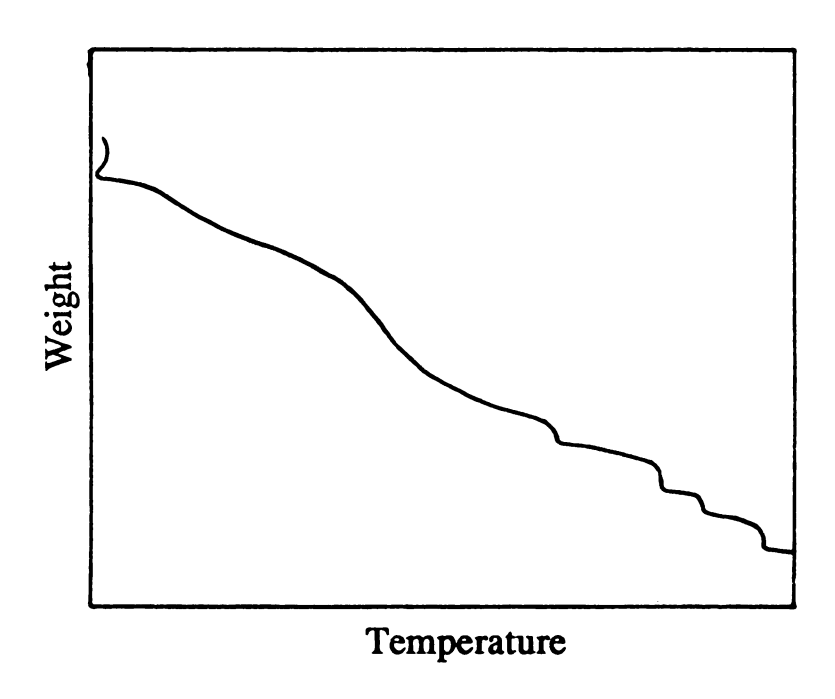
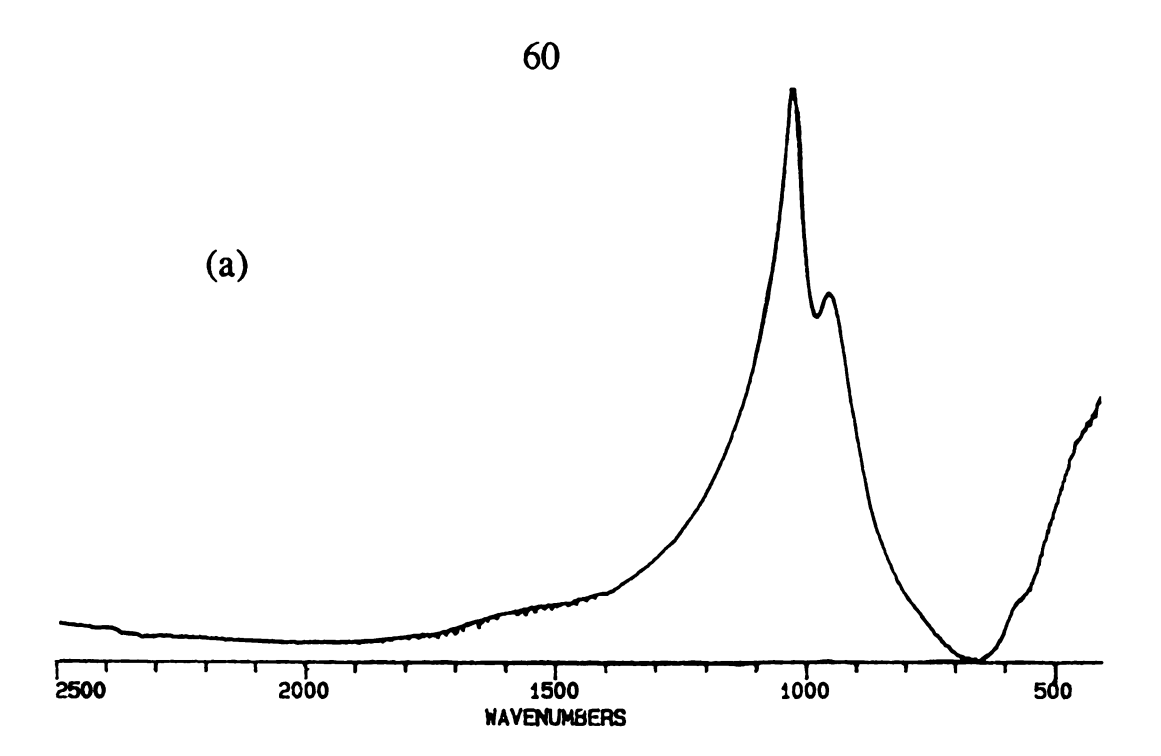


Figure 22. Display of the thermogravimetric analysis measurement of [Re₂(NCCH₃)₈][Mo₆O₁₉]₂.



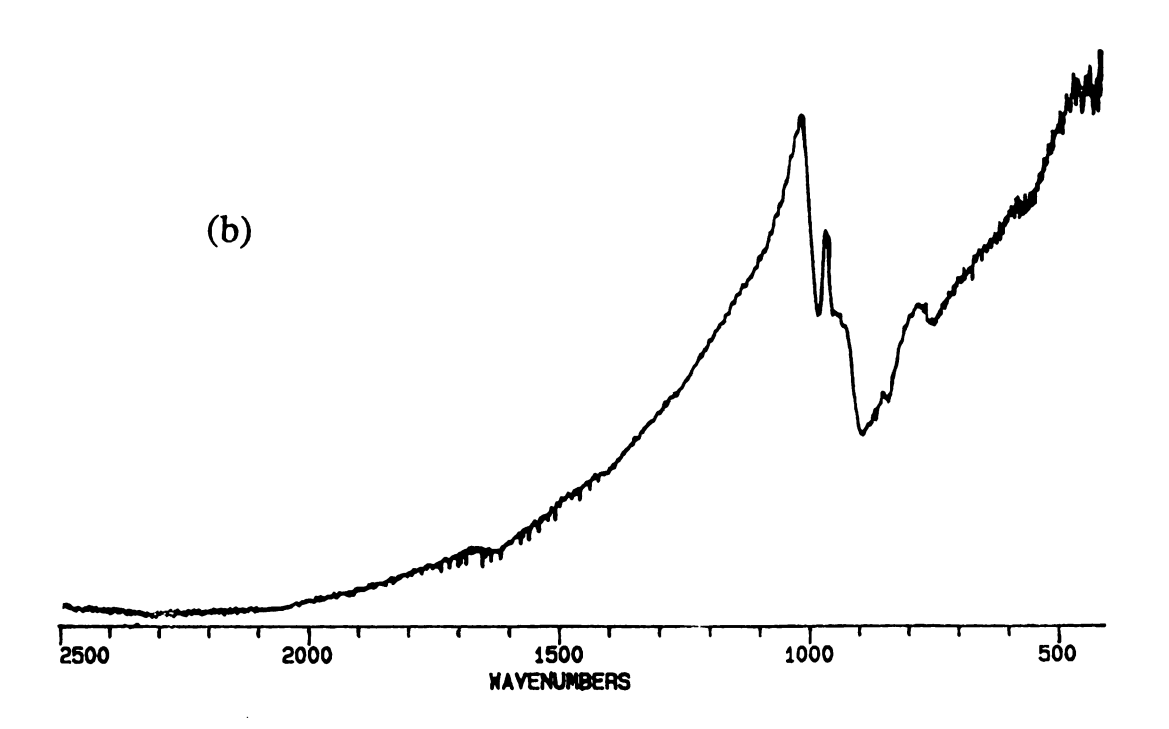


Figure 23. Infrared spectra of the desolvated materials (a) " $Re_2(Mo_6O_{19})_2$ " and (b) " $Mo_2(Mo_6O_{19})_2$ ".

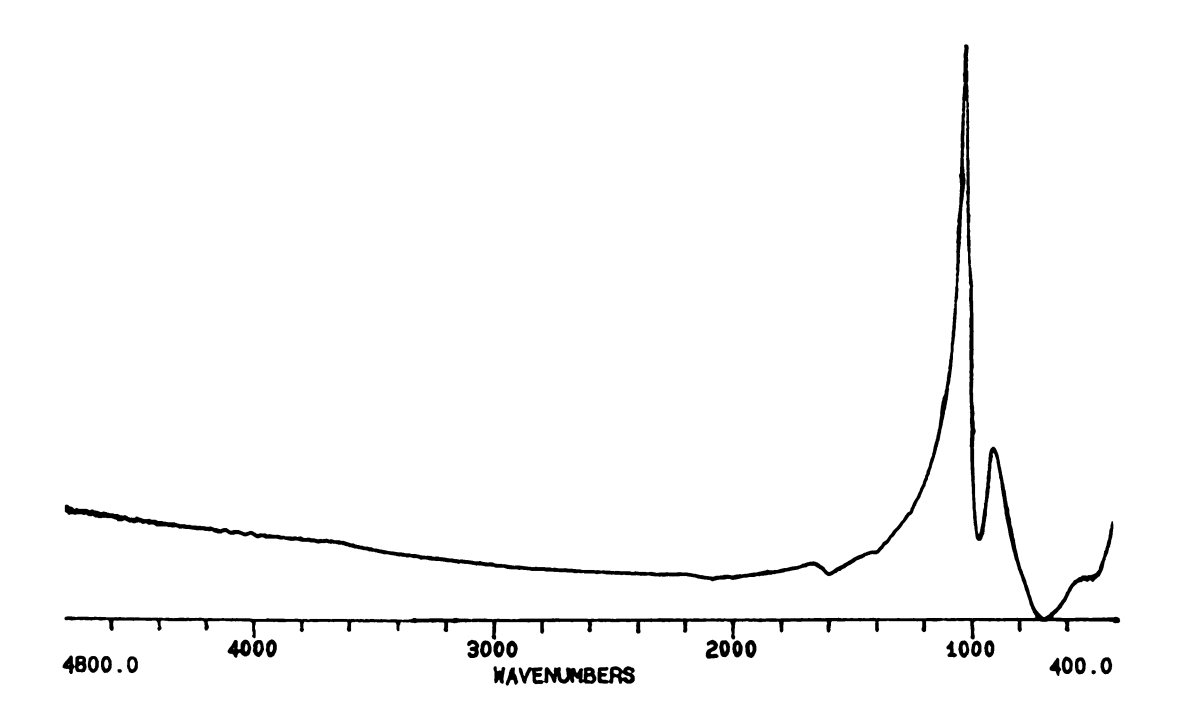


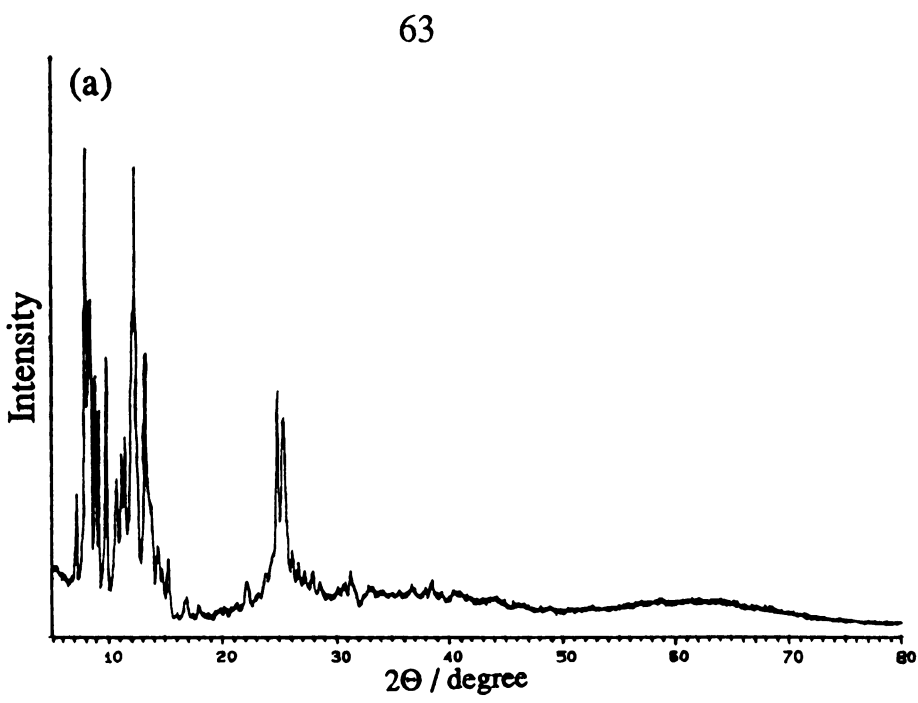
Figure 24. Infrared spectrum of the desolvated material "Rh₂(Mo₆O₁₉)₂"

C. X-ray Diffraction

1. Powder X-ray Diffraction.

The new crystalline polyoxoanion compounds were investigated by powder X-ray diffraction techniques. Figures 25-27 depicts a qualitative comparison of the diffraction patterns at 2Θ angles between 5 and 80° of the solvated polyoxometalate complexes, with the exclusion of $[Mo_2(NCCH_3)_8][Mo_6O_{19}]_2$, since solid samples were found to be unstable in the X-ray beam. The *n*-tetrabutylammonium polyoxometalate salts are also provided for comparison in Figures 28-29. The resemblance of the intensities at corresponding angles of 2Θ indicates that the structures of the solvated polyoxoanion complexes are similar, thereby lending more support for general characterization.

As expected, the X-ray powder diffraction of the desolvated materials generally yield patterns indicative of amorphous behavior, since removal of the coordinated acetonitrile ligands usually destroys the crystalline properties of the complexes. An investigation of the TGA products confirmed this with one exception; desolvation of [Mo₂(NCCH₃)₈][Mo₆O₁₉]₂ produces a very crystalline deep blue material that gives rise to an intense diffraction pattern (Figure 30). The peak position and indices given in Table 4 constitute an unit cell of orthorhombic symmetry. Work is in progress to elucidate the structure of this material.



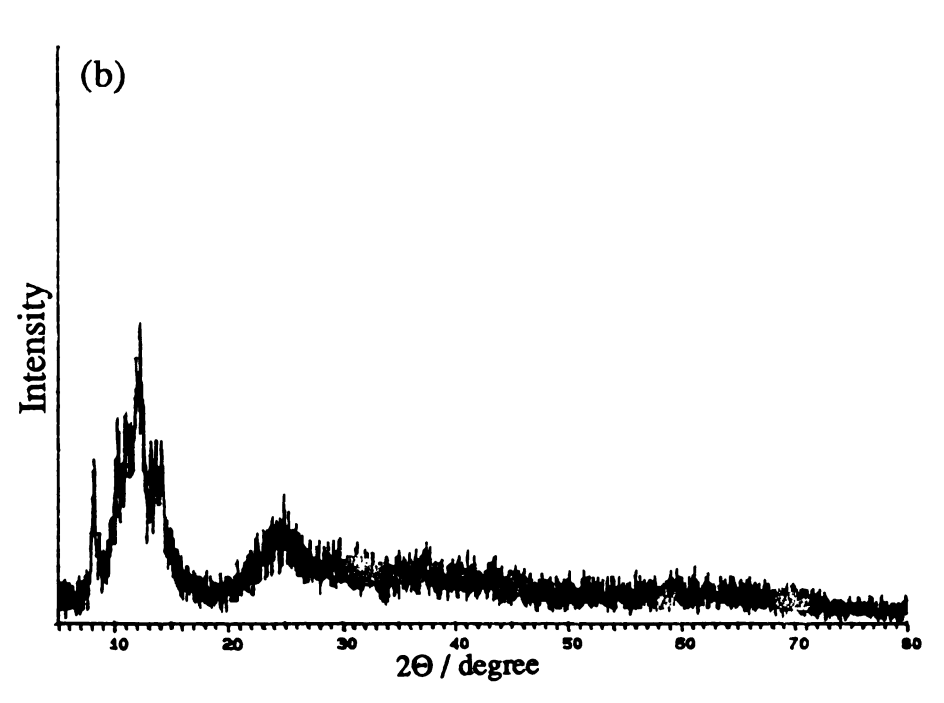
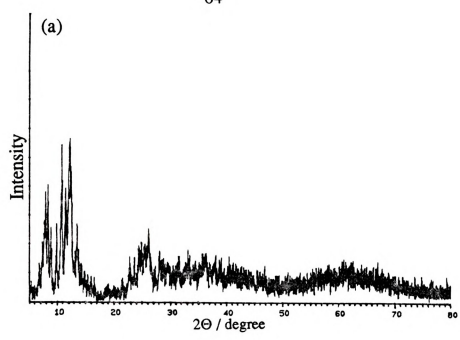
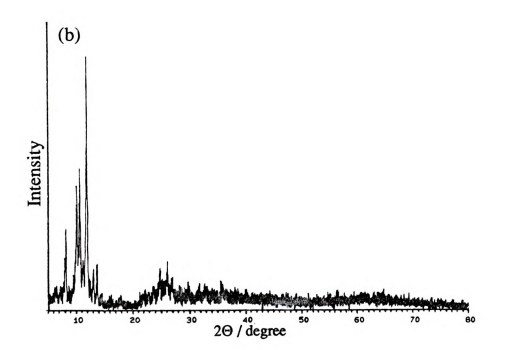


Figure 25. Powder X-ray diffraction patterns for (a) $[Rh_2(NCCH_3)_{10}][Mo_6O_{19}]_2 \ and \ (b) \ [Re_2(NCCH_3)_8][Mo_6O_{19}]_2.$





 $\label{eq:Figure 26.} \textbf{Figure 26.} \quad \text{Powder X-ray diffraction patterns for (a)} \\ [\text{Rh}_2(\text{NCCH}_3)_{10}][W_6O_{19}]_2 \text{ and (b) } [\text{Mo}_2(\text{NCCH}_3)_8][W_6O_{19}]_2.$

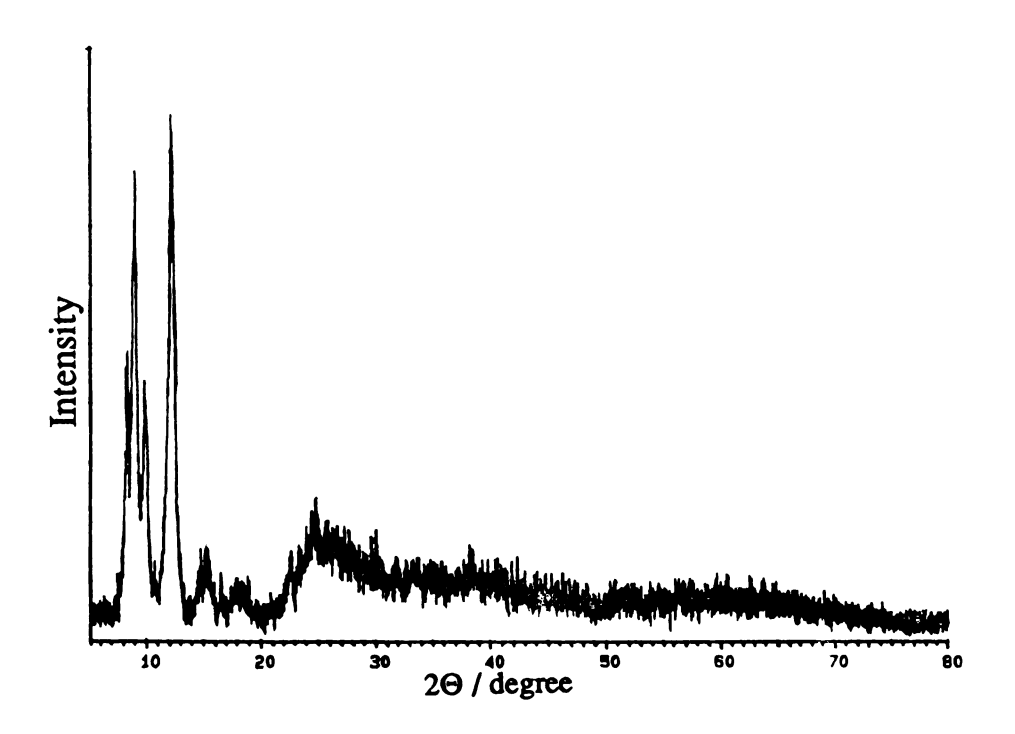
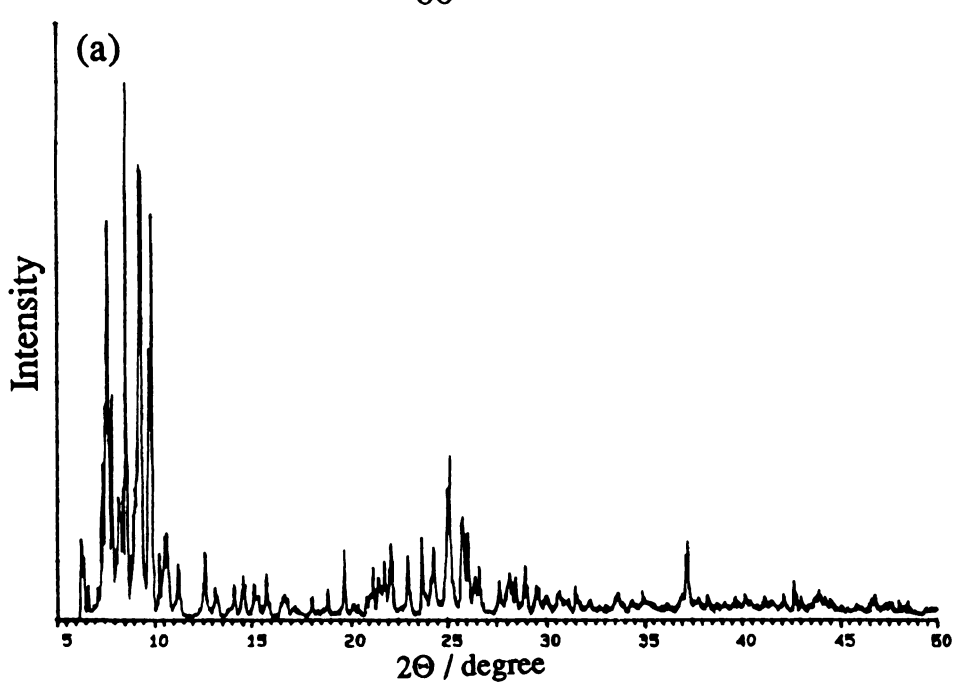


Figure 27. Powder X-ray diffraction pattern for [Rh₂(NCCH₃)₁₀][Mo₈O₂₆].



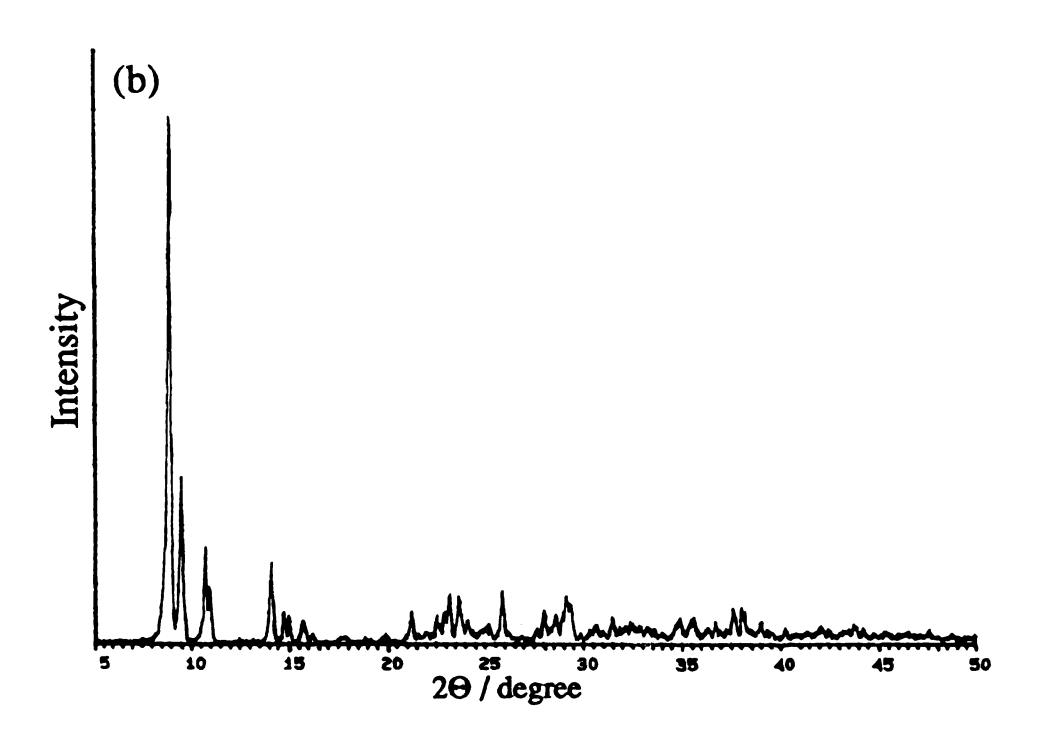


Figure 28. Powder X-ray diffraction patterns for $[(n-C_4H_9)_4N]_2[M_6O_{19}]$: (a) M = Mo; (b) M = W.

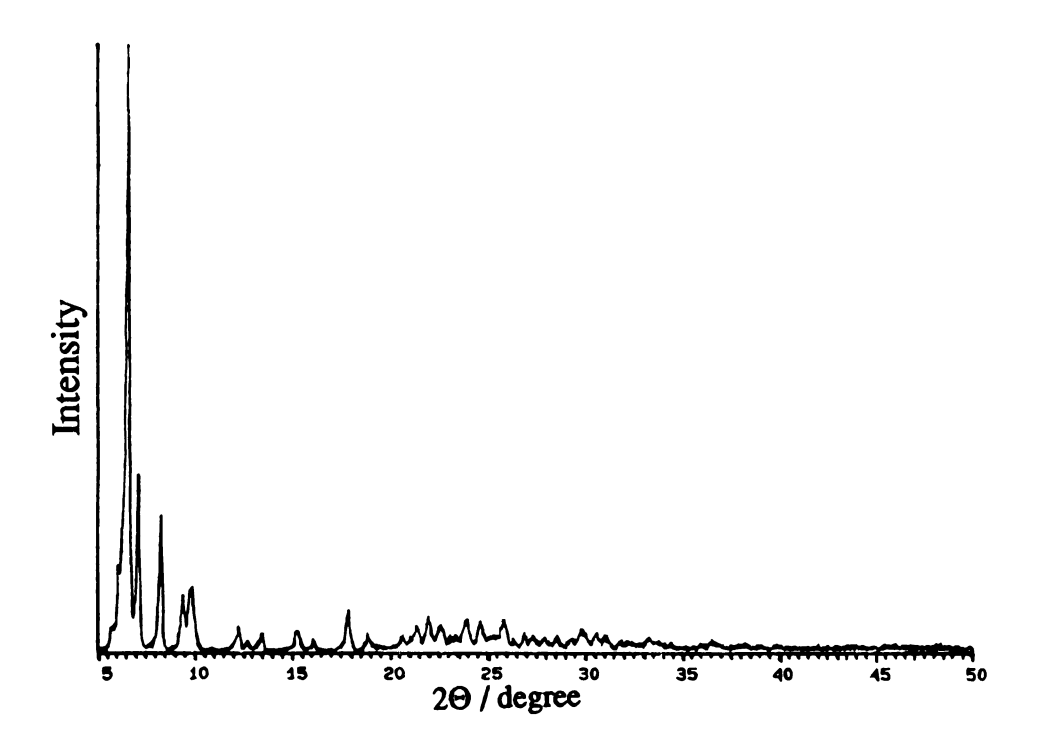


Figure 29. Powder X-ray diffraction pattern for $[(n-C_4H_9)_4N]_4[Mo_8O_{26}]$.

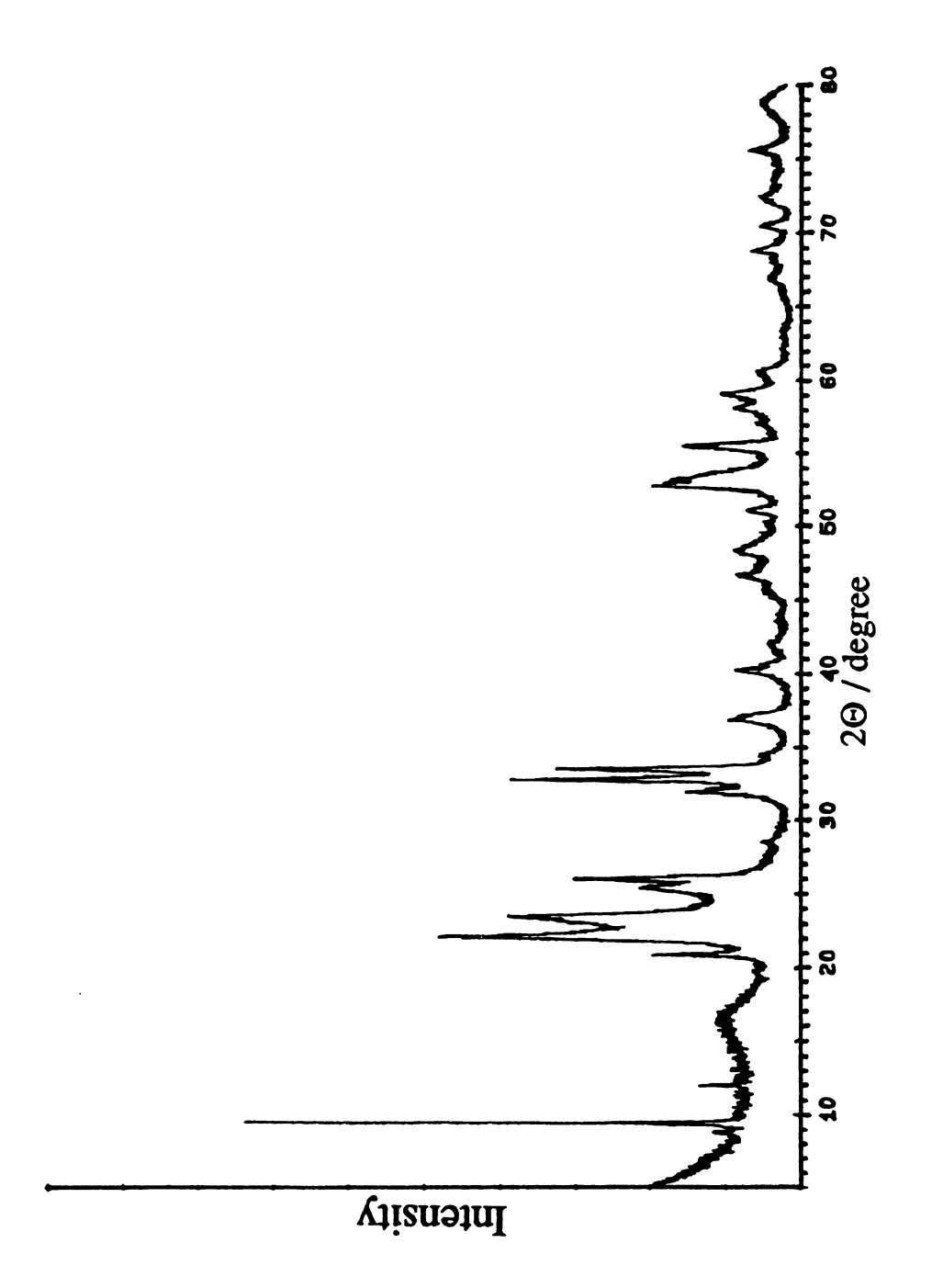


Figure 30. Powder X-ray diffraction pattern for the desolvated material obtained from the TGA of [Mo₂(NCCH₃)₈][Mo₆O₁₉]₂.

Table 4. The Peak Positions and Indices of the X-ray Diffraction Pattern of the TGA Product for $[Mo_2(NCCH_3)_8][Mo_6O_{19}]_2$.

(hkl)	2Θ / degree _{obs}	2⊕ / degree _{calc}
(1 1 0)	9.080	9.036
(0 2 0)	_	9.144
(2 0 0)	9.440	9.437
(2 1 0)	12.000	12.025
(1 0 1)	16.241	16.226
(1 2 0)	_	16.282
(3 2 0)	20.880	20.857
(0 2 1)	22.140	22.117
(0 3 0)	23.520	23.522
(4 1 1)	25.420	25.408
(3 2 1)	26.100	26.127
(1 4 0)	_	31.886
(6 0 1)	_	31.901
(6 2 0)	31.931	31.931
(1 1 2)	_	32.757
(2 0 2)	32.820	32.789
(6 1 1)	_	32.888
(3 2 3)	52.801	52.801
(8 5 0)	55.539	55.540

^aLattice constants are a = 19.33(2) Å, b = 11.337(8) Å, c = 5.690(1) Å, α = β = γ = 90°, V = 1246.72 Å³.

2. Single Crystal X-ray Diffraction.

A. $[Re_2(NCCH_3)_8(CH_3CN)_2][BF_4]_4$

(i) Data Collection and Reduction.

A blue hexagon crystal having approximate dimensions of 0.5 x 0.36 x 0.18 mm³ was mounted in a glass capillary, covered with vacuum grease, and cooled to -100 °C. All measurements were performed on a Rigaku AFC6-S diffractometer equipped with Mo K_α radiation $(\lambda_{\bar{\alpha}} = 0.71069 \text{ Å})$. A fast data collection was used to locate 21 strong reflections which led to reduced cell dimensions of a = b = c = 29.22(1) Å, $\alpha = \beta = \gamma = 90^{\circ}$ and indicated that the crystal was cubic. Based on the formula unit, Z = 24 and F. W. = 1130.108, the calculated density is 1.899 g cm⁻³. An ω scan motion was employed to a maximum 2Θ value of 50° at 4°/min (in omega) to collect 5379 reflections. The intensities of three representative reflections which were measured after every 97 reflections declined by -5.4 %. A linear correction factor was applied to the data to account for this. An empirical absorption correction based on three Ψ scans taken a χ near 90° resulted in transmission factors from 0.7748 to 1.00. The data were corrected for Lorentz and polarization effects.

B. $[Re_2(NCCH_3)_8(CH_3CN)_2][Mo_6O_{19}]_2 \cdot 4CH_3CN \cdot 2H_2O$

(i) Data Collection and Reduction.

A green-blue crystal of approximate dimensions $0.39 \times 0.26 \times 0.08 \text{ mm}^3$ was mounted at the end of a glass fiber with vacuum grease and cooled to - $100 \, ^{\circ}\text{C}$. Geometric and intensity data were obtained on a Rigaku AFC6-S diffractometer equipped with graphite-monochromated Mo K_{α} radiation ($\lambda_{\overline{\alpha}} = 0.71069 \, \text{Å}$). An automatic search routine was used to

preliminary cell was indexed. After a fast data collection in the range $20 \le 2\Theta \le 30^{\circ}$, the reduced cell dimensions of a = 18.352(3) Å, b = 22.659(4) Å, c = 17.390(3) Å, β = 90.32° indicated that the crystal was monoclinic which was subsequently confirmed by axial photography. The space group was determined to be C2/c (#15) based on the systematic absences of hkl: $(h + k) \ne 2n$; h0l: $l \ne 2n$. An ω -2 Θ scan motion was used to scan 6736 data points in the range $6 \le 2\theta \le 50^{\circ}$, of which 6508 were unique. The structure factors were obtained after correction for Lorentz and polarization effects. During data collection, the intensities of three check reflections were measured every 97 reflections and revealed a significant decay of -60 %; a linear correction factor was applied to the data to account for this phenomenon. Azimuthal scans of 3 reflections with Eulerian angle χ near 90° were used as a basis for an empirical absorption correction which was applied and resulted in transmission factors ranging from 0.46 to 1.00.

(ii) Structure Solution and Refinement.

The structure was solved by direct methods [47]. The positions of the Re and Mo atoms were obtained by the program DIRDIF [48]. A sequence of successive difference Fourier maps and least-squares cycles led to full development of the coordination sphere. The final full-matrix refinement involved 298 parameters and 2805 observations with $F_0^2 > 3\sigma(F_0^2)$ for a data-to-parameter ratio of 9.14. The refinement converged with residuals of R = 0.066 and $R_w = 0.083$ and quality of fit of 2.56. Three hkl reflections: (3,1,1), (1,3,-2), (0,4,-1) were removed due to their large errors in intensity values. The largest shift / esd in the final cycle was 0.13. The maximum peak on the final difference Fourier map

corresponded to $1.95 e^{-}/\text{Å}^3$ and was associated with the Re atom. The minimum peak was $-1.4 e^{-}/\text{Å}^3$.

(iii) Molecular Structure.

The complex was crystallized by slow diffusion of the appropriate starting materials as acetonitrile solutions to give blue-green crystals, one of which was examined by single crystal X-ray diffraction methods. The crystallographic data are shown in Table 5, and selected bond distances and angles for [Re₂(NCCH₃)₈(CH₃CN)₂]⁴⁺ and [Mo₆O₁₉]²⁻ are given in Tables 6 An ORTEP plot of the molecular structure is depicted in Figure 31. The complex crystallizes as discrete cation and anion units which reveals a 1:2 cation:anion formulation; this immediately indicates that the Re atoms had undergone a reduction in the initial reaction from Re₂^{III,III} [Re₂Cl₈]²- to form a dinuclear Re₂^{II,II} solvated cation. coordination geometry of each Re^{II} center is pseudo-octahedral with a square plane occupied by four CH₃CN groups and two additional vertices defined by a weaker interacting axial CH₃CN ligand and the other Re atom; the cation adopts a twisted conformation in which two Re(NCCH₃)₄ units are rotated by $\chi_{av} = 44.5 [1]^{\circ}$ from an eclipsed geometry. Figure 32 displays a space-filling model of the cation which reveals the unsaturation of the molecule, and shows a clear depiction of the staggered arrangement of the ligands. A Re-Re bond distance value of 2.259(4) Å is comparable with other dirhenium compounds containing metal-metal triple bonds of the electron rich $\sigma^2 \pi^4 \delta^2 \delta^{*2}$ configuration. A crystal packing diagram within a 10 Å radius from the center of the Re-Re bond revealed that the

Table 5. Crystal Data for $[Re_2(NCCH_3)_8(CH_3CN)_2][Mo_6O_{19}]_2 \cdot 4CH_3CN \cdot 2H_2O$

Formula	$C_{28}H_{46}N_{14}O_{40}Mo_{12}Re_2$
Formula weight	2742.44
Crystal system	monoclinic
Space group	C2/c (#15)
a, Å	18.352(3)
b, Å	22.659(4)
c, Å	17.390(3)
α, deg	90
β , deg	90.32(1)
γ, deg	90
v, Å ³	7231(4)
Z	4
d _{calc} , g/cm ³	2.508
Crystal size, mm ³	0.39 × 0.26 × 0.08
μ (Mo K α), cm ⁻¹	54.03
Radiation (monochromated in incident beam)	Mo K _{α} ($\lambda_{\overline{\alpha}} = 0.71069 \text{ Å}$)
Scan method	ω - 2Θ
Temperature, °C	-90
Trans. factors, max., min.	1.00, 0.4639
R ^a	0.066
R _w ^b	0.083

 $[\]overline{a_{R} = \Sigma \mid |F_{o}| - |F_{c}| |/\Sigma |F_{o}|}$

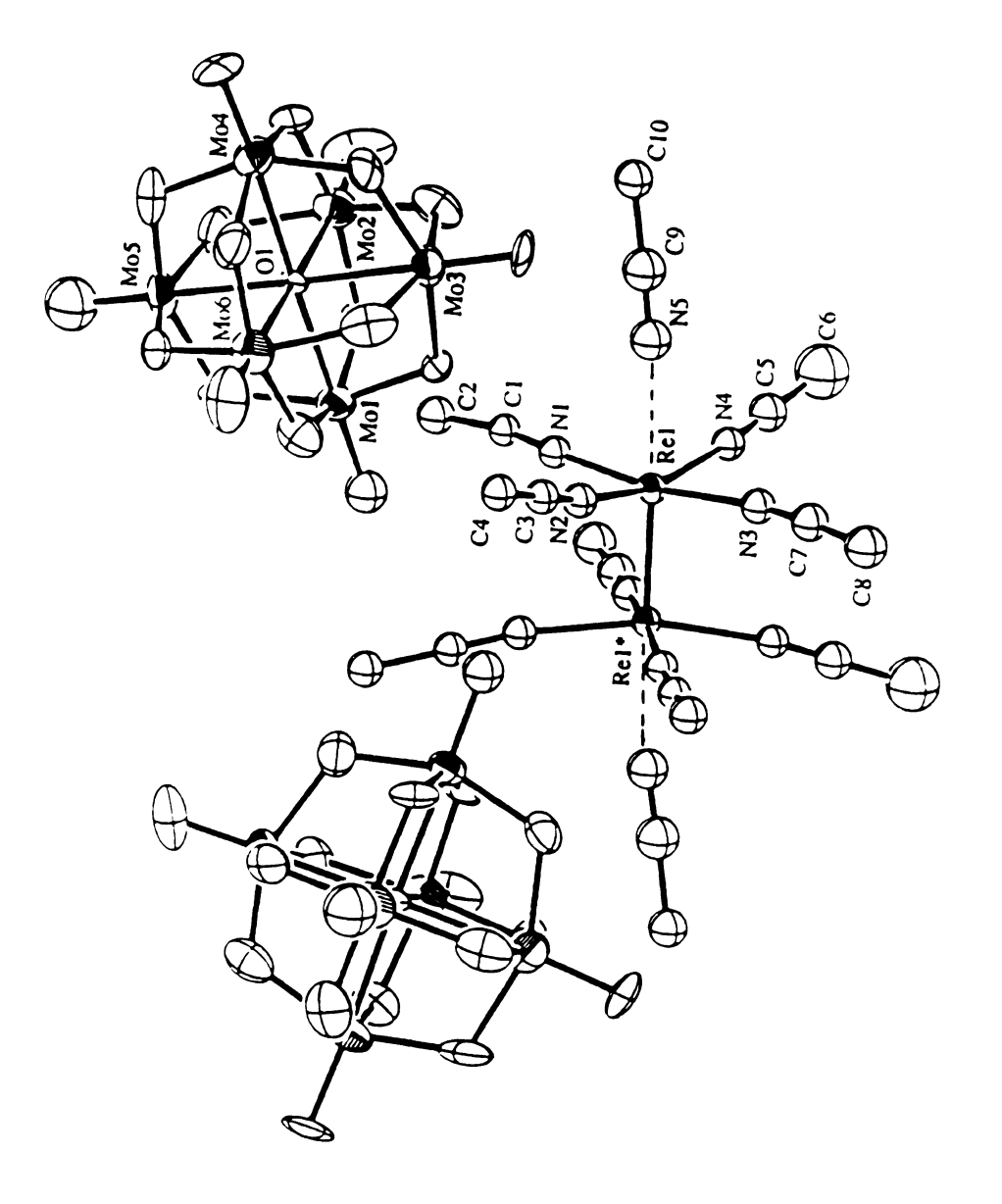
 $^{{}^{}b}R_{w} = [\Sigma w \mid F_{o} \mid - \mid F_{c} \mid)^{2}/\Sigma w \mid F_{o} \mid^{2}]^{1/2}; w = 1/\sigma^{2}(\mid F_{o} \mid)$

Table 6. Selective Bond Distances (Å) and Angles (deg) for the Molecular [Re₂(NCCH₃)₈(CH₃CN)₂]⁴⁺ Cation.

(1)* 2.259 (4) N (1) C ((2) 2.02 (3) N (3) C ((4) 2.16 (3) N (5) C ((5) 2.51 (3) C (5) C ((5) 2.51 (3) C (5) C ((6) 2.51 (3) C (5) C ((7) Re (1) N (1) P (4) N (2) C (3) C (3) C (3)	Atom 1	Atom 2	Distance) (Ce	A	Atom 1	Atom 2	Distance
N (2) 2.02 (3) N (3) C N (4) 2.16 (3) N (5) C N (5) C 2.51 (3) C (5) C Atom 2 Atom 3 Angle Atom 1 Atom 2 Re (1)* N (1) 97.8 (6) Re (1) N (1) Re (1)* N (2) 92.6 (7) Re (1) N (2) Re (1)* N (5) 176.6 (6) Re (1) N (5) C (1) C (2) 179 (4) N (2) C (3)	Re (1)	Re (1)*	2.259	(4)	~	4 (1)	C (1)	1.06 (3)
N (4) 2.16 (3) N (5) C N (5) 2.51 (3) C (5) C Atom 2 Atom 3 Angle Atom 1 Atom 2 Re (1)* N (1) 97.8 (6) Re (1) N (1) Re (1)* N (2) 92.6 (7) Re (1) N (2) Re (1)* N (5) 176.6 (6) Re (1) N (5) C (1) C (2) 179 (4) N (2) C (3)	Re (1)	N (2)	2.02 (3)		V (3)	C (5)	1.18 (3)
N (5) 2.51 (3) C (5) C Atom 2 Atom 3 Angle Atom 1 Atom 2 Re (1)* N (1) 97.8 (6) Re (1) N (1) Re (1)* N (2) 92.6 (7) Re (1) N (2) Re (1)* N (5) 176.6 (6) Re (1) N (5) C (1) C (2) 179 (4) N (2) C (3)	Re (1)	N (4)	2.16 (3)		V (5)	C (9)	1.09 (3)
Atom 2 Atom 3 Angle Atom 1 Atom 2 Re (1)* N (1) 97.8 (6) Re (1) N (1) Re (1)* N (2) 92.6 (7) Re (1) N (2) Re (1)* N (5) 176.6 (6) Re (1) N (5) C (1) C (2) 179 (4) N (2) C (3)	Re (1)	N (5)	2.51 (3)	•	C (5)	C (6)	1.37 (4)
Re (1)* N (1) 97.8 (6) Re (1) N (1) Re (1)* N (2) 92.6 (7) Re (1) N (2) Re (1)* N (5) 176.6 (6) Re (1) N (5) C (1) C (2) 179 (4) N (2) C (3)	Atom 1	Atom 2	Atom 3	Angle	Atom 1	Atom 2	Atom 3	Angle
Re (1)* N (2) 92.6 (7) Re (1) N (2) Re (1)* N (5) 176.6 (6) Re (1) N (5) C (1) C (2) 179 (4) N (2) C (3)	Re (1)	Re (1)*	N (1)	(9) 8.76	Re (1)	N (1)	C (1)	170 (3)
Re (1)* N (5) 176.6 (6) Re (1) N (5) C (1) C (2) 179 (4) N (2) C (3)	Re (1)	Re (1)*	N (2)	92.6 (7)	Re (1)	N (2)	C (3)	176 (2)
C(1) C(2) 179 (4) N(2) C(3)	Re (1)	Re (1)*	N (5)	176.6 (6)	Re (1)	N (5)	C (9)	168 (3)
	Re (1)	C (1)	C (2)	179 (4)	N (2)	C (3)	C (4)	172 (3)

Table 7. Selective Bond Distances (Å) and Angles (deg) for the [Mo₆O₁₉]². Anion.

Atom 1	Atom 2	Distance	v		Atom 1	Atom 2	Distance
Mo (3)	0 (14)	1.63 (2)			Mo (3)	0 (5)	1.81 (2)
Mo (3)	0 (1)	2.28 (2)			Mo (3)	0 (8)	1.97 (2)
Mo (4)	0 (15)	1.70 (2)			Mo (6)	0 (4)	1.91 (2)
Mo (5)	0(1)	2.36 (2)	(Mo (6)	0 (17)	1.98 (3)
Atom 1	Atom 2	Atom 3	Angle	Atom 1	Atom 2	Atom 3	Angle
Mo (1)	0 (1)	Mo (2)	(7) 0.06	Mo (5)	0 (1)	Mo (6)	89.1 (8)
Mo (2)	0(1)	Mo (3)	90.8 (8)	Mo (1)	0 (1)	Mo (4)	178.1 (9)
Mo (3)	0(1)	Mo (4)	90.5 (7)	Mo (2)	0 (1)	Mo (6)	178 (1)
Mo (4)	0(1)	Mo (5)	(7) 6.88	Mo (3)	0 (1)	Mo (5)	179.4 (9)



showing the atom labeling scheme. Unlabeled atoms are related to labeled Figure 31. ORTEP drawing of [Re₂(NCCH₃)₈(CH₃CN)₂][Mo₆O₁₉]₂, ones by a two-fold axis at the midpoint of the Re-Re* bond.

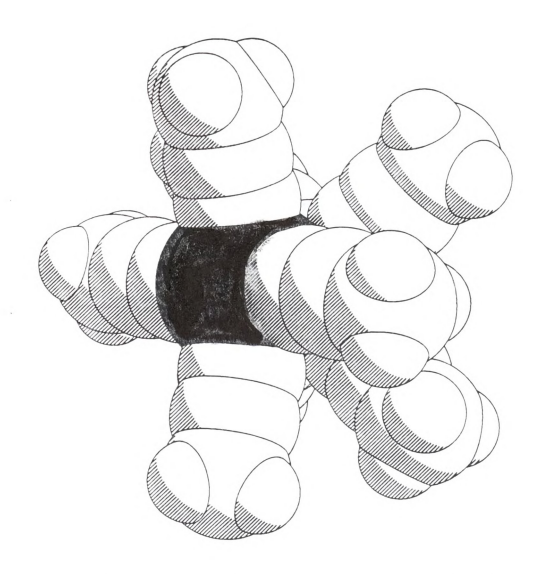


Figure 32. Computer generated space-filling model of the $[Re_2(NCCH_3)8]^{4+}$ cation. The Re atom is denoted by the black ball.



dirhenium species resides in pseudo-octahedral sites formed by the $[Mo_6O_{19}]^{2-}$ units; this denotes the lattice structure similar to that of fluorite.

The structure of the anion consists of an octahedral arrangement of Mo^{VI} ions with each molybdenum bound to the central oxygen assigned as O1. Additionally, each Mo atom bonds with one terminal oxygen and four bridging oxygens that form the faces of the polyhedra. Each molybdenum atom adopts a distorted octahedral geometry; the average Mo-O distances of 1.67 Å (Mo-O_t), 2.31 Å (Mo-O_c), and 1.93 Å (Mo-O_b) correlate well with the distances reported for the *n*-tetrabutylammonium salt [49]. Four molecules of acetonitrile solvent reside within the lattice of the crystal, of which several are disordered; attempts to model the disorder in a chemically sensible manner proved unsatisfactory. Two molecules of water are positioned near a bridging and terminal oxygen of the polyoxoanion (3.32(5) Å, 3.51(4) Å).

C. $[Rh_2(NCCH_3)_{10}][BF_4]_4$

(i) Data Collection and Reduction.

Investigations of the reactions of $[Rh_2(NCCH_3)_{10}][BF_4]_4$ led to the discovery that the molecule crystallizes in two different crystallographic symmetries. Initial reports revealed the crystal system to be monoclinic with dimensions a = 18.123(2) Å, b = 29.287(4) Å, c = 12.690(4) Å, $\beta = 99.58(1)^0$ [10]. Recrystallization of the complex from a CH_3CN/CH_2Cl_2 solvent mixture produced a crystal of orthorhombic symmetry with cell dimensions: a = 22.982(4) Å, b = 29.287(4) Å, c = 12.690(4) Å. The space group was determined to be Fddd (#70) based on the systematic absences of hkl: h + k, k + l, (h + l); Okl: $(k + l) \neq 4n$;

h01: $(h+1) \neq 4n$; hk0: $(h+k) \neq 4n$. Geometric and intensity data were obtained on a Rigaku AFC6-S diffractometer equipped with Mo K_{α} radiation ($\lambda_{\overline{\alpha}}$ = 0.71069 Å) at room temperature. An automatic search routine was used to locate 23 reflections in the range $18 \leq 2\Theta \leq 21.16^{\circ}$.

Data reduction was carried out with the use of well-established computational procedures. An ω -2 Θ scan motion was used to scan 2072 data points in the range $4 \le 2\Theta \le 50^{\circ}$. Structure factors were obtained after Lorentz and polarization corrections. During intensity data collection three check reflections were measured at regular intervals; an average loss in intensity of -14 % was observed; a linear correction factor was applied to correct for this. Azimuthal scans of three reflections with Eulerian angle χ near 90° were used as a basis for an empirical absorption correction; DIFABS was applied, and resulted in transmission factors ranging from 0.631 to 1.00. After averaging equivalent reflections, there remained 1084 reflections with $F_0^2 > 3\sigma(F_0^2)$.

(ii) Structure Solution and Refinement.

The structure was solved by direct methods [50]. The position of the unique Rh atom was obtained by the application of DIRDIF [48]. A sequence of successive difference Fourier maps and least-squares cycles led to full development of the coordination sphere. The final full-matrix refinement involved 76 variable parameters and 1084 observed reflections, for a data-to-parameter ratio of 14.26. The refinement converged with residuals of R = 0.088 and $R_w = 0.116$ and quality-of-fit 4.10. The largest parameter shift was 0.26 times its esd. The maximum and minimum peaks

on the final difference Fourier map corresponded to 0.93 and -0.94 e/Å³ respectively.

(iii) Molecular Structure.

Red needles of [Rh₂(NCCH₃)₁₀][BF₄]₄ were grown from a CH₃CN/CH₂Cl₂ solvent mixture; they were of a higher crystallographic symmetry than the previously reported structure. The crystallographic data are shown in Table 8 and selected bond distances and angles are given in Table 9 for both of the adopted symmetries. In the case of the orthorhombic system, a slight decrease of bond distances and angles was observed in comparison to the monoclinic structural solution. Axial acetonitrile ligands are disordered in the orthorhombic structure, and each carbon atom was found to occupy two positions related by a two-fold rotation of the molecule along the axial N-Rh-Rh-N axis. An ORTEP plot of the molecule generated from the orthorhombic system is depicted in Figure 33.

D. $[Rh_2(NCCH_3)_{10}][Mo_6O_{19}]_2 \cdot 4CH_3CN$

(i) Data Collection and Reduction.

An orange crystal of approximate dimensions $0.96 \times 0.10 \times 0.07 \text{ mm}^3$ was mounted on a glass fiber with petroleum oil, and cooled to -75 ± 1 °C in a nitrogen cold stream on a Nicolet P3/F upgraded to a Siemens P3/V diffractometer equipped with graphite monochromated Cu K α radiation ($\lambda_{\bar{\alpha}} = 1.54184 \text{ Å}$) and a low temperature device. Cell parameters of a = 18.457(2) Å, b = 22.723(2) Å, c = 17.190(2) Å, b = 90.07(1)° were determined from 25 reflections with $40 \le 2\Theta \le 60°$; axial photographs confirmed this assignment. The space group was determined to be C2/c (#15) based on the systematic absences of hkl: (h + k) $\ne 2n$;

Table 8. Crystal Data for [Rh₂(NCCH₃)₁₀][BF₄]₄

Formula	C ₂₀ H ₃₀ B ₄ N ₁₀ F ₁₆ Rh ₂
Formula weight	963.55
Crystal system	orthorhombic
Space group	Fddd (#70)
a, Å	22.982 (4)
b, Å	29.287 (4)
c, Å	12.690 (4)
α , deg	90
β, deg	90
γ, deg	90
v, A ³	8542 (5)
Z	8
dcalc, g/cm ³	1.498
μ (Mo Kα), cm ⁻¹	8.54
Radiation (monochromated in incident beam)	Mo K _{α} ($\lambda_{\overline{\alpha}} = 0.71069 \text{ Å}$)
Data collection instrument	Rigaku AFC6-S
Scan Method	ω - 2 0
Temperature, °C	23
Trans. factors, max., min.	1.00, 0.6311
Ra	0.088
R _w b	0.116

 $[\]overline{a_{R} = \Sigma \mid |F_{O}| - |F_{C}| / \Sigma |F_{O}|}$

 $b_{\mathbf{R}_{\mathbf{W}}} = [\Sigma \mathbf{w} \mid \mathbf{F}_{\mathbf{O}} \mid - \mid \mathbf{F}_{\mathbf{C}} \mid) 2/\Sigma \mathbf{w} \mid \mathbf{F}_{\mathbf{O}} \mid 2] 1/2; \ \mathbf{w} = 1/\sigma^2(\mid \mathbf{F}_{\mathbf{O}} \mid)$

Table 9. Selected Bond Distances (Å) and Angles (deg) for the Molecular [Rh₂(NCCH₃)₁₀]⁴⁺ Cation Derived from Orthorhombic and Monoclinic Crystal Systems.

Atom 1	Orthorhombic Atom 2	Distance			Δtom 1	Monoclinic	
					1 11000	A10111 2	Distance
Rh (1)	Rh (1)*	2.619 (4)			Rh (1)	Rh (1)*	2.624 (1)
Rh (1)	N (1)	1.94 (2)			Rh (1)	N (1)	1.986 (4)
Rh (1)	N (3)	2.14 (3)			Rh (1)	N (5)	2.191 (5)
N (1)	C(1)	1.12 (3)			Z (E)	C(1)	1.131 (5)
C (1)	C (2)	1.55 (3)			C(1)	C (2)	1.460 (7)
	Orthorhombic					Monoclinic	
Atom 1	Atom 2	Atom 3	Angle	Atom 1	Atom 2	Atom 3	Angle
Rh (1)	Rh (1)*	N (3)	180.00	Rh (1)	Rh (1)*	N (5)	178.1 (1)
Rh (1)	N (1)*	C(1)	173 (2)	Rh (1)	N (!)	C (1)	176.2 (4)
Rh (1)	N (3)	C (5)	144 (2)	Rh (1)	N (5)	C (9)	166.1 (5)

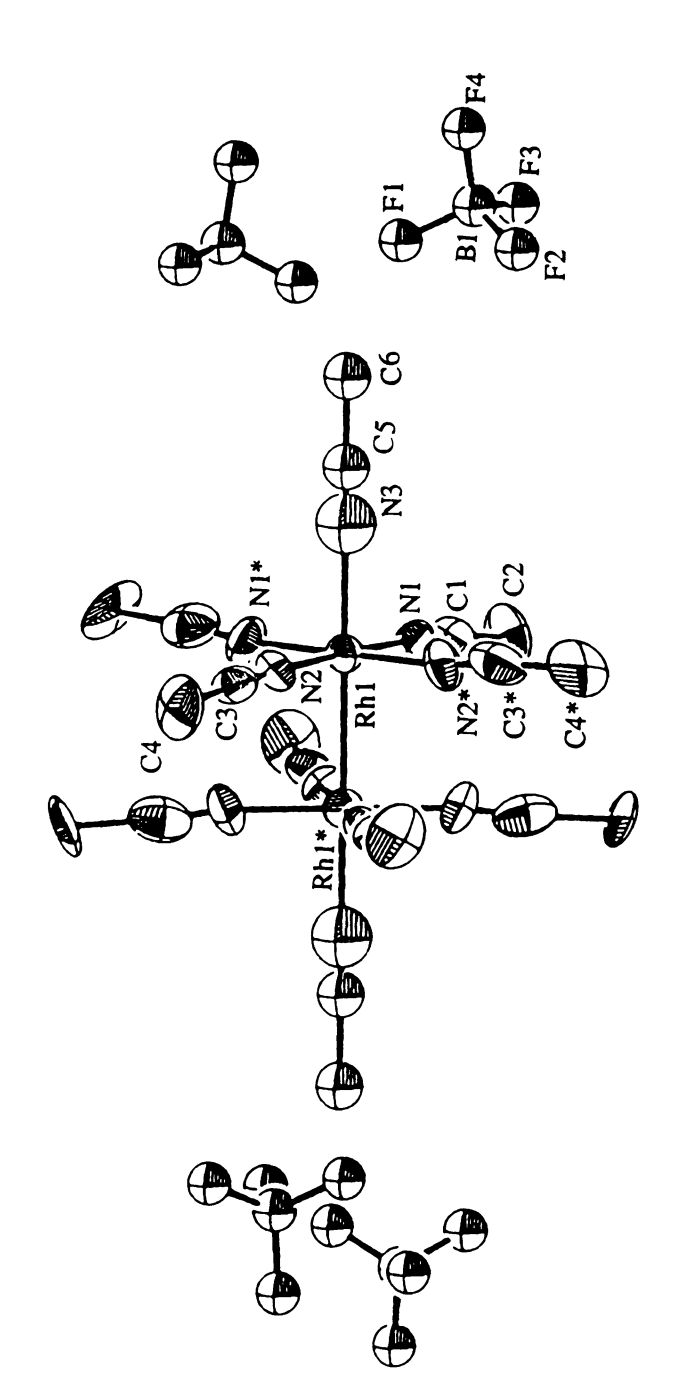


Figure 33. ORTEP diagram of $[Rh_2(NCCH_3)_{10}][BF_4]_4$ in an orthorhombic crystal system.

h0l: $1 \neq 2n$. Intensity data were collected using an ω scan mode in the range $4 \leq 2\Theta \leq 114^{\circ}$ with a scan speed of 4° /min. Three standard reflections measured at constant intervals showed no significant decay in intensities. Data were corrected for Lorentz and polarization effects. A linear absorption correction was applied based on Ψ scans of three reflections with χ near 90°. The program DIFABS [51] was applied to the data to account for electron density that was not corrected by the initial absorption correction and resulted in transmission factors from 0.39 to 1.00.

(ii) Structure Solution and Refinement.

The structure was solved by direct methods [47]. The positions of heavy atoms were located by DIRDIF [48], and a sequence of successive difference Fourier maps and least-squares cycles led to the location of the remaining non-hydrogen atoms. The final full-matrix refinement involved 389 variable parameters and 3772 observed reflections with $F_0^2 > 3\sigma(F_0^2)$ for a data-parameter ratio of 9.70. The refinement converged with residuals of R = 0.079 and $R_w = 0.051$ and goodness of fit 3.90.

(iii) Molecular Structure.

Crystallographic data for this complex are listed in Table 10. Selected bond distances and angles for the cation and anion are shown in Table 11. Figure 34 depicts an ORTEP plot of the complex. The complex contains four molecules of acetonitrile within its lattice; several are disordered, and attempts to model the disorder proved unsatisfactory. The cation adopts the configuration of its precursor; the Rh(CH₃CN)₄ units are rotated by $\chi_{av} = 45$ [8]^o from an eclipsed geometry. The slight differences

Table 10. Crystal Data for [Rh₂(NCCH₃)₁₀][Mo₆O₁₉]₂ • 4CH₃CN

Formula	C36H42N14O38Mo12Rh2
Formula weight	2636.03
Crystal system	monoclinic
Space group	C2/c (#15)
a, Å	18.457 (2)
b, Å	22.723 (2)
c, Å	17.190 (2)
α, deg	90
β , deg	90.07 (1)
γ, deg	90
v, Å ³	7209 (2)
Z	4
dcalc, g cm ⁻³	2.301
Crystal size, mm	0.959 x 0.104 x 0.065
μ (Cu Kα), cm ⁻¹	213.470
Radiation (monochromated in incident beam)	Cu K_{α} ($\lambda_{\overline{\alpha}} = 1.54184 \text{ Å}$)
Data collection instrument	P3/V
Scan method	ω
Temperature, °C	-75
Trans. factors, max., min.	1.00, 0.3917
Ra	0.079
R _w b	0.059

 $[\]overline{a_{R} = \Sigma \mid |F_{O}| - |F_{C}| / \Sigma |F_{O}|}$

 $^{{}^{}b}R_{\mathbf{w}} = [\Sigma \mathbf{w} \mid F_{0} \mid - \mid F_{c} \mid) 2/\Sigma \mathbf{w} \mid F_{0} \mid 2] 1/2; \ \mathbf{w} = 1/\sigma^{2}(\mid F_{0} \mid)$

Table 11. Selected Bond Distances for [Rh₂(NCCH₃)₁₀][Mo₆O₁₉]₂ • 4CH₃CN.

Atom 1	Atom 2	Distance	Atom 1	Atom 2	Atom 3	Angle
Rh (1)	Rh (1)*	2.616 (3)	(I) N	Rh (1)	N (2)	90.1 (6)
Rh (1)	N (1)	1.97 (2)	Rh (1)	N (2)	C (3)	175 (2)
Rh (1)	N (3)	2.15 (2)	N (3)	C (4)	C (7)	179 (2)
N (1)	C(2)	1.12 (2)	Rh (1)	Rh (1)*	N (3)	177.5 (5)
C(1)	C (10)	1.52 (3)				
Mo (1)	0 (1)	2.31 (1)	Mo (1)	0(1)	Mo (2)	179.4 (6)
Mo (1)	0 (8)	1.68 (2)	Mo (2)	0(1)	Mo (3)	90.6 (4)
Mo (1)	0 (15)	1.94 (1)	Mo (4)	0 (1)	Mo (5)	90.3 (4)
Mo (1)	0 (18)	1.92 (1)	Mo (5)	0(1)	Mo (6)	89.5 (4)

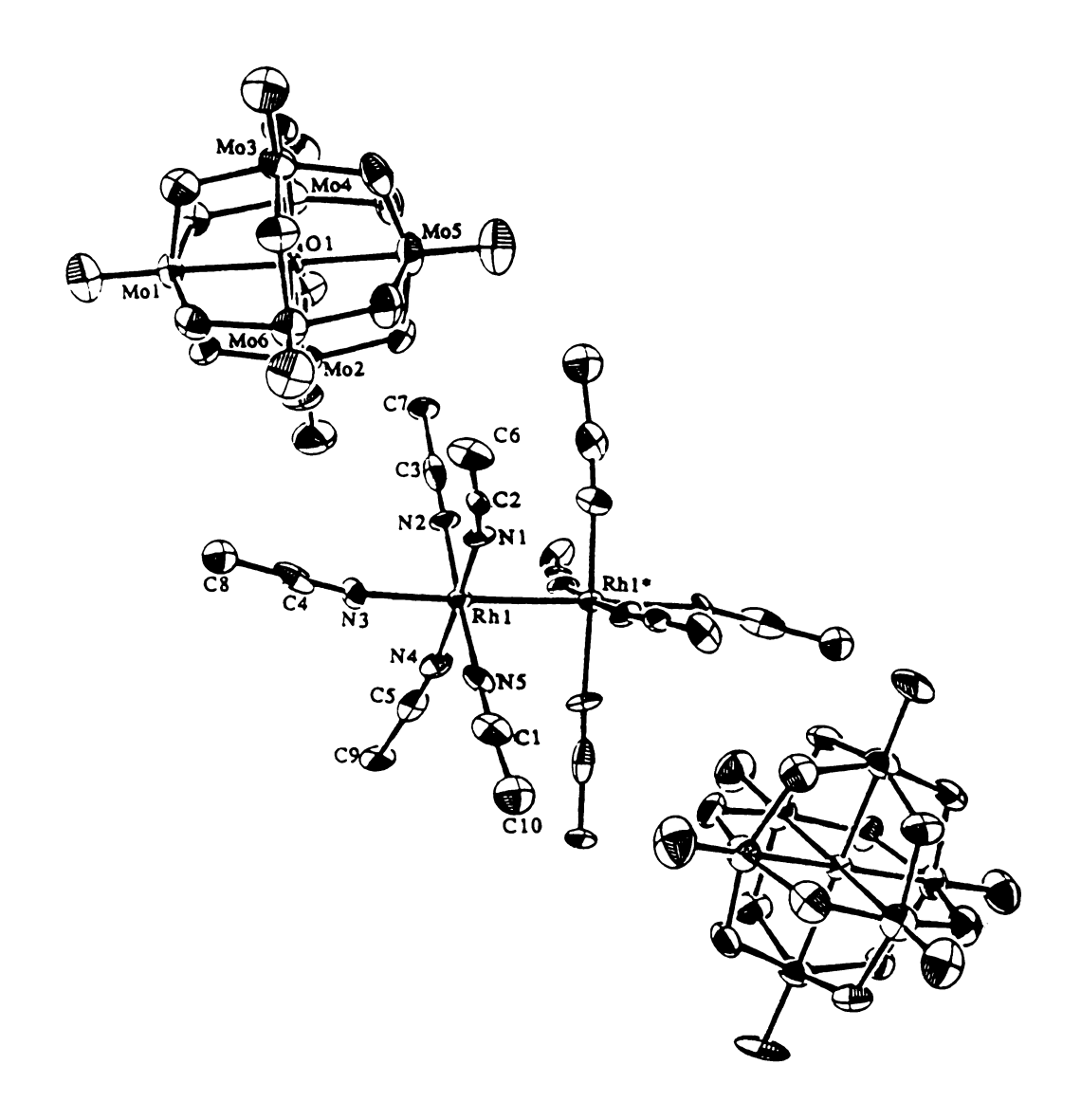


Figure 34. ORTEP diagram of $[Rh_2(NCCH_3)_{10}][Mo_6O_{19}]_2$ showing the atom labeling scheme. Unlabeled atoms are related to labeled ones by a two-fold axis at the midpoint of the Rh-Rh* bond.

in distances and angles may be attributed to crystal packing forces. The bond distances for the molecular anion $[Mo_6O_{19}]^{2-}$ are The slight differences in distances and angles may be attributed to crystal packing forces. The bond distances for the molecular anion $[Mo_6O_{19}]^{2-}$ are in good agreement with the *n*-tetrabutylammonium salt; the average distances are 1.69 Å, 2.31 Å, and 1.93 Å, for Mo-O_t, Mo-O_c, and Mo-O_b, respectively.

E. $[Rh(\eta^3-TMPP)_2][W_6O_{19}] \cdot 4CH_3CN$

(i) Data Collection and Refinement.

A purple crystal of approximate dimensions 0.60 x 0.21 x 0.18 mm³ was mounted on a glass fiber with vacuum grease, and cooled to -90 °C in a nitrogen cold stream on a Nicolet P3/F upgraded to a Siemens P3/V diffractometer equipped with graphite monochromated Mo K_{α} radiation ($\lambda_{\bar{\alpha}} = 0.71073$ Å). Cell parameters of a = 25.782(5) Å, $b = 11.862(2) \text{ Å}, c = 26.5345(4) \text{ Å}, \beta = 102.19(1)^{\circ}$ were determined from 25 reflections with $20 \le 2\Theta \le 26^{\circ}$. The space group was determined to be P2/c (#13) based on the systematic absence of h0l: $1 \neq 2n$. Intensity data were collected using the ω -scan mode in the range $4 \le 2\Theta \le 50^{\circ}$ with a scan speed of 4°/min. Structure factors were obtained after Lorentz and polarization corrections. Due to the extensive amount of absorption, a linear absorption correction was applied based on Y scans of three reflections with χ near 90° In addition, an empirical absorption correction using the program DIFABS [51] was applied which resulted in transmission factors of 0.204 to 1.00. During data collection, the intensities of three check reflections were measured every 100 reflections and revealed that the crystal had slightly decayed; a linear correction factor was applied to the data to account for this After averaging equivalent reflections, there remained 7148 reflections with $F_0^2 > 3\sigma(F_0^2)$.

(ii) Structure Solution and Refinement.

The structure was solved by direct methods [47]; the heavy atoms were found by the program DIRDIF [48]. A sequence of successive difference Fourier maps and least-squares cycles led to the full-matrix refinement. The program DIFABS [51] was applied to the data after the heavy atoms were found due to the extreme amount of radiation the crystal had absorbed. The final full-matrix refinement involved 491 parameters and 7148 observations. The refinement converged with residuals of R = 0.06 and $R_w = 0.046$ and goodness-of-fit of 3.49. The largest shift/esd in the final cycle was 0.34.

(iii) Molecular Structure.

Crystallographic data are given in Table 12, and Table 13 shows some important bond distances and angles for the complex. Crystals of purple needles were grown overnight in an acetonitrile solution of the starting materials, in which one was chosen for a crystallographic determination. An ORTEP plot is depicted in Figure 35. The $[W_6O_{19}]^{2-}$ anion resides on a special position containing a two-fold symmetry, and the cation is situated on a general position. The Rh atom adopts a pseudo-octahedral geometry with bond distances and angles comparable to the starting material [45]. The $[W_6O_{19}]^{2-}$ anion contains the same geometry as the analogous Mo polyoxoanion. The average W-O distances are 1.74 Å, 2.325 Å, 1.93 Å for the terminal, central, and bridging oxygens, respectively. Figure 36 depicts a packing diagram of the complex.

Table 12. Crystal Data for $[Rh(\eta^3-TMPP)_2][W_6O_{19}] \cdot 4CH_3CN$

Formula	C ₆₂ H ₇₈ N ₄ O ₃₇ P ₂ RhW ₆
Formula weight	2739.26
Crystal system	monoclinic
Space group	P2/c (#13)
a, Å	25.782 (5)
b, Å	11.862 (2)
c, Å	26.534 (4)
α, deg	90
β , deg	102.19 (1)
γ, deg	90
v, Å ³	7932 (4)
Z	4
d _{calc} , g cm ⁻³	2.294
μ (Mo Kα), cm ⁻¹	91.806
Radiation (monochromated in incident beam)	Mo K _{α} ($\lambda_{\overline{\alpha}} = 0.71073 \text{ Å}$)
Data collection instrument	P3/V
Scan method	ω
Temperature, °C	-90
Trans. factors, max., min.	1.00, 0.2044
Ra	0.060
R_w^b	0.046

 $a_R = \Sigma \mid |F_0| - |F_c| |/\Sigma |F_0|$

 $^{{}^{}b}R_{w} = [\Sigma w \mid F_{o} \mid - \mid F_{c} \mid)^{2}/\Sigma w \mid F_{o} \mid^{2}]^{1/2}; w = 1/\sigma^{2}(\mid F_{o} \mid)$

Table 13. Some Important Bond Distances (Å) and Angles (deg) for [Rh(η³-TMPP)₂][W₆O₁₉].

	Atom 2	Distance			Atom 1	Atom 2	Distance
Rh (1)	P (1)	2.208 (7)			P(1)	C (1)	1.82(3)
Rh (1)	P (2)	2.214 (6)			W(1)	0(1)	1.75 (2)
Rh (1)	0 (4)	2.34 (1)			W(1)	O (8)	2.321 (1)
Rh (1)	0 (3)	2.42 (2)			W(1)	0 (12)	1.98 (2)
Atom 1	Atom 2	Atom 3	Angle	Atom 1	Atom 2	Atom 3	Angle
P (1)	Rh (1)	P (2)	102.4 (2)	W (1)	0 (1)	W (1)	178 (2)
P (1)	Rh (1)	O (4)	172.0 (5)	W (1)	0 (1)	W (2)	180.00
0 (4)	Rh (1)	0 (5)	103.2 (6)	W (3)	0 (1)	W (4)	89.93 (5)

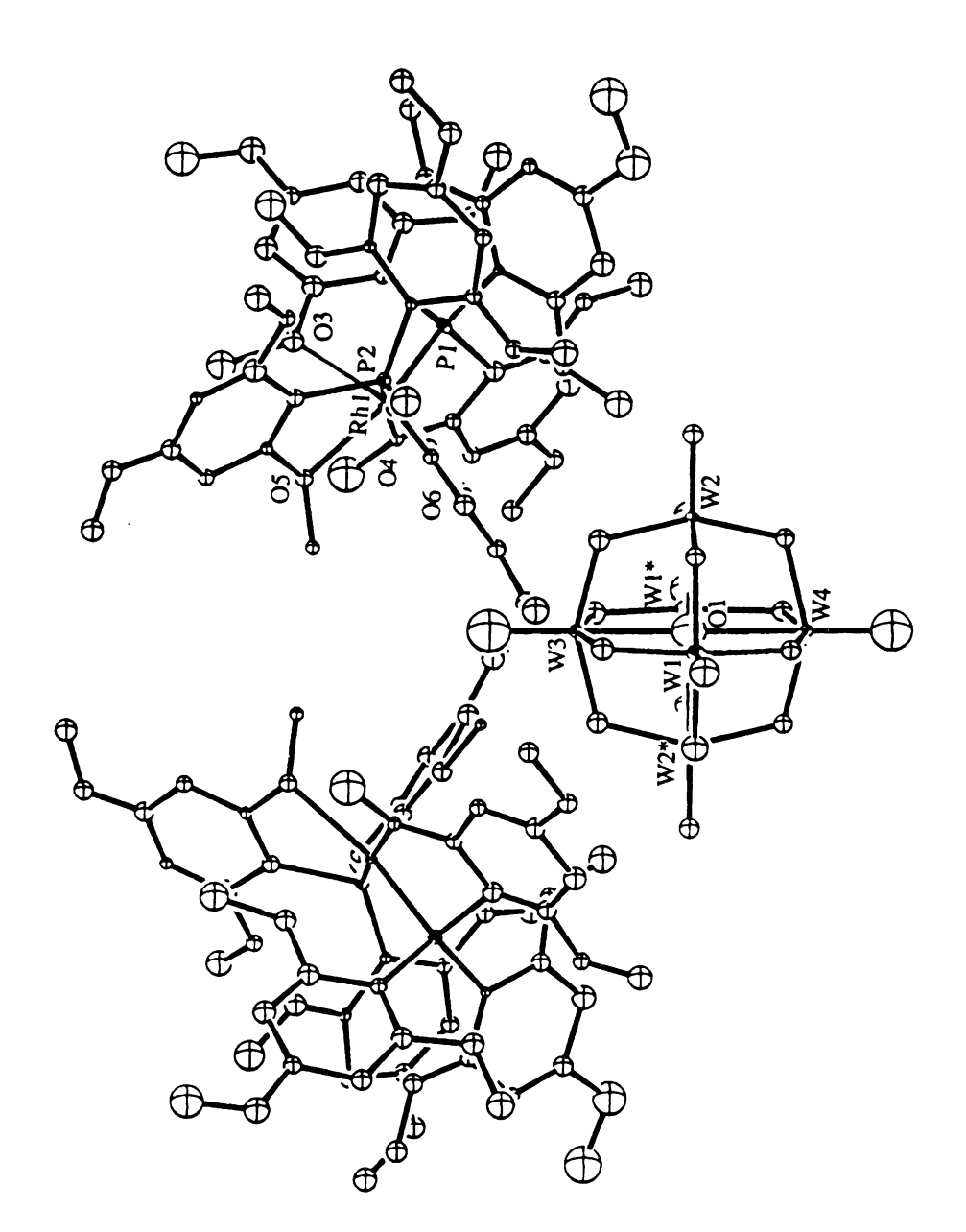


Figure 35. ORTEP drawing of $[Rh(\eta^3-TMPP)_2][W_6O_{19}]$. The $[W_6O_{19}]^2$ anion resides on a site of two-fold symmetry.

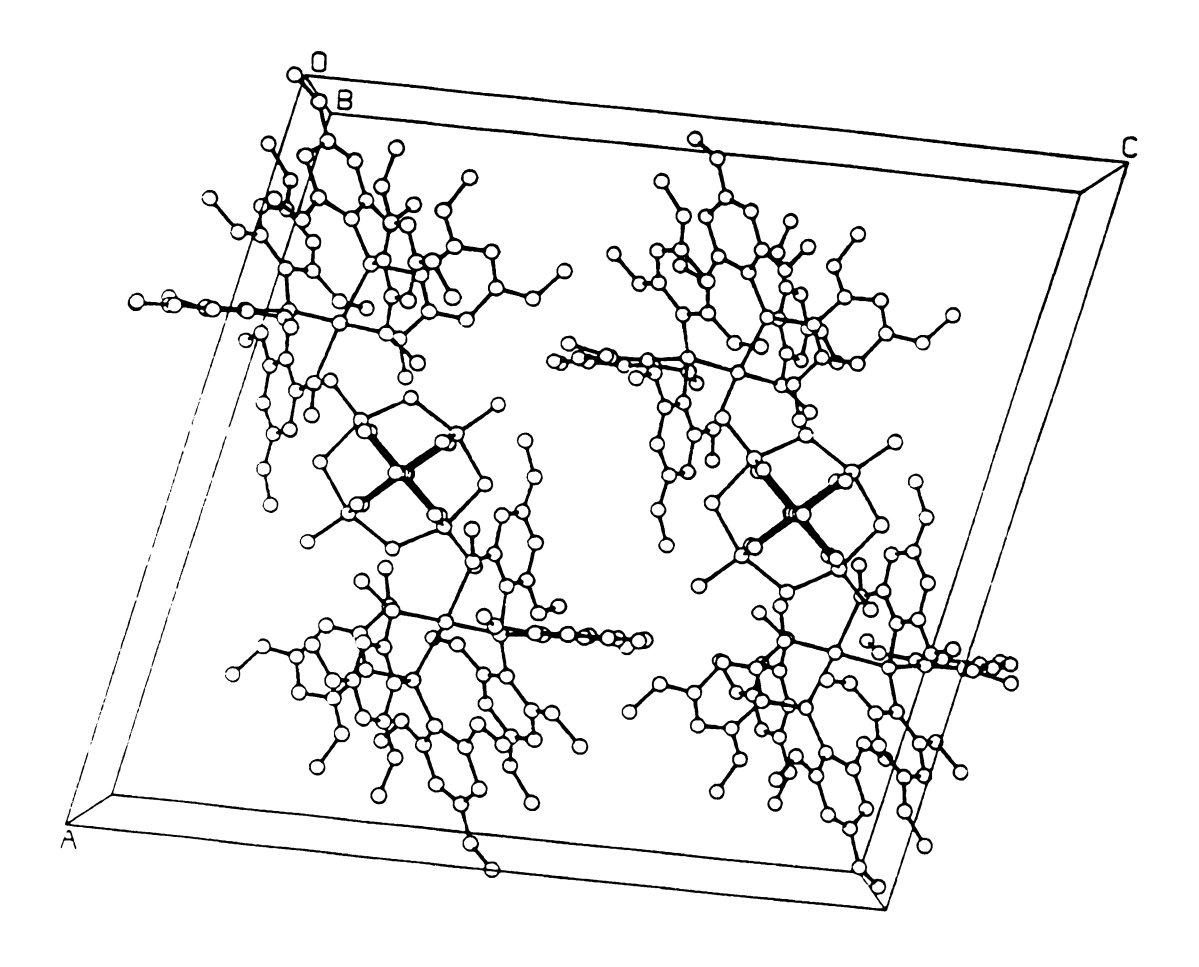


Figure 36. A view of a packing diagram of $[Rh(h^3-TMPP)_2][W_6O_{19}]$ along the b - axis.

F. $[Rh(\eta^3-TMPP)_2][Mo_6O_{19}] \cdot 4CH_3CN$

(i) Data Collection and Reduction.

A purple crystal of dimensions 1.4 x 0.10 x 0.08 mm was mounted on a glass fiber with vacuum grease and placed under a cooled nitrogen stream at - 90 °C. All measurements were performed on a Rigaku AFC6-S diffractometer with monochromated Mo K_{α} ($\lambda_{\overline{\alpha}} = 0.71069 \text{ Å}$). Cell constants were obtained using 21 centered reflections in the range $11 \le$ $2\Theta < 26^{\circ}$ and corresponded to a monoclinic cell with dimensions: a =25.792(8) Å, b = 11.846(8) Å, c = 26.542(6) Å, β = 102.03(2)°. The space group was determined to be P2/c (#13) based on the systematic absence of h0l: $1 \neq 2n$. The data were collected using the ω -scan technique to a maximum 2Θ value of 50° at 4°/min (in omega), of which 14707 were unique. The intensities of three representative reflections were measured after every 97 reflections decreased by - 2.4%, and a correction factor was applied to the data to account for this. An empirical absorption correction based on azimuthal scans of several reflections of χ near 90° was applied and resulted in transmission factors ranging from 0.92 to 1.00. The data were corrected for Lorentz and polarization effects.

(ii) Structure Solution and Refinement.

The structure was solved by direct methods [47]; positions of heavy atoms were obtained by DIRDIF [48]. The cycle of full matrix least-squares refinement was based on 3870 observed reflections with $F_0^2 > 3\sigma(F_0^2)$. Unfortunately the structure could not be completely refined due to problems arising from the length of the platelet crystal in comparison to the width of the X-ray beam of the diffractometer. Crystallographic data for the complex are listed in Table 14.

Table 14. Crystal Data for $[Rh(\eta^3-TMPP)_2][Mo_6O_{19}] \cdot 4CH_3CN$

Formula	C ₆₂ H ₇₈ N ₄ O ₃₇ P ₂ Mo ₆ Rh
Formula weight	2211.80
Space group	monoclinic
Crystal system	P2/c (#13)
a, Å	25.792(8)
b, Å	11.846(8)
c, Å	26.542(6)
α, deg	90
β , deg	102.03(2)
γ, deg	90
v, Å ³	7931(10)
Z	4
dcalc, g/cm ³	1.852
Crystal size, mm ³	1.420 × 0.104 × 0.078
μ (Mo Kα), cm ⁻¹	12.25
Radiation (monochromated in incident beam)	Mo K $_{\alpha}$ ($\lambda_{\vec{\alpha}} = 0.71069$)
Scan method	ω - 2 0
Temperature, °C	-100
Trans. factors, max., min.	1.00, 0.92
R ^a	0.192
R _w b	0.235

 $a_R = \Sigma \mid |F_0| - |F_c| |/\Sigma |F_0|$

 $^{{}^{}b}R_{w} = [\Sigma w \mid F_{O} \mid - \mid F_{C} \mid) 2/\Sigma w \mid F_{O} \mid 2] 1/2; w = 1/\sigma^{2}(\mid F_{O} \mid)$



Chapter 4 CONCLUSIONS AND FUTURE OUTLOOK

The properties of dinuclear homoleptic acetonitrile complexes and their chemistry with isopolyoxometalates are of considerable interest in the context of affording a new class of materials that may serve as valuable catalysts. The reason for this is unquestionably due to the nature of the acetonitrile ligand, which can be easily removed from electrophilic metal centers. Furthermore, polyoxometalates provide an oxymetalate cluster lattice that incorporates these metal centers in their interstitial sites that can exhibit intercluster chemistry. These properties may enhance their catalytic capabilities in that these materials are now bifunctional [37].

Our efforts to extend the instances of homoleptic dinuclear acetonitrile complexes have been successful, and provide us with an opportunity to investigate their syntheses, properties, redox chemistry and solid state structures. As we have demonstrated, a homoleptic dinuclear acetonitrile complex of rhenium may be synthesized from reactions of $[(n-C_4H_9)N]_2[Re_2Cl_8]$ with tetrafluoroboric acid etherate solutions to form the reduced species. Subsequent X-ray structural studies have shown the crystals to be $[Re_2(NCCH_3)_8(axial-CH_3CN)_2]^{4+}$. This cation complex is easily characterized by infrared and ¹H NMR spectroscopies. Investigations of the electronic spectroscopy revealed two overlapping

features in the visible region of near equal intensity ($\varepsilon = 629 \text{ M}^{-1}\text{cm}^{-1}$), and several higher energy transitions. The assignments of these require detailed spectral studies coupled with molecular orbital calculations. The electrochemical properties of the complex indicate that reduction of the metal centers is very favorable, rather than an oxidation which would form an even more highly charged metal core.

Simple metathesis reactions of the acetonitrile complexes with isopolymetalates of formulae $[M_6O_{19}]^{2-}$ (M = Mo, W) and $[Mo_8O_{26}]^{4-}$ have complexes of general molecular formula afforded $[M'_2(NCCH_3)_x][M_6O_{19}]_2$ (x = 8, 10; M' = Re, Rh, Mo) and $[M'_2(NCCH_3)_x][Mo_8O_{26}]$ (M' = Rh, Mo). There are several key features to note about these new salts. One relates to the factors governing the crystallization of the complexes. Replacement of [BF₄] anions with the larger polyoxometalate counterions provides a favorable means of reducing the crystal symmetry for complexes that inherently prefer to crystallize in a high symmetry space group, thus finally providing us with a successful structural determination of the $[Re_2(NCCH_3)_8(CH_3CN)_2]^{4+}$ cation. The identities of these complexes were confirmed by X-ray diffraction techniques. Infrared spectroscopy also provides a good tool for identifying these species by the characteristic stretching frequencies which arise from the coordinated acetonitrile and the distinctive v(Mo-O) features exhibited by polyoxoanions. These new salts accommodate cations in which the metal atoms are very reactive by virtue of the facile removal of their weakly ligating acetonitrile ligands. When these complexes are heated, the acetonitrile is volatilized until the complex is completely desolvated, thereby forming new solid-state materials derived from molecular anionic metal oxide clusters. Desolvation of the rhodium and rhenium complexes

yields new amorphous materials of general formulae Rh_xMo_yO_z and Re_xMo_yO_z. To our knowledge, there exists only one example of a ternary rhodium oxide, whereas instances of such mixed ReMo oxides have never been reported [52]. The thermal decomposition of $[Mo_2(NCCH_3)_8][Mo_6O_{19}]_2$ results in significantly different observations from the others in this work. Formation of a highly crystalline blue solid of orthorhombic symmetry resulted, as evidenced by powder X-ray diffraction. The advantage of the present methods is that low temperature synthesis by desolvation of the precursor salts should provide a material wherein the constituent metals are evenly dispersed over the entire oxide surface, and with an exact stoichiometry of metals to oxide.

Finally, studies aimed at incorporating the mononuclear Rh(II) cation, $[Rh(\eta^3\text{-TMPP})_2]^{2+}$ within the polyoxometalate lattice resulted in the syntheses of the new salts $[Rh(\eta^3\text{-TMPP})_2][M_6O_{19}]$ (M = Mo, W). Upon reaction with carbon monoxide, the solid-state form of the mononuclear Rh(II) cation undergoes redox chemistry to form the now well-established Rh^{II} and Rh^{III} products [45], as well as what we speculate to be $[Rh(TMPP)_2(CO)]^{2+}$.

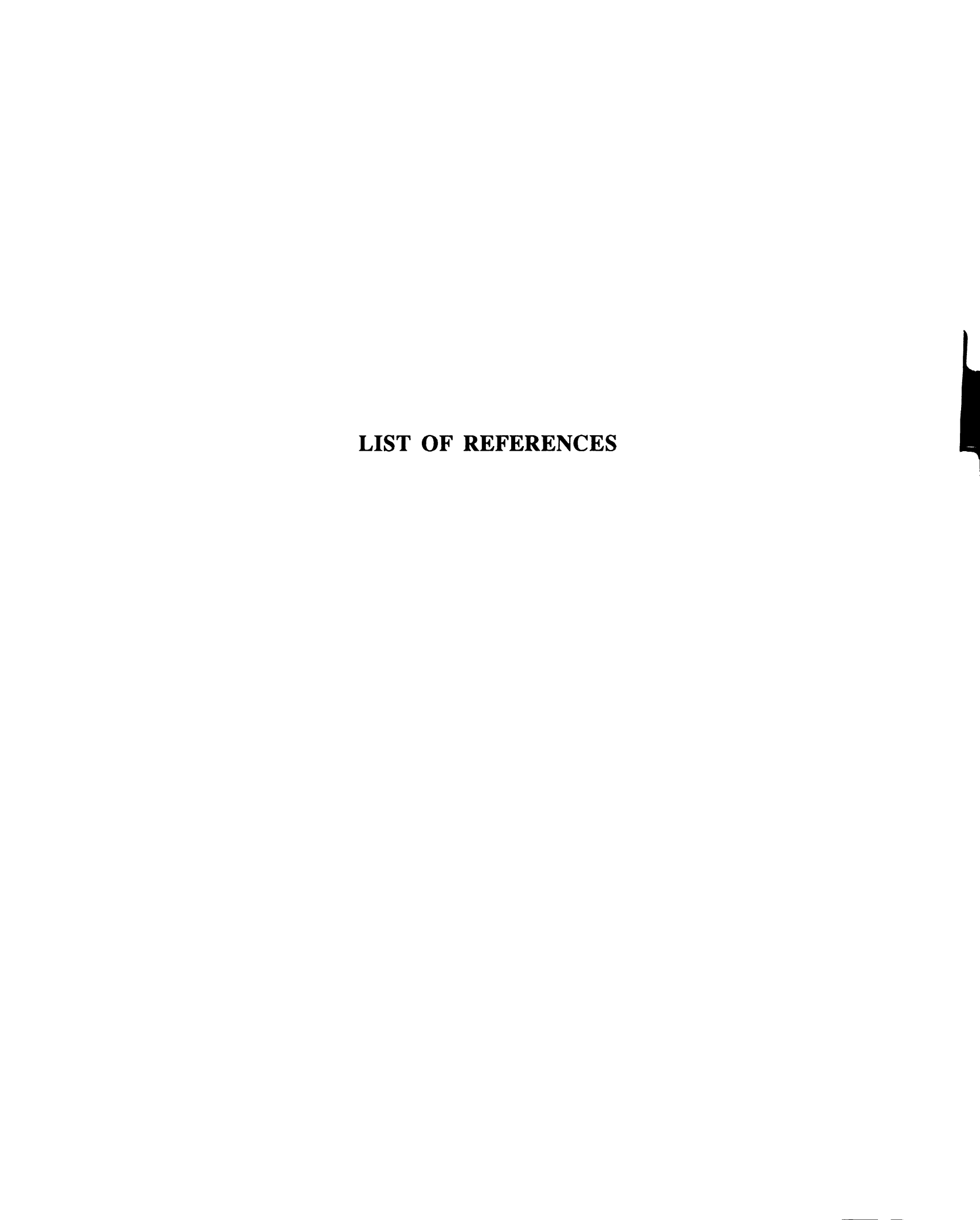
The results presented in this thesis are a promising beginning to a new area of research based on metal-metal bonded transition metal complexes and clusters. An attractive feature is the use of homoleptic acetonitrile complexes since they serve as excellent *in situ* starting materials for metal incorporation reactions. A modification of the preparation of the new acetonitrile species [Re₂(NCCH₃)₈]⁴⁺ is a major goal in order to obtain an optimum yield of product. An alternative route is to begin with an already reduced dinuclear Re₂⁴⁺ core, so precious metal would not be sacrificed during the reaction, as in the case of reactions beginning with

 $[Re_2Cl_8]^{2-}$. Starting materials such as $Re_2Cl_4(P^nBu_3)_4$ or $Re_2(O_2CCF_3)_4$ have an advantage since they contain ligands that may be labilized by reagents such as HBF_4 under similar reaction conditions to those used with $[Re_2Cl_8]^{2-}$.

Association of the isopoly metal oxide clusters with the acetonitrile cations extends their interesting characteristics. In this regard, crystallization of additional transition metal acetonitrile cations and polyoxometalate anions will expand this entirely new class of oxymetalates. Other areas of interest involve the incorporation of the acetonitrile cations, both mono- and dinuclear, into films derived from Ti or Zr network polymers that can lead to other desired catalytic properties [53]. Low temperature thermal degradation leading to loss of volatile organic groups is an effective technique for converting these films into new materials. Since characterization of the materials is difficult, techniques like extended X-ray absorption fine structure (EXAFS) and small angle neutron scattering, performed in collaboration with Dr. K. Prassides of the University of Sussex, will lend more insight into the structure of the amorphous materials including the fate of the M-M bonded unit in the oxide cluster framework. X-ray photoelectron spectroscopy (XPS) will be used as a complementary technique in order to observe the oxidation states of the metal atoms after thermal decomposition. Surface techniques like this may be performed in collaboration with Dr. J. Ledford at Michigan State University or at the Composite Materials Center on campus. Single crystal and powder X-ray diffraction will be employed whenever possible to elucidate structures of crystalline products acquired after thermal decomposition such as [Mo₂(NCCH₃)₈][Mo₆O₁₉]₂. One method that may be

successful to obtain a single crystal is a gradual heating of the sample, with subsequent slow cooling by use of a tube furnace.

The formation of clusters from acetonitrile precursors is practically limitless. Preliminary results have already been obtained from reactions of $[Rh_2(NCCH_3)_{10}][BF_4]_4$ with H_2S at low temperatures, as well as at room temperature. Currently there are only a handful of compounds formulated with rhodium and sulfur, and reactions of this type should prove extremely interesting for the synthesis of clusters. Interest in devising new mild low temperature routes into clusters will also be extended to chemistry with compounds containing metal-metal multiple bonds, since these have already proven to be excellent precursors for the formation of small clusters, in light of the condensation reactions reported by McCarley, et al. that lead to extended M-M bond network polymers [54].





LIST OF REFERENCES

- 1. Henke, W. Justus Liebigs Ann. Chem. 1858, 106, 280.
- (a) Walton, R. A. Q. Rev. Chem. Soc. 1965, 19, 126. (b)
 Storhoff, B.N.; Lewis Jr., H. C. Coord. Chem. Rev. 1977, 23, 1. (c)
 Davies, J. A.; Hartley, F. R. Chem. Rev. 1981, 81, 79.
- 3. (a) Zuur, A. P.; Groeneveld, W. L. Recl. Trav. Chim. Pays-Bas. 1967, 86, 1089. (b) Reedijk, J.; Groenveld, W.L. Recl. Trav. Chim. Pays-Bas. 1967, 86, 1103. (c) Reedijk, J.; Zuur, A. P.; Groenveld, W. L. Recl. Trav. Chim. Pays-Bas. 1967, 86, 1127. (d) Reedijk, J.; Groeneveld, W. L. Recl.Trav. Chim. Pays-Bas. 1968, 87, 513, 553, 1079. (e) Reedijk, J. Recl. Trav. Chim. Pays-Bas. 1969, 88, 86.
- (a) Hathaway, B.J.; Underhill, A. E. J. Chem. Soc. 1960, 3705.
 (b) Hathaway, B.J.; Holah, D. G.; Underhill, A. E. J. Chem. Soc. 1962, 2444.
 (c) Hathaway, B.J.; Holah, D. G. J. Chem. Soc. 1964, 2400.
- (a) Rapaport, I.; Helm, L.; Merbach, A. E.; Bernhard, P.; Ludi, A. Inorg. Chem. 1988, 27, 873. (b) Bown, M.; Fontaine, X. L. R.; Greenwood, N. N.; Kennedy, J. D.; Thornton-Pett, M. J. J. Chem. Soc. Dalton Trans. 1987, 1169. (c) Sen, A.; Lai, T-W. J. Am. Chem. Soc. 1981, 103, 4627. (d) Thomas, R. R.; Sen, A. Inorg. Synth. 1989, 26, 128. (e) Alesbury, C. K.; Symons, M. C. R. J. C. S. Faraday, I. 1980,

- 76, 244. (f) Nilsson, K.; Oskarsson, A. Acta., Chem. Scan. A. 1984, 38,
- 79. (g) Bruckner, A.; Vogt, H.; Riesel, L. Z. Chem. 1987, 27, 415.
- (h) De Renzi, A.; Panunzi, A.; Vitagliano, A.; Paiaro, G. J. Chem. Soc. Chem. Commun. 1976, 47. (i) Johnson, P. R.; Pratt, J. M.; Tilley, R. I. J. Chem. Soc. Chem. Commun. 1978, 606.
- 6. Thomas, R. R.; Chebolu, V.; Sen, A. J. Am. Chem. Soc. 1986, 108, 4096.
- 7. Mayer, J. M.; Abbott, E. H. *Inorg. Chem.* 1983, 22, 2774.
- 8. Cotton, F. A.; Wiesinger, K. J. Inorg. Chem. 1991, 30, 871.
- 9. (a) Bowen, A. R.; Taube, H. J. Am. Chem. Soc. 1971, 93, 3287.
- (b) Inorg. Chem. 1974, 13, 2245.
- 10. Dunbar, K. R. J. Am. Chem. Soc. 1988, 110, 8247.
- 11. Baranovskii, I. B.; Zhilyaev, A. N.; Dikareva, L. M. Russ. J. Inorg. Chem. 1988, 33, 1802.
- 12. (a) Ibrahim, M. A.; Michl, J. "Towards a Square-Grid Polymer Using a Molecular Size Tinkertoy' Construction Set." 201st ACS National Meeting, Division of Polymer Chemistry, Atlanta, Georgia, April 14 19, 1991. (b) Shin, Y. Ph. D. Dissertation, Michigan State University, 1991; Shin, Y.; Nocera, D. J. Am. Chem. Soc. 1992, 114, 0000.
- 13. (a) Jiang, Z.; Sen, A. J. Am. Chem. Soc. 1990, 112, 9655. (b)
 Sen, A.; Lai, T-W. Inorg. Chem. 1984, 23, 3257. (c) J. Am. Chem.
 Soc. 1982, 104, 3520. (d) Organometallics. 1982, 1, 415. (e) J. Am.

- Chem. Soc. 1981, 103, 4627. (f) Sen, A.; Thomas, R. Organometallics. 1982, 1, 1251. (g) Sen, A. Acc. Chem. Res. 1988, 21, 421.
- 14. (a) Doyle, M. P. Acc. Chem. Res. 1986, 19, 348. (b) Chem. Rev. 1986, 86, 919.
- 15. (a) Misono, M. Catal. Rev. Sci. Eng. 1987, 29, 269. (b) Tanabe, K.; Misono, M.; Ono, Y.; Hattori, H. New Solid Acids and Bases, Elsevier, New York, 1989. (c) Urabe, K.; Tanake, Y.; Izumi, Y. Chem. Lett. 1985, 1595. (d) Izumi, Y.; Tanaka, Y.; Urabe, K. Chem. Lett. 1982, 679.
- 16. Pope, M. T.; Muller, Ä. Angew. Chem. Intl. Ed. Engl. 1991, 30, 34.
- 17. Berzelius, J. Pogg. Ann. 1826, 6, 369, 380.
- 18. (a) Marignac, C. C. R. Acad. Sci. **1862**, 55, 888. (b) Ann. Chim. **1862**, 25, 362.
- 19. (a) Keggin, J. F. Nature 1933, 131, 908. (b) Proc. Roy. Soc. A 1934, 144, 75.
- 20. Lipscomb, W. N. Inorg. Chem. 1965, 4, 132.
- 21. Pope, M. T. Heteropoly and Isopoly Oxometalates, Springer Verlag, New York, 1983.
- 22. Evans, H. T., Jr. Acta Cryst. 1974, B30, 2095.
- 23. Dexter, D. D.; Silverton, J. V. J. Am. Chem. Soc. 1968, 90, 3589.

- 24. (a) Rocchiccioli-Deltcheff, C.; Thouvenot, R.; Fouassier, M. Inorg. Chem. 1982, 21, 30. (b) Rocchiccioli-Deltcheff, C.; Fournier, R. F.; Thouvenot, R. Inorg. Chem. 1983, 22, 207. (c) Rocchiccioli-Deltcheff, C.; Fournier, M.; Frank, R.; Thouvenot, R. Spectrosc. Lett. 1986, 19, 765. (d) Rocchiccioli-Deltcheff, C.; Thouvenot, R. J. Chem. Research (S), 1977, 46.
- 25. (a) Rao, C. N. R.; Gopalakrishnan, J. Acc. Chem. Res. 1987, 20, 228. (b) Green, M. L. H.; Hamnett, A.; Qin, J.; Baird, P.; Bandy, J. A.; Prout, K.; Marseglia, E.; Obertelli, S. D. J. Chem. Soc. Chem. Commun. 1987, 1811. (c) Casellato, U.; Guerriero, P.; Tambunini, S.; Sitran, S.; Vigato, P. A. J. Chem. Soc. Dalton Trans. 1991, 2145. (d) Borvornwattananont, A.; Moller, K.; Bein, T. J. Phys. Chem. 1987, 93, 4205.
- 26. Day, V. W.; Klemperer, W. G. Science 1985, 228, 533.
- 27. (a) Che, T. M.; Day, V. W.; Francesconi, L. C.; Fredrich, M. F.; Klemperer, W. G.; Shum, W. *Inorg. Chem.* 1985, 24, 4055. (b) Klemperer, W. G.; Shum, W. *J. Chem. Soc. Chem. Commun.* 1979, 60.
- 28. Day, V. W.; Fredrich, M. F.; Klemperer, W. G.; Thompson, M. R. J. Am. Chem. Soc. 1981, 103, 3597.
- 29. Klemperer, W. G.; Yagasaki, A. Chem. Lett. 1989, 2041.
- 30. (a) Besecker, C. J.; Klemperer, W. G. J. Am. Chem. Soc. 1980, 102, 7600. (b) Besecker, C. J.; Day, V. W.; Klemperer, W. G.; Thompson, M. R. Inorg. Chem. 1985, 24, 44. (c) J. Am. Chem. Soc. 1984, 106, 4125.

- 31. Besecker, C. J.; Klemperer, W. G. J. Am. Chem. Soc. 1982, 104, 6158.
- 32. Day, V. W.; Klemperer, W. G.; Main, D.J. *Inorg. Chem.* **1990**, 29, 2345, 2355.
- 33. Finke, R. G.; Droege, M. W. J. Am. Chem. Soc. 1984, 106, 7274.
- 34. (a) Finke, R. G.; Rapko, B.; Domaille, P. J. Organometallics 1986, 5, 175. (b) Edlund, D. J.; Saxton, R. J.; Lyon, D. K.; Finke, R. G. Organometallics 1988, 7, 1692. (c) Finke, R. G.; Lyon, D. K.; Nomiya, K.; Sur, S.; Mizuno, N. Inorg. Chem. 1990, 29, 1787, 1789.
- 35. Siedle, A. R. New J. Chem. 1989, 13, 719.
- 36. (a) Siedle, A. R.; Newmark, R. A. J. Am. Chem. Soc. 1989, 111, 2058. (b) Organometallics 1989, 8, 1442. (c) Sieldle, A. R.; Newmark, R. A; Sahyun, M. R. V.; Lyon, P. A.; Hunt, S. L.; Skarjune, R. P. J. Am. Chem. Soc. 1989, 111, 8346. (d) Siedle, A. R.; Markell, C. G.; Lyon, P. A.; Hodgson, K. O.; Roe, A. L. Inorg. Chem. 1987, 26, 220.
- 37. Siedle, A. R.; Newmark, R. A.; Gleason, W. B.; Skarjune, R. P.; Hodgsen, K. O.; Roe, A. L.; Day, V. W. Solid State Ionics 1988, 26, 109.
- 38. Rempel, G.A.; Legzdins, P.; Smith, H.; Wilkinson, G. *Inorg. Synth. Vol.* 13, **1972**, 90.
- 39. Dunbar, K. R.; Pence, L. E. Inorg Synth. Vol. 29, in press.
- 40. Cotton, F. A.; Wiesinger, K. J. Inorg. Synth. Vol. 29, in press.



- 41. (a) Lawton, D.; Mason, R. J. Am. Chem. Soc. 1965, 82, 921.
- (b) Stephenson, T. A.; Bannister, E; Wilkinson, G. J. Chem. Soc. 1964, 4150.
- 42. Fuchs, J.; Jahn, K. F. Z. Naturforsch. Teil B 1968, 23, 1380.
- 43. Che, M.; Fournier, M.; Launay, J. P. J. Chem. Phys. 1979, 71, 1954.
- 44. Klemperer, W. G. Inorg. Synth. Vol. 27 1990, 71.
- 45. (a) Dunbar, K. R.; Haefner, S. C.; Pence, L. E. J. Am. Chem. Soc.
 1989, 111, 5504. (b) Haefner, S. C.; Dunbar, K. R.; Bender, C. J. Am. Chem. Soc. 1991, 113, 9540.
- 46. TEXSAN TEXRAY Structure Analysis Package, Molecular Structure Corporation, 1985.
- 47. Sheldrick, G.M.; SHELXS86. Program for the solution of crystal structures. Univ. of Gottingen, Germany.
- 48. Beurskens, P. T.; DIRDIF: Direct Methods for Difference Structures an automatic procedure for phase extensions and refinement of difference structure factors. Technical Report 1984/1 Crystallography Laboratory, Toernooiveld, 6525 Ed Nijmegen, Netherlands.
- 49. Dahlstrom, P.; Zubieta, J.; Neaves, B.; Dilsworth, J. R. Cryst. Struct. Commun. 1982, 11, 463.
- 50. Gilmore, C. J. MITHRIL an integrated direct methods computer program. Univ. of Glasgow, Scotland, J. Appl. Cryst. 1984, 17, 42.

- 51. Walker, N.; Stuart, D. DIFABS. Acta Cryst. 1983, A39, 158.
- 52. Badaud, J., et al. C. R. Seances Acad. Sci., Ser. C 1977, 284, 921.
- 53. Haefner, S. C.; Dunbar, K. R.; Dulebohn, J. I.; Berglund, K. A. submitted to *Chemistry of Materials*.
- 54. Beers, W. W.; McCarley, R. E. Inorg. Chem. 1985, 24, 468.







11CHIGAN STATE UNIV. LIBRARIES 31293007929130